THE UNIVERSITY OF MANITOBA

THE EFFECT OF EDGE TREATMENT ON FATIGUE STRENGTH OF 2024-T3 ALUMINUM ALLOY

by

ALY M.A.NAWWAR

A THESIS

SUBMITTED TO THE FACULTY OF GRADUATE STUDIES

IN PARTIAL FULFILMENT OF THE REQUIREMENTS FOR THE DEGREE

OF DOCTOR OF PHILOSOPHY

DEPARTMENT OF MECHANICAL ENGINEERING

WINNIPEG, MANITOBA

October 1976

"THE EFFECT OF EDGE TREATMENT ON FATIGUE STRENGTH OF 2024-T3 ALUMINUM ALLOY"

by

ALY M.A. NAWWAR

A dissertation submitted to the Faculty of Graduate Studies of the University of Manitoba in partial fulfillment of the requirements of the degree of

DOCTOR OF PHILOSOPHY

© 1976

Permission has been granted to the LIBRARY OF THE UNIVERSITY OF MANITOBA to lend or sell copies of this dissertation, to the NATIONAL LIBRARY OF CANADA to microfilm this dissertation and to lend or sell copies of the film, and UNIVERSITY MICROFILMS to publish an abstract of this dissertation.

The author reserves other publication rights, and neither the dissertation nor extensive extracts from it may be printed or otherwise reproduced without the author's written permission.

ABSTRACT

This thesis presents a new approach to improving the fatigue strength of sheet and thin plate material by edge treatment. The improvement is achieved by inducing compressive residual stresses along the edge. The technique consists of creating misfit between a finite portion of the edge and the surrounding material, thus resulting in a residual compression in the critical region to fatigue. The parameters of the edge dimpling procedure are optimized in order to attain a useful condition of maximum fatigue strength improvement with minimum scatter of results.

To accurately assess the effect of edge dimpling on the fatigue strength improvement the resulting residual stress distribution is determined. For this purpose, an analytic-numerical method is developed in which an approximate procedure to determine the distribution of residual deformation, based on idealized stress-strain relations, is employed. The finite element technique is used at some stage of the solution to determine the stress field produced by a system of body and boundary forces. Final stresses are calculated for given dimpling parameters and material properties. For the necessary verification of the results of this analytic-numerical method an experimental investigation of residual stresses due to edge dimpling is conducted. For this purpose a modified hole-drilling technique is developed which eliminates the major disadvantages associated with the conventional hole-drilling procedure. Preliminary experiments on aluminum alloy sheet specimens show that the modified technique can yield

measurements within ±5 percent accuracy. The modified technique is employed to measure the average residual stresses in edge dimpled specimens. The results are found to be in good agreement with those obtained by the analytic-numerical technique.

An experimental fatigue testing program is conducted using 2024-T3 aluminum alloy notched sheet specimens. The study of results backed by extensive statistical analysis of data, indicates a fatigue strength improvement of approximately 100 percent at one million stress-cycles to failure. The fatigue strength reduction factor is almost halved at the same life. Further fatigue testing of dimpled-preloaded-notched specimens indicates that preloading does not significantly influence the level of fatigue strength improvement obtained by edge dimpling.

An attempt is made to correlate the strength improvement with the residual stress. A procedure is developed for predicting the S-N curve for dimpled-notched specimens. The predictions are based on the fact that residual stress at the stress raiser lowers the actual stress-concentration effect and subsequently lowers the effective fatigue strength reduction factor. Predictions are determined from the S-N data for plain material, the geometry of and the residual stress at the notch or the stress concentrator. Good correlation is shown between the measured residual stress and fatigue strength for the 2024-T3 edge-dimpled specimens.

ACKNOWLEDGEMENTS

The author wishes to express his deepest gratitude to his advisor Dr. J. Shewchuk for his continuous encouragement, valuable advice and suggestions and generous support throughout the course of the study. Sincere appreciation is also due to Dr. K. McLachlan for his constructive criticism and useful discussions during the experimental study of the residual stress determination. Thanks are also extended to other staff members and collegues who contributed in one way or the other to the completion of this work.

The financial support of the University of Manitoba through a Graduate Fellowship and the National Research Council of Canada through an NRC Postgraduate Scholarship and the Operating Grant No.4131 to Dr. J. Shewchuk are greatly appreciated.

Lastly, and perhaps most importantly, particular appreciation is due to my wife Amany Nawwar for her patience and understanding over the long period of the study and preparation of this dissertation and also to my mother, brothers and sister for their sincere support and encouragement across the thousands of miles that seperate us.

TABLE OF CONTENTS

	Page
ABSTRACT	i
ACKNOWLEDGEMENTS	iii
TABLE OF CONTENTS	iv
LIST OF TABLES	viii
LIST OF FIGURES	x
NOMENCLATURE	xv
CHAPTER 1 INTRODUCTION	1
1.1 Introduction	1
1.2 Statement of Problem	2
1.3 Scope of Thesis	4
CHAPTER 2 REVIEW OF LITERATURE ON FATIGUE AND RESIDUAL STRESSES	5
2.1 Introduction	5
2.2 Residual Stresses and Fatigue	6
2.3 Fatigue Improvement by Reducing Alternating Stress	8
2.4 Fatigue Improvement by Reducing Mean Stress	10
2.4.1 Thermal Techniques	10
2.4.2 Metallurgical Techniques	11
2.4.3 Mechanical Techniques	12
i Overloading Techniques	13
ii Shot-Peening and Strain-Peening	17
iii Coining Techniques	18
iv Dimpling Techniques	22
2.5 SUMMARY	26

Page

CHAPTER 3 FATIGUE STRENGTH IMPROVEMENT BY EDGE TREATMENT 27

3.1 Introduction 27

3.2 The Edge Dimpling Technique 27

3.2.1 Description 27

3.2.2 Dimpling Apparatus 33

3.2.3 Dimpling Parameters 35

3.2.4 Characteristic Curve of Edge Dimpling . . 41

3.3 Summary 43

CHAPTER 4 ANALYTICAL DETERMINATION OF RESIDUAL STRESS DUE TO EDGE DIMPLING 45

4.1 Introduction 45

4.2 Method of Solution 47

4.2.1 Assumption of Fictitious Forces 47

4.2.2 Distribution of Residual Deformation . . . 50

4.2.3 Removal of Fictitious Forces 65

4.2.4 Residual Stress Distribution 69

4.3 Effect of Preloading 71

4.4 Summary 75

CHAPTER 5 THE MEASUREMENT OF RESIDUAL STRESSES 76

5.1 Review of Residual Stress Measuring Techniques . 76

5.1.1 Non-destructive Techniques 76

5.1.2 Destructive Techniques 78

5.1.3 Summary 82

Page

5.2 The Modified Hole-Drilling Technique 82

5.2.1 Theoretical Analysis 83

5.2.2 Practical Considerations 87

5.2.3 Experiments 90

5.2.4 Results 94

5.2.5 Discussion 94

5.2.6 Summary 106

5.3 Residual Stresses Due to Edge Dimpling 107

5.3.1 Extension to Biaxial Stress Measurement . 107

5.3.2 Additional Considerations 111

5.3.3 Experiment 118

5.3.4 Results and Analysis 120

5.4 Comparison of Results 128

5.5 Summary 130

CHAPTER 6 EXPERIMENTAL FATIGUE TESTING PROGRAM 131

6.1 Objectives 131

6.2 Experimental Program 132

6.2.1 Test Specimens 132

6.2.2 Test Equipment 133

6.2.3 Test Procedure 138

6.3 Results and Analysis 139

6.4 Discussion 140

6.4.1 The Fatigue Strength Improvement 140

6.4.2 The Effect of Preloading on Fatigue Strength 147

Page

6.4.3 The Correlation of Fatigue Strength Improvement and Residual Stress 149

6.5 Summary 156

CHAPTER 7 SUMMARY AND CONCLUSIONS 159

7.1 Summary 159

7.2 Conclusions 160

7.3 Suggestions for Further Study 161

BIBLIOGRAPHY 163

APPENDIX A PRESENTATION AND STATISTICAL ANALYSIS OF FATIGUE DATA 171

A.1 Comparison of Notched Specimens Types-A and B . 171

A.2 Optimization Testing: Series 1 176

A.3 Fatigue Life Distribution of Dimpled Specimens: Series 9 183

A.4 Primary Fatigue Testing: Series 2, 3 and 4 . . 188

A.5 Preloading Fatigue Testing: Series 5, 6, 7 and 8 200

LIST OF TABLES

Table		Page
2.1	Fatigue Strength Improvement by Preloading.	15,16
2.2	Fatigue Testing Results of 7075-T6 Aluminum Alloy, Edge Roll Grooved and V-notched Specimens [31]	23
5.1	The Measured Relaxation Strains for O.D.S. Specimen (Microstrain)	121
5.2	Apparent Stress Changes and Residual Stresses, psi	123
5.3	Changes of Stress and Residual Stresses (psi) With Consideration of Biaxiality	125
5.4	Percentage Reduction of Residual Stresses due to the Redistribution	127
6.1	Nominal Chemical and Mechanical Properties of 2024-T3 Alclad Aluminum Alloy Sheet	135
6.2	Comparison of Predicted and Experimental Fatigue Strengths for Notched-dimpled Specimens	157
A.1	Results of Comparative Tests	172
A.2	Tests of Significance - Summary of Results	174
A.3	Test Series No. 1 - Results of Preliminary Optimization Testing	177
A.4	Test Series No. 9 - Results of Fatigue Life Distribution .	184
A.5	Test Series No. 2 - Results of Fatigue Testing for Notched Specimens	189

Table		Page
A.6	Test Series No. 3 - Results of Fatigue Testing for Dimpled-Notched Specimens	190
A.7	Test Series No. 4 - Results of Fatigue Testing for Plain Specimens	191
A.8	Statistical Parameters for Determining Confidence Limits (of the mean) and Standard Deviation	195
A.9	Statistical Analysis of Series 2, 3 and 4	197
A.10	Test Series No. 5 - Results of Preliminary Preloading Testing	201
A.11	Test Series No. 6 - Results of Fatigue Testing with Preloading - R_{ps} = 0.65	204
A.12	Test Series No. 7 - Results of Fatigue Testing with Preloading - R_{ps} = 1.00	205
A.13	Test Series No. 8 - Results of Fatigue Testing with Preloading - R_{ps} = 1.17	206
A.14	Statistical Analysis of Series 6, 7 and 8	207

LIST OF FIGURES

Figure		Page
1.1	Fatigue Failure of Access Door Opening into a Wing Structure (Front spar), [3]	3
2.1	Basic Methods of Fatigue Improvement on Modified Goodman Diagram	7
2.2	Change of Stress Cycle with Interference Fits. Results of Photoelastic Studies by Ligenza [9]	9
2.3	Diagramatic Illustration of Axial Stress Distributions due to Preloading at the Minimum Section of a Specimen with Central Hole [19]	14
2.4	Variation in Fatigue Life with Depth of Penetration of a Ring Coining Die [32]	20
2.5	Coining Techniques Developed by Speakman [3]	21
2.6	Concentric Dimpling Developed by Shewchuk and Roberts [37]	25
3.1	Edge Dimpling Process and Resulting Residual Compressive Stress	28
3.2	Bending Effect in Edge Dimpling of an Elemental Strip	30
3.3	Bending Effect after the Second Dimple in Reversed Edge Dimpling	32
3.4	Edge Dimpling Apparatus	34
3.5	Illustration of Steps of Edge Dimpling	36
3.6	Geometry of Edge Dimple	38

Figure		Page
3.7	The Average Edge Strain vs. Dimpling Ratio for Various Values of $0 \leq K \leq 1.0$	40
3.8	The Characteristic Dimpling Curve	42
4.1	Subdivision of Elemental Strips	48
4.2	Edge Dimpling Procedure Represented on the Idealized Stress-Strain Curve	51
4.3	Characteristic Regions of Edge Dimpling for 2024-T3 Alclad Aluminum Alloy Material	55
4.4	Dimpling Head Profile	57
4.5	Values of the Characteristic Parameter $\bar{\varepsilon}$ for the Given Conditions	59
4.6	The Distribution of $\varepsilon_x^0(y)$	61
4.7	The Necessary Boundary Pressure (non-dimensional) to Suppress an Elemental Strip at a Distance y from the Edge to its Original Planar Dimensions	63
4.8	Summary of Procedure of Determining the Residual Strain Distribution, $\varepsilon_x^0(y)$	64
4.9	The Elemental Strips Joined Together in an Integral Body	66
4.10	The Finite Element Mesh for Edge Dimpled Specimens	68
4.11	The Stresses Created by the Removal of Fictitious Forces	70
4.12	The Analytical Solution of Residual Stresses ($x = 0$)	72

Figure		Page
4.13	The Effect of Preloading	74
5.1	Values for the Radial Relaxation Coefficient	84
5.2	Values for the Tangential Relaxation Coefficient	86
5.3	Error in Evaluating Stress due to the Effect of Local Plastic Yielding	91
5.4	Test Specimen and Strain Gage Layout	92
5.5	Results for Longitudinal Gages - Specimen I	95
5.6	Results for Transverse Gages - Specimen I	96
5.7	Results for Longitudinal Gages - Specimen II	97
5.8	Results for Transverse Gages - Specimen II	98
5.9	Values for the Relaxation Component due to the Machining Stresses	99
5.10	Values of ε_p for a Radial Gage at $\theta = 0$	102
5.11	The Percentage Error in Determining the Stress as a Function of λ	104
5.12	Strain Gage Arrangement for Measuring Bi-axial Stresses	108
5.13	Effect of Hole Location, Savin [88]	113
5.14	Interaction Between Two Holes in a Plate, Savin [88]	115
5.15	Iso-relaxation Lines for a Radial Gage in the Vicinity of a Hole Drilled at the Origin O in The Stress Field σ_x	116
5.16	Specimen and Strain Gage Layout	119
5.17	The Residual Stress Distribution in Edge-Dimpled Specimen	129

Figure		Page
6.1	Types of Fatigue Specimens: Shape and Size	134
6.2	Sonntag-Baldwin Fatigue Testing Machine (Model SF-1-U)	136
6.3	Specimen Type-B as Clamped	137
6.4	Best Fitting S-N Curves for Fatigue Testing - Strength Improvement Results	141
6.5	Best Fitting S-N Curves for Fatigue Testing Results - Preloading Effect	142
6.6	Fatigue Strength Improvement vs. Life (Log Scale)	143
6.7	The Decrease in F.S.R.F. vs. Life	145
6.8	The Variation in F.S.R.F. due to Dimpling	146
6.9	Log-life Ratio vs. Prestress Ratio at Various Preload Levels. N_i, i = 6, 7, 8, is the Life of Respective Series and N_3, is the Life of Specimens without Preload	148
6.10	Change of Fatigue Strength Improvement by Preloading	150
6.11	Change of F.S.R.F. of Dimpled Specimens by Preloading	151
A.1	Average Edge Strain, $\bar{\varepsilon}_e$, vs. LogN Plot	179
A.2	Residual Stress Distribution for $\bar{\varepsilon}_e$ in the Elastic Stage	180
A.3	Median Life Improvement Factor vs. $\bar{\varepsilon}_e$	181
A.4	Cumulative Probability Plot for Data - Series 9	186
A.5	Log-Normal Probability Plot for Data of Series 9	187
A.6	Log-Log Plots of the Best Estimate of Standard Deviation of the Population, σ, vs. the Maximum Fatigue Stress, S_{max}	198

Figure		Page
A.7	S-N Curves for Fatigue Strength Test Series	199
A.8	The Effect of Prestress Ratio on Fatigue Life, at the Same Stress Level	202
A.9	Log-Log Plots of the Best Estimate of Standard Deviation of the Population, σ, vs. the Maximum Fatigue Stress, S_{max}	208
A.10	Effect of Preloading	209

NOMENCLATURE

A	= statistical parameter, psi (MPa)
a	= material notch alleviation factor, $in.^{1/2}$ ($mm^{1/2}$)
B	= statistical parameter, kilocycles (kc)
B_x	= body force in the x direction, lb.(kg)
$2b$	= span of dimpling apparatus, in.(mm)
C	= centre distance, in.(mm)
C_d	= drilling clearance, in.(mm)
C'_d	= corrected drilling clearance, in.(mm)
d	= hole size, in.(mm)
d	= dimpling ram movement, in.(mm)
d'	= effective dimpling ram movement, in.(mm)
E	= modulous of elasticity, psi (MPa)
E'	= plastic modulous, psi (MPa)
f	= empirical material constant, dimensionless
GL	= gage length of strain gage, in.(mm)
K	= dimpling constant, dimensionless
K'	= dimpling constant at a distance y from the plate edge, dimensionless
K_f	= FSRF (Fatigue Strength Reduction Factor) @ 10^7 cycles, dimensionless
K'_f	= FSRF for dimpled notched specimens @ 10^7 cycles, dimensionless

$K_f(N)$ = FSRF @ N kc, dimensionless

$K_f'(N)$ = FSRF for dimpled notched specimens @ N kc, dimensionless

$K_r(\lambda,\theta)$ = radial relaxation coefficient, dimensionless

$K_\theta(\lambda,\theta)$ = tangential relaxation coefficient, dimensionless

K_t = theoretical stress concentration factor, dimensionless

K_t' = effective theoretical stress concentration factor, dimensionless

m = statistical parameter, dimensionless

N = fatigue life, kc

$p_x(y), p_y(y)$ = boundary pressures in the x and y directions; respectively, psi (MPa)

q = notch sensitivity, dimensionless

R_b = dimpling-span ratio, dimensionless

$R_b'(y)$ = dimpling-span ratio at a distance y, dimensionless

R_{ps} = prestress ratio = preload ratio, dimensionless

R_t = dimpling-thickness ratio, dimensionless

r = distance from hole centre to strain gage centre, in.(mm)

r_1, r_2, r_3 = radii of dimpling ram, fillets, and upward curvature of the dimpling ram; respectively, in.(mm)

S = fatigue strength of notched specimens, psi (MPa)

S' = fatigue strength of dimpled notched specimens @ 10^7 cycles, psi (MPa)

S_e = fatigue strength at a large number of cycles to failure (usually 5×10^8 cycles), psi (MPa)

S_{max} = maximum fatigue stress, psi (MPa)

S_p = fatigue strength of plain specimens, psi (MPa)

S_u = ultimate tensile strength, psi (MPa)

t = material thickness, in.(mm)

y_{max} = maximum contact distance during dimpling, in.(mm)

$\alpha(\lambda)$ = ratio of relaxation coefficients, dimensionless

β = biaxiality ratio, dimensionless

γ = Bauschinger effect parameter, dimensionless, centre distance ratio, dimensionless

$\Delta(y)$ = correction factor for R_b and K, dimensionless

δ = sign operator = ± 1

ε = strain, in./in. (m/m)

ε_R = net relaxation strain

ε_{Ri} = net relaxation strain for gages i= a,b or c

$\varepsilon_{Rr}, \varepsilon_{R\theta}$ = relaxation strain in the radial and tangential directions; respectively

$\varepsilon_{Rx}, \varepsilon_{Ry}$ = net relaxation strain in the x and y directions, respectively

ε_T = total strain relaxation as measured

ε_m = relaxation strain component due to machining stresses

ε_p = relaxation strain component due to localized yielding

$\varepsilon_r, \varepsilon_\theta$ = radial and tangential strains in the vicinity of the drilled hole

$\varepsilon_x^o, \varepsilon_y^o$ = residual strains due to dimpling, in the x and y directions respectively

$\varepsilon_r^o, \varepsilon_\theta^o$ = radial and tangential strains in a uniform stress field

$\bar{\varepsilon}(y)$ = average dimpling strain at a distance y from the edge

$\bar{\varepsilon}_e$ = characteristic parameter : average edge dimpling strain (at y = 0)

$\Delta\varepsilon$ = strain relaxation due to unclamping

$\Delta\varepsilon_x, \Delta\varepsilon_y$ = changes in strain in the x and y directions, respectively

θ = angle, radians

λ = parameter defined by d/r, dimensionless

ν = Poisson's ratio of the material, dimensionless

ϕ_i = indicates hole diameter after the ith drilling sequence

σ = stress, psi (MPa)

σ = nominal stress

σ_B = Bauschinger stress

σ_F = forward yield strength

σ_R = reverse yield strength

σ_{ps} = prestress

$\sigma_r, \sigma_\theta, \sigma_{r\theta}$ = radial, tangential and shear stress components

σ_x, σ_y = stresses in the x and y directions, respectively

$\Delta\sigma_x, \Delta\sigma_y$ = changes in σ_x and σ_y, respectively

σ_x' = remaining residual stress in the x direction

$\Delta\sigma_x'$ = change in σ_x'

σ_x'' = stress component which is not measured

σ_{yp} = yield strength of the material

σ_x^o = maximum possible residual stress in an elemental strip in the x direction

$\sigma_x^{RS}(x,y), \sigma_y^{RS}(x,y), \sigma_{xy}^{RS}(x,y)$ = total residual stress

$\sigma_x^{I}(y), \sigma_y^{I}(y)$ = components of residual stress due to the first step of solution

$\sigma_x^{II}(x,y), \sigma_y^{II}(x,y), \sigma_{xy}^{II}(x,y)$ = components of residual stress due to the second step of solution which are determined by numerical technique

CHAPTER 1

1.1 INTRODUCTION

Fatigue in metals is known to have two characteristics. The first is its surface nature; in most cases, fatigue cracks initiate at the exposed surface of the material. The exposed surfaces are inherently weaker than the interior grains that are confined by bonds with adjoining grains. Sines [1] explains the surface weakness by comparing plain and surface treated (shot-peened) specimens. All fibers are subjected to the same imposed stresses and yet an improvement is obtained; therefore, "the interior grains must have been much stronger than the surface to account for the increased strength". The second characteristic of fatigue is its tensile nature; fatigue cracks propagate into the material under tensile stresses.

In sheet material, thin plates or components with small thickness compared to surface area, the likeliest region to fatigue is the edge. The absence of edges in round bar material may explain why it has a somewhat higher fatigue resistance than sheets of the same material [2]. The additional presence of geometrical concentrations at the edge of a plate, due to cuts, notches, curvatures or openings, will greatly aggravate the fatigue situation. The fatigue cracks, initiating at the surface or edge of the stress concentration configuration will propagate upon the application of normal tensile fatigue loads.

In such cases fatigue strength (or life) may be enhanced by the introduction of residual compressive stresses. These stresses will improve the fatigue resistance through:

1. lowering the actual stress concentration effect, thus delaying crack initiation; and
2. reducing the effective tensile stresses at the critical region, thus slowing the rate of crack propagation.

Therefore, the overall strength of the structure may be increased by improving the detailed fatigue resistance at free edges or where high stress concentrations exist. If the weak points of the structure are strengthened, a condition of uniform fatigue resistance could possibly be approached. Theoretically, this condition of uniformity corresponds to the optimum use of material where all links of the chain have the same strength.

1.2 STATEMENT OF PROBLEM

This thesis introduces a new method of improving the fatigue resistance of sheet and thin plate material by edge treatment. This treatment is useful in cases of plates with large scale geometrical stress concentrations. Most structures, and particularly aircraft structures, are made up of a large number of such functionally necessary concentrations. Typical examples are an unstressed access door opening into a wing structure as shown in Figure 1.1, panels of window doublers in aircraft and other similar applications.

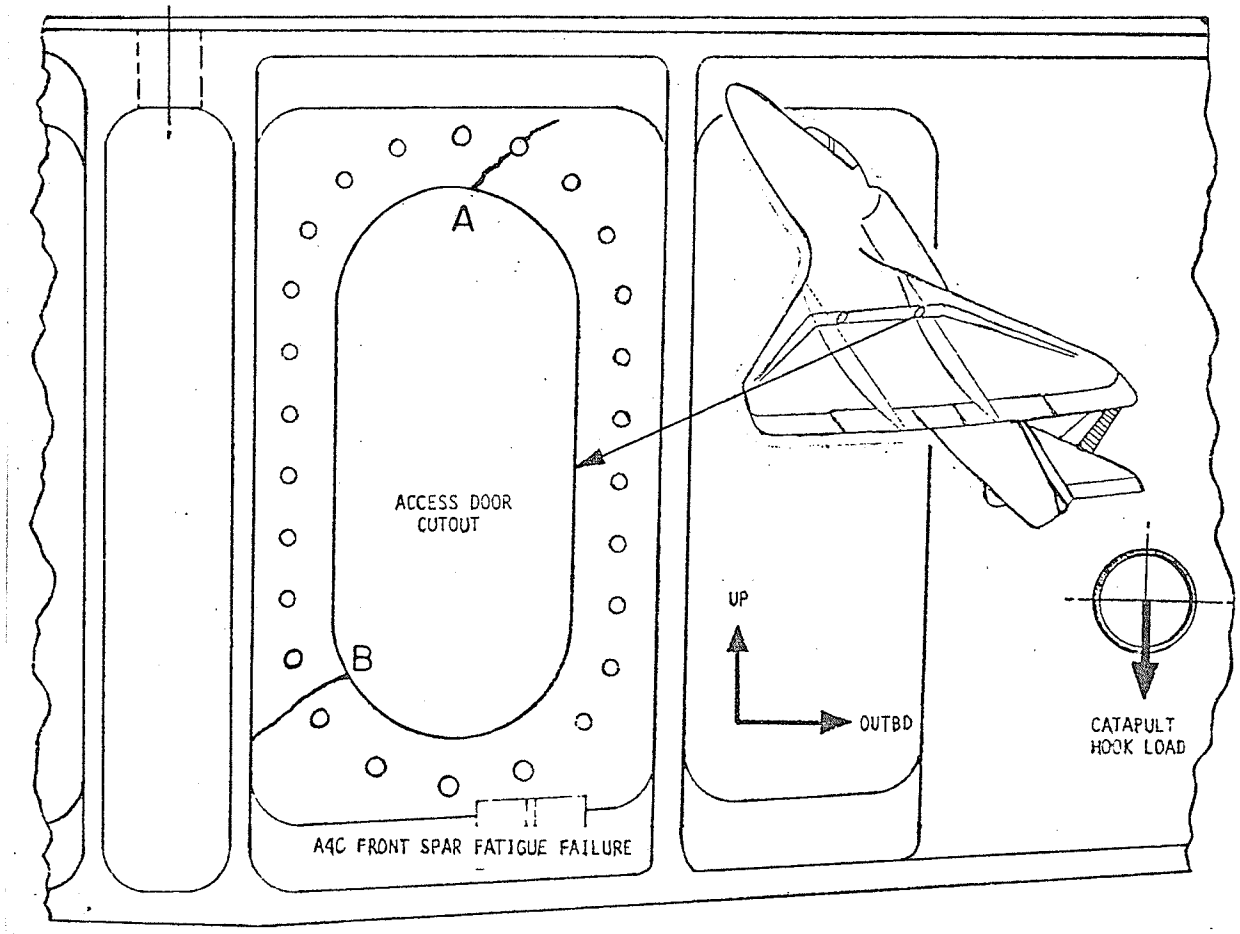

Figure 1.1 Fatigue failure of an access door opening into a wing structure (Front spar), [3].

1.3 SCOPE OF THESIS PRESENTATION

The thesis is divided into six chapters.

Chapter 1 is an introduction to the problem of fatigue at stress concentrations in sheet and thin plate materials and how to improve their fatigue resistance by inducing residual stresses.

Chapter 2 is a review of previous work on the influence of residual stresses on fatigue and the various techniques of inducing such stresses in the critical regions.

Chapter 3 includes a description of the new technique of edge treatment by edge dimpling and gives definitions of the associated parameters.

Chapter 4 presents an analytic determination of residual stresses in edge dimpled specimens.

Chapter 5 describes the experimental measurement of residual stresses and a modified hole-drilling technique is outlined.

Chapter 6 is devoted to a description of the experimental fatigue testing program which was carried out to assess the effect of edge dimpling on fatigue strength of aluminum alloy specimens. An attempt is made to correlate the fatigue strength improvement with the residual stresses at the critical region.

Chapter 7 is the summary, conclusions and recommendations for further study.

A bibliography is presented at the conclusion of the thesis. Appendix A presents detailed statistical analysis of the results of fatigue testing.

CHAPTER 2

REVIEW OF LITERATURE ON FATIGUE AND RESIDUAL STRESS

2.1 INTRODUCTION

Residual stresses are those which remain in a body (or mating bodies) in the absence of any external load or constraint. From the early beginning of fatigue studies residual stresses have been associated with fatigue failures. In 1946, Norton et al. [4] made the following statement concerning the state of understanding of the exact role of residual stress in fatigue.

"Despite extensive research, the influence of residual stress on the fatigue behaviour of metal parts in general and welded joints in particular still remains one of the most controversial engineering problems of today. Most of the work done in welding seems to indicate that the residual stress has little or no influence on the fatigue performance of welded joints. On the other hand, there is strong feeling among many investigators that residual compressive stress has much to do with the improvement of the fatigue behaviour of metal parts,...."

Since then, several investigations on the relation between residual stress and fatigue have followed, and it is now established that, in general, residual compressive stresses exert a favourable influence on fatigue strength while residual tensile stresses have a detrimental effect. Exceptions, however, may occur depending on the nature of the stresses and the loading. An example of this will be shown in the discussion on interference stresses in Section 2.3.

Residual stresses may result from certain manufacturing processes such as metal forming, machining, welding, casting or assembling. Such residual stresses are the fortuitous products of manufacturing processes and their influence on fatigue may or may not be favourable depending on their distribution and the nature of the service loading.

On the other hand, residual stresses may be intentionally induced to improve the fatigue resistance of metals. The following sections include a critical review of the literature pertaining to "intentional" residual stresses in relation to fatigue.

2.2 RESIDUAL STRESSES AND FATIGUE

Residual stresses may be used to improve the fatigue resistance of metals. The conditions in the critical regions are ameliorated by one of two basic methods:

1. reduction in alternating stress.
2. reduction in mean stress.

These are illustrated in Figure 2.1 by means of the modified Goodman diagram [5]. In the first method, going from point A of life N_1 to point B of higher life N_3, the improvement is achieved by lowering the alternating stress while the maximum stress is kept essentially unchanged. Meanwhile, the same improvement in fatigue life could be achieved by lowering the mean stress while the alternating stress is kept unchanged, i.e., going from point A to point C of life N_3 in the figure. The various residual stress techniques may be classified into one of these two categories. The mechanisms associated with the above will be discussed in the subsequent sections.

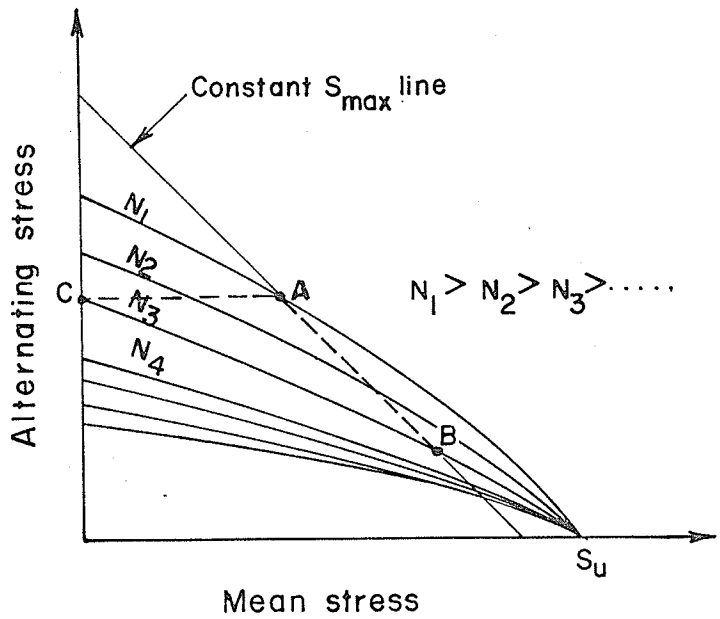

Figure 2.1 Basic methods of fatigue improvement on modified Goodman diagram.

2.3 FATIGUE IMPROVEMENT BY REDUCING ALTERNATING STRESS

Techniques of this category utilize the high residual stresses at the hole edge, caused by interference fits, to lower the alternating stress range while maintaining the maximum stress at essentially the same level, thus resulting in an increase in the fatigue life. It is interesting to note that although the residual stress in the critical region is tensile, considerable improvement in the fatigue life could be obtained.

Smith [6] investigated the effect of pressed in bushing interference on fatigue life of 7075-T6 aluminum lugs. His results indicate that there is an optimum interference fit to give the greatest fatigue life improvement. He later experimented on taper pin interference [7] and reported similar trends of improvement in the short cycle fatigue range up to 100 kilocycles.

In 1963, Mittenberg and Beall [8] experimented on pin-loaded lug joints with different values of interference. They studied the effect of interference and bolt torque on fatigue strength and observed that the marked strength improvement at high pin interference values is accompanied by large scatter and possible damage of pin holes during assembling.

Ligenza [9] conducted photoelastic studies on pin loaded holes with different amounts of interference. His results, as shown in Figure 2.2, confirm that the maximum cyclic stress in the critical section is slightly reduced at high interferences while the minimum stress is considerably increased resulting in a major contribution to fatigue improvement.

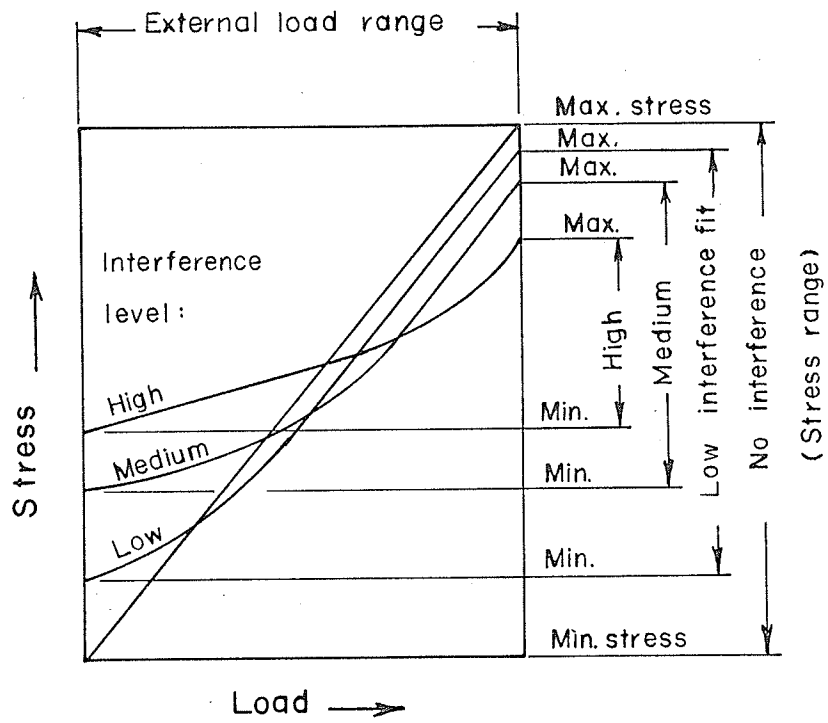

Figure 2.2 Change of stress cycle with interference fits. Results of photoelastic study by Ligenza [9].

Furthermore, it has been confirmed analytically by Koplik and Klassen [10] that inserts with optimum interference can be used to reduce the stress concentration and alternating stress range around holes in plates.

2.4 FATIGUE IMPROVEMENT BY REDUCING MEAN STRESS

Techniques of this category utilize residual compressive stresses which may have different origins: thermal, metallurgical and mechanical. In the following sections techniques employing these sources of residual stress will be discussed.

2.4.1 THERMAL TECHNIQUES

The sudden application of steep temperature gradients can produce high levels of residual compressive surface stress and, hence, provide for reduced critical mean stress in load applications. A good example of pure thermal effects, i.e., no transformation, is demonstrated by Lee and Rogers [11] in the production of toughened glass (although not generally associated with fatigue). The sudden cooling of glass surfaces leads to a non-uniform thermal contraction and tensile stresses at the surfaces. These stresses cause viscoelastic flow in the hot internal regions. This internal deformation becomes "frozen in" when the temperature falls to normal, and in turn causes residual compression at the surfaces.

In crystalline materials (metals and alloys) residual stresses resulting from sudden cooling of a body are generated in the same manner.

The principal difference is that the pure thermal effects may or may not be accompanied by other metallurgical changes in the structure due to high temperatures.

In 1966, Rathbun and Coffin [12] performed experiments on AISI-316 stainless steel plates which experiences no phase transformation. Pure thermal residual stresses of up to 36 ksi were produced at the surface.

If the heating is performed with a very high intensity and in a very short period of time it is known as "thermal shocking". Hsu [13] applied the laser beam thermal shock technique to generate residual compressive stresses around holes in 2024-T3 aluminum alloy specimens. This was done by thermal shocking a concentric annular area. The theoretical solution of the stress field introduced by thermal shock was reported by Hsu and Trasi [14]. Their analytical results indicate a residual tangential compressive stress at the hole edge of 0.2 of the yield strength of the material. This compression is balanced by relatively high tensile stresses, in the interior region, ranging from 0.4 to more than 0.8 of the yield strength.

2.4.2 METALLURGICAL TECHNIQUES

Metallurgical sources of residual stresses include both phase transformation and surface absorption. To distinguish between thermal and phase transformation effects consider, for instance, steel. The heating of steel, in general, to a temperature above the lower critical point followed by rapid cooling from the austenite region to room temperature results in the transformation of austenite to martensite and,

hence, in an appreciable increase in volume. Thus, if heating was restricted to the surface the volume of the surface layers will increase. The sudden cooling (quenching) of the hot surfaces will freeze the martensite in the surface layers resulting in high residual surface compression. In this case both transformation and thermal residual stresses occur. While if the temperature is kept below the lower critical value only thermal residual stresses are possible [15].

Weiner and Huddleston [16] made an analytical study of the residual stresses in heat treated cylinders. In their analysis, they included the phase transformation effect as an equivalent temperature change, for both result in similar volume dilatation. Their results are in good agreement with experimental results presented by Bühler and Scheil [17] for residual stresses in water-quenched solid cylinders.

A year later, Landau and Zwicky [18] studied the various factors affecting residual stresses in quenched cylinders. They used the same analogy of phase transformation and temperature change and found that "the length of transformation interval had a significant effect on the calculated stress near the cylinder centre, but much less effect on the values near the surface."

2.4.3 MECHANICAL TECHNIQUES

Residual compressive stresses may be induced by mechanical means. Several techniques have been used such as: (i) overloading, (ii) shot-peening and strain-peening, (iii) coining and (iv) dimpling.

(i) Overloading Techniques

Prior tensile overloading produces residual compressive stresses at sections with stress raisers such as notches, and leads to an improvement in fatigue strength only when the overload and the fatigue mean load are applied in the same direction. The effect of prior overloading on the resulting stress distribution in a typical notched part is illustrated by Heywood [19] as shown in Figure 2.3. The influence of prior overloads (preloads) on fatigue strength has been examined by several investigators and some of their results are given in Table 2.1.

Heywood [24] has shown that periodic overloads produce greater improvements in fatigue strength than single or repeated overloads prior to fatigue cycling. He found that the beneficial effect is smaller when the fatigue stresses are comparatively high. He attributed this reduction to the progressive loss or "fading" of residual stresses during the fatigue test. However, the fading effect was counteracted by periodic overloading to restore the original level of residual stress. Alternatively, fatigue cracks may form during the early stages of a fatigue test, and the subsequent application of a high load might produce residual stresses at the crack extremities, thus preventing or retarding further progression.

Vitovec[25] investigated the effect of prestraining of notched and unnotched specimens made of different materials on their fatigue resistance. He found the effect of strain hardening to be of secondary importance compared to the effect of residual stress. He also indicated that, at high prestress levels, cracks were developed in some cases along

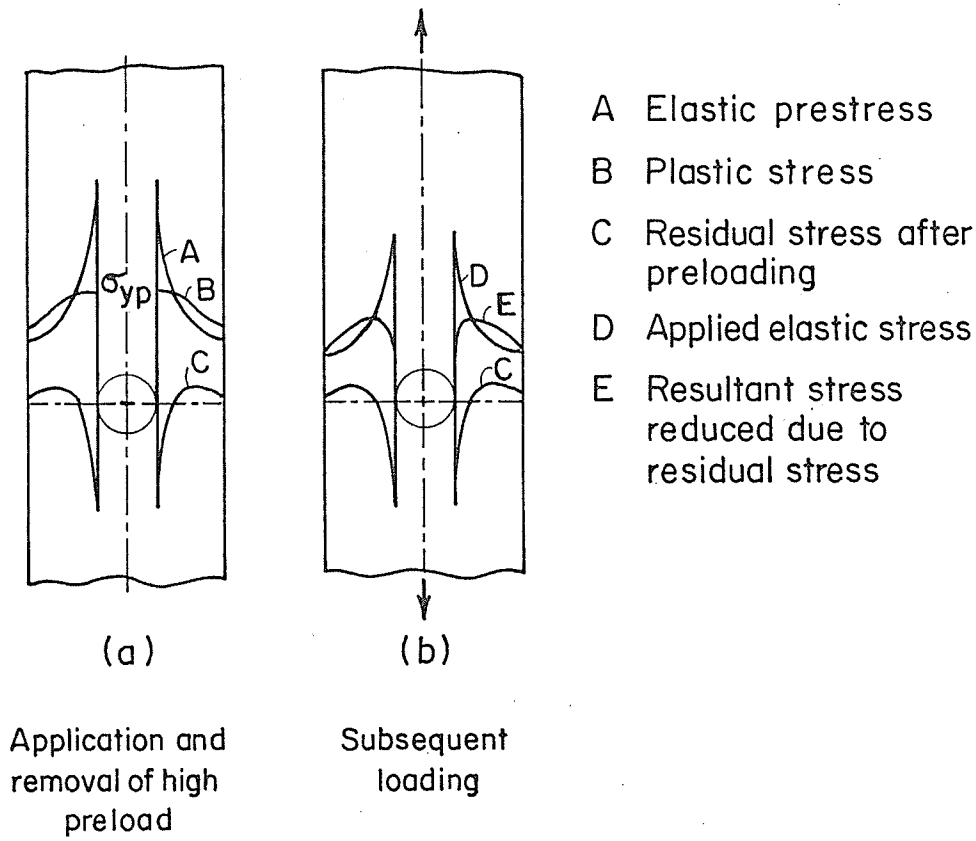

Figure 2.3 Diagrammatic illustration of the axial stress distribution due to preloading at the minimum section of a specimen with central hole [19].

Table 2.1 Fatigue Strength Improvement by Preloading

Preload level	Specimen & material	Fatigue strength improvement at 10 Mc.	Remarks	Ref. NO.
0.1 % proof stress	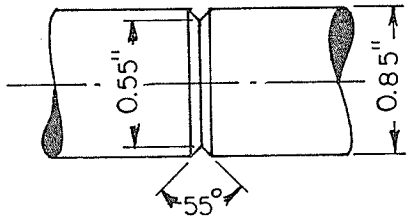 Round bars	Mild steel 55 % Carbon steel 45 % Nickel steel 55 % Aluminum alloys 85 % Rotating bending	As compared to stress relieved specimens	20
0.63 σ_{yp} 1.0 σ_{yp} 1.2 σ_{yp}	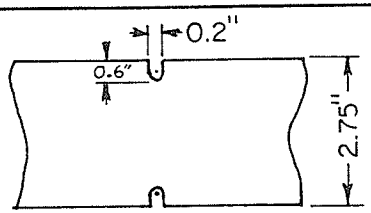 0.19% C steel, 1/2" thickness	4 % 33% 11 % Reverse bending	All figures determined by extrapolation.	4
0.83 σ_{yp} 1.15 σ_{yp}	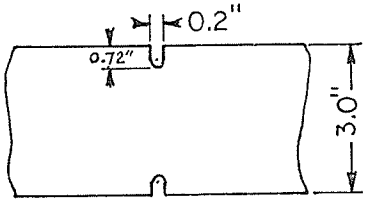 61S aluminum alloy, 0.353" thick.	Insignificant improvement. $>10\%$ Reverse bending	Specimens stress relieved after machining.	21

Table 2.1 (continued)

Preload level	Specimen & material	Fatigue strength improvement at 10 Mc.	Remarks	Ref. NO.
Sp = - 1.0 Sp = - 0.75 Sp = + 0.75 Sp = 1.00 Sp = 1.34	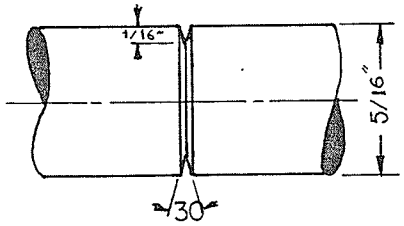 7075-T6 aluminum alloy bars.	- 53 % - 47 % + 12 % 59 % 124 % Rotating bending	Sp is defined as the nominal prestress divided by the ultimate tensile strength of the material.	22
1.0 σ_{yp}	Medium carbon steel S25C plain specimen without notch.	~ 5 % Reverse bending	Improvent is due to strain hardening.	23
0.8 σ_{yp}	Materials: a. 61S-T (hard) b. 61S-T (soft) 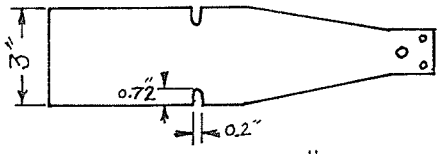 3/8" thickness	a. Reverse bending 33 % Pulsating bending 31 % b. No appreciable improvement.	In soft material fading of residual stress occurs in the first few cycles.	12

the circumference of the root of the notch, but due to the high compressive residual stress acting on the crack the fatigue strength, apparently, was not affected. He also concluded that "the volume of material in which the critical residual stress occurs seems to affect significantly the relaxation mechanism and thus influences the effect of residual stress on fatigue behaviour."

(ii) Shot-peening and Strain-peening

Shot peening is one of the most effective and widely used techniques to improve fatigue strength by inducing residual compressive stresses. It is accomplished by impinging the surface with round shot which is directed on to the work at high velocity by means of an air blast or centrifugal wheel. Surface residual compressive stresses due to shot peening range from 60 to 150 ksi, depending on the conditions of peening and the materials being treated.

Taira and Murakami [23] conducted fatigue tests on shot peened medium carbon steel. In their analysis, they define the factors affecting fatigue strength as the work hardening at and near the surface and the favourable residual stress, on one hand, and the indentation produced by shot impact as a notch effect, on the other hand. However, the combined effect amounts to an improvement in the fatigue limit of about 26 percent of which only 62 percent or less was contributed by residual compressive stress of approximately 46 kg/mm^2 (65 ksi).

In 1968, Esquivel and Evans [26] investigated the residual stress distribution in shot peened AISI 4130 steel. They found that residual

compressive stresses were produced in a thin layer of 0.014-in. deep and exhibit a small negative stress gradient at the surface. Subsequent fatigue cycling reduced the magnitude of residual compression at the surface from 90 ksi to approximately 60 ksi after 100 kilocycles. They suggest that "a direct correlation exists between residual stress relaxation at the surface and the residual stress gradient."

In 1973, Bogs and Byrne [27] studied the stability of residual stresses in shot peened alloys. They observed that residual stresses were stable in low stacking fault energy alloys while decay was observed in high stacking fault energy alloys. This was attributed to the greater ease of dislocation motion particularly as the cyclic stress exceeded the yield stress of the material.

Strain peening, shot peening of a surface of a specimen while it is under tensile strain, was first recommended by Straub and May [28]. This treatment results in higher residual compressive stress at the surface and is more beneficial in fatigue strengthening. Fuchs [29] indicates a residual stress of 130 percent over shot peening for steel specimens peened under 0.54 percent strain. Mattson and Roberts [30] studied the fatigue strength improvement caused by strain peening and reported an additional fatigue strength improvement of up to 50 percent.

(iii) Coining Techniques

Coining is a mechanical method for inducing residual compressive stresses by compression yielding of the material. In 1961, Phillips [31] proposed coining as a means of significantly improving fatigue life of

structural components without adding additional weight and without necessitating major design changes. In Phillips' experiments, coining was done by pressing a concentric groove around the opening to be protected. He observed that there is an optimum groove depth and location for greatest gatigue improvement. Deeper grooves may cause internal shear cracking and, subsequently, a loss of the fatigue strength. No influence was found of delay in testing of coined specimens.

Two years later, Whaley [32] examined the effect of various techniques of coining using conical and ring shaped dies. Experiments conducted on 7075-T651 aluminum alloy specimens confirmed the results of Phillips and further indicated the superiority of coining both sides of the specimen. He found that fatigue life increased rapidly with increasing depth of penetration of a ring type die but tended to reach an optimum when the initiation of the crack moved from the coined area to the edge of the plate. This trend is illustrated in Figure 2.4.

In 1964, Kasgard et al. [33] conducted an exploratory study on optimizing the coining technique. They obtained measurements of the residual stress distribution for different coining loads and coining ring diameters. They defined the optimum coining as that which has a residual stress level such that the resultant stress at the hole edge would be reduced to the nominal stress of the specimen. Their analysis was supplemented by favourable fatigue testing results.

Later in 1970, Speakman [34] reported the development of new coining techniques known as: radius stress coining, pad stress coining and stress coin hole expansion. These techniques are illustrated in Figure 2.5.

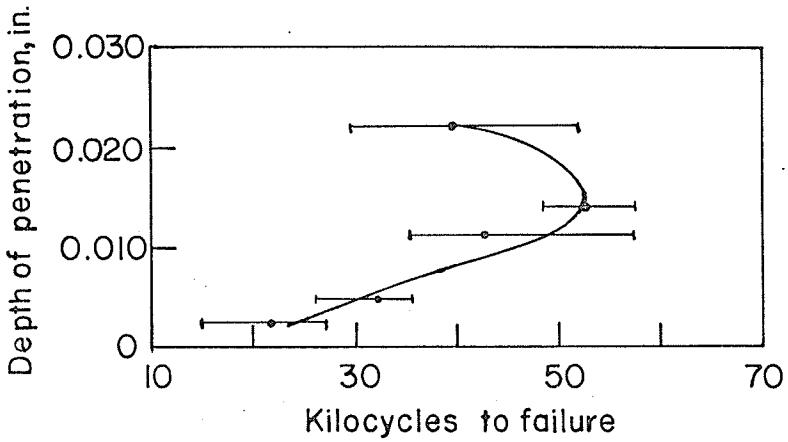

Figure 2.4 Variation in fatigue life with depth of penetration of a ring die[32].

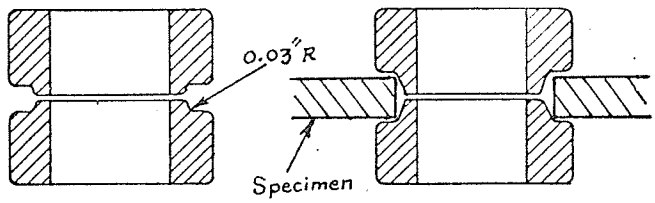

Type A
For Material Thickness .090 To .190

Type B
For Material Thickness .190 and Thicker

a. Radius coin dies for holes 1/2" diameter and larger.

b. Round hole pad coining dies.

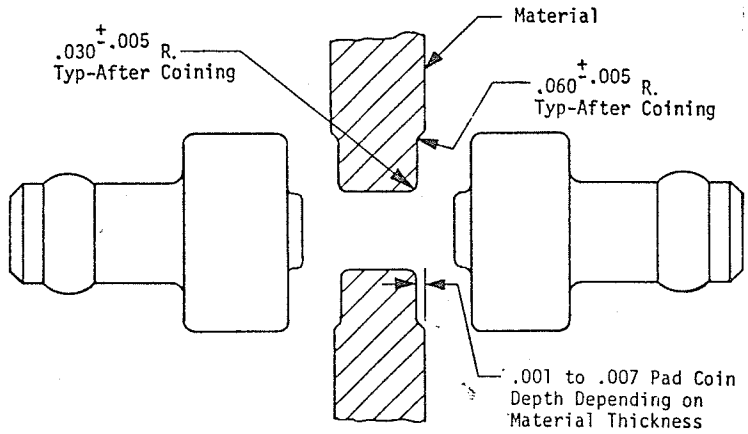

C. STRESS COINING HOLES - EXPANSION PIN

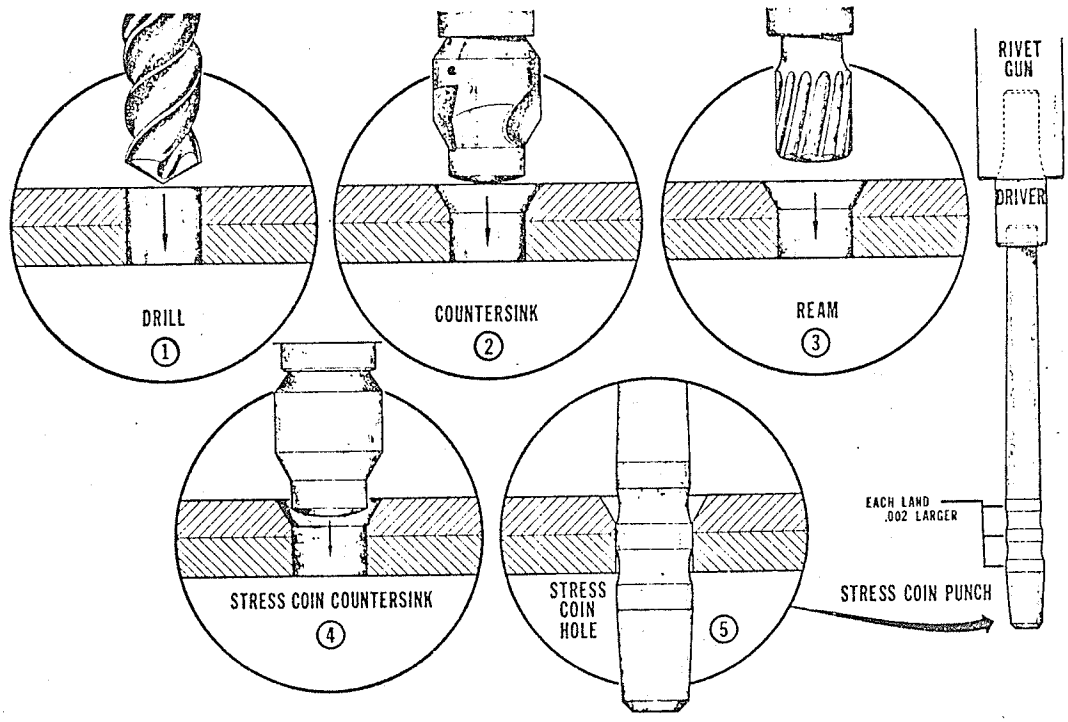

Figure 2.5 Coining techniques developed by Speakman [3]

The first technique cold works a highly polished 0.030-in. radius around the edges of the stress concentrator, while the second is completed by forming an impression, approximately 0.004-in. deep, in the surface material surrounding the hole or slot. Both techniques are adequate for thicknesses of up to 0.182 in. (4.6 mm.). In thicker materials of up to 5 in., the third technique is used for additional treatment for the holes in which they are expanded to size by a lubricated expanding pin. These coining techniques are shown to improve the fatigue life of test specimens for various aricraft materials by a factor of approximately four.

Smith [35] suggested that if it were possible to have a combination of coining and interference fit, a subsequent increase in fatigue resistance could be obtained. Although there is no experimental evidence of this benefit, coining has been used in conjunction with low interference fits only for practical reasons [3].

It should be mentioned that Phillips [31] conducted comparative fatigue tests on specimens which were v-notched and edge-roll coined versus uncoined specimens. His results are reproduced in Table 2.2. To the author's knowledge, no further work on edge coining has been conducted since then except for some practical applications as indicated by Speakman [36].

(iv) Dimpling Technique

Dimpling is a mechanical method for creating residual compressive stress by bulge-stretching and subsequent flattening of sheet material.

Table 2.2

Fatigue Testing Results of 7075-T6 Aluminum Alloy,

Edge Roll Grooved and V-Notched Specimens [31]

Axial Tension Fatigue R = +0.2

Material Thickness	Groove Condition	V-notched before or after grooving	Maximum Stress, Ksi	Life ratio*
.102" Bare	one side	before	20	>7
.102" Bare	one side	after	20	>20
.102" Bare	both sides	before	25	>450
.062" Alclad	one side	before	20	>84
.062" Alclad	both sides	before	20	>82

* Life ratio of grooved to ungrooved.

Although a form of dimpling has been used in association with riveted connections [6], the intent was at permitting one flat surface in a thin plate lap joint using flat head rivets. Recently, Shewchuk and Roberts [37] developed a new method called dimpling for creating favourable residual compressive stresses in the vicinity of loaded holes. The technique, as shown in Figure 2.6, consists of dimpling the material centering about the intended hole location, thus producing tensile plastic strain. The dimple is then flattened and the hole drilled so that the region around the hole is in residual compression. They conducted experiments on 2024-T3 aluminum alloy specimens which indicated that the fatigue strength of loaded holes improved by a factor of nearly three at one million cycles to failure. The corresponding residual stress was measured to be close to -27 ksi or approximately 60 percent of the yield strength of the material.

Shewchuk [38] investigated the effect of dimpling on the fatigue strength of unloaded holes. His experiments on 0.050-in. (1.27 mm) thick 2024-T3 alclad aluminum alloy specimens show that the fatigue strength reduction factor is reduced by dimpling by 36 percent for one million cycles to failure.

In 1976, Kuc and Shewchuk [39] reported on the effects of combined concentric dimpling and interference fits on the fatigue strength of loaded holes. Their experiments, on 2024-T3 aluminum alloy specimens, indicate considerable improvements due to the unloading effect of interference in addition to the residual compression induced by concentric dimpling.

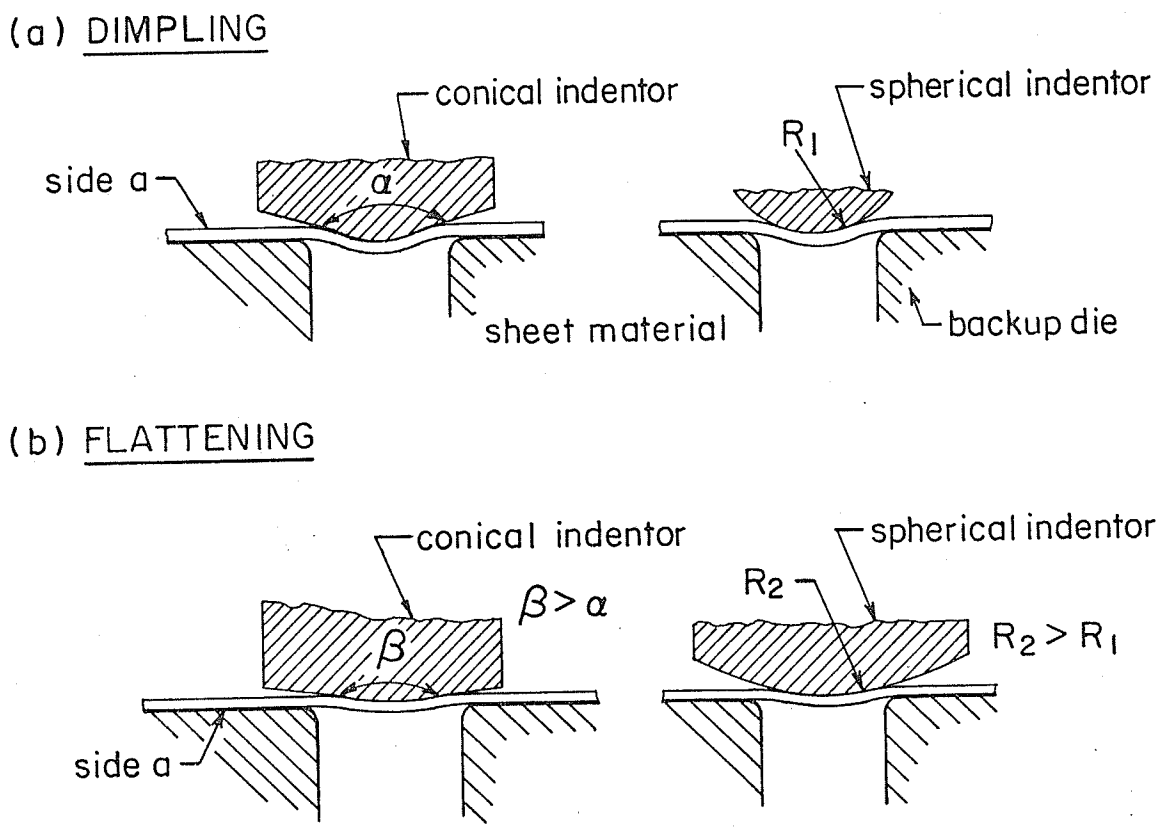

Figure 2·6 Concentric dimpling developed by Shewchuk and Roberts [37]

2.5 SUMMARY

It has generally been recognized that residual compression exerts a favourable influence on fatigue strength while residual tension has a detrimental effect. Residual stresses may result as a by-product of manufacturing operations or may intentionally be induced by several methods. These methods may be classified as: thermal, metallurgical and mechanical. Thermal techniques usually overlap with metallurgical techniques as thermal effects may induce microstructural changes. Mechanical techniques are, in fact, the most desirable as they are capable of inducing residual compression in a larger volume of the material. Dimpling of sheet material appears to be the most effective mechanical method due to the deep residual compressive stresses. The overloading technique provides a simple method of studying the effects of residual stress on fatigue behaviour of materials. It has been found from the survey that edge treatment of plate material has not been given adequate consideration as a potential technique for improving fatigue strength. Therefore, a new technique for fatigue strength improvement by edge treatment will be described in the following chapter.

CHAPTER 3

FATIGUE STRENGTH IMPROVEMENT BY EDGE TREATMENT

3.1 INTRODUCTION

Fatigue strength of plates may be enhanced by placing the edge region into a state of residual compression. In this chapter, a new method of edge treatment, in which residual stresses are mechanically induced in a limited portion of the free edge, is considered. This method, called "edge dimpling," is described and the various parameters of the method are defined and related to the residual stress.

3.2 THE EDGE DIMPLING TECHNIQUE

3.2.1 DESCRIPTION

Edge dimpling is a mechanical method of producing a controllable gradient of residual stress in a finite length of the free edge of sheet metallic materials. The procedure of edge dimpling is illustrated in Figure 3.1. It consists of firmly clamping the plate around the area to be treated to restrict slip during subsequent dimpling, as shown in Figure 3.1(a). Then the area is "dimpled" or stretched by moving the ram to a precalculated depth resulting in the dimple as shown in Figure 3.1(b). Finally, the dimple is flattened to its original flat shape provided that the flattening ram moves a distinct distance beyond the initial position to compensate for the elastic springback, as illustrated in Figures 3.1(c) and (d). The resulting stress distribution, in

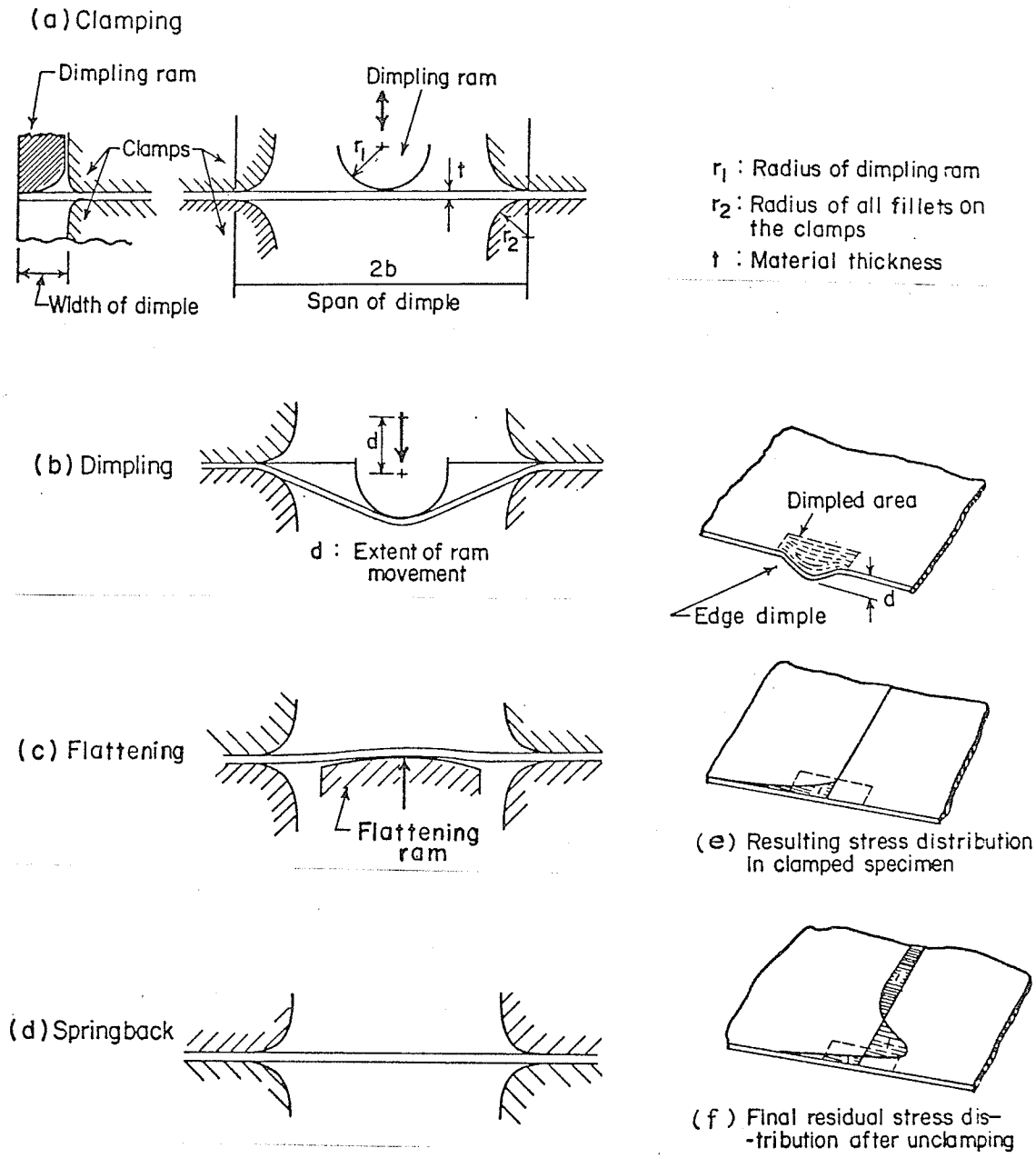

Figure 3.1 Edge dimpling process and resulting residual compressive stresses.

the clamped state, as shown in Figure 3.1(e), is referred to as the maximum possible residual stress and will be denoted by MPRS. It is a function of the various dimpling parameters which will be defined in Sec. 3.2.2. When the clamps are released, the residual stress partly relaxes and redistributes in the nature shown in Figure 3.1(f). The amount of relaxation, for a given material, is a function of the shape and dimensions of the undimpled region of the plate as compared to those of the dimpled region.

The process of edge dimpling is accompanied by a secondary effect of bending which is undesirable for two reasons:

1. The plastic strain, and consequently the stress, throughout the thickness will be non-uniform. This requires three dimensional stress analysis and, as a result, the determination of residual stresses becomes more complicated.
2. The effective value of residual stress, which is the minimum value of the distribution throughout the thickness, will be lowered. Hence, a lower fatigue strength improvement will have to be expected. This effect becomes more pronounced as the material thickness increases.

The effect of bending may qualitatively be illustrated by considering an elemental strip along the edge of the dimple area, as shown in Figure 3.2. For this qualitative illustration the Bauschinger effect will be neglected. Subscripts 0, 1, and 2 designate edge points on the neutral axis, the concave side in contact with the ram and the convex side of the specimen respectively. The strain distribution due to bending

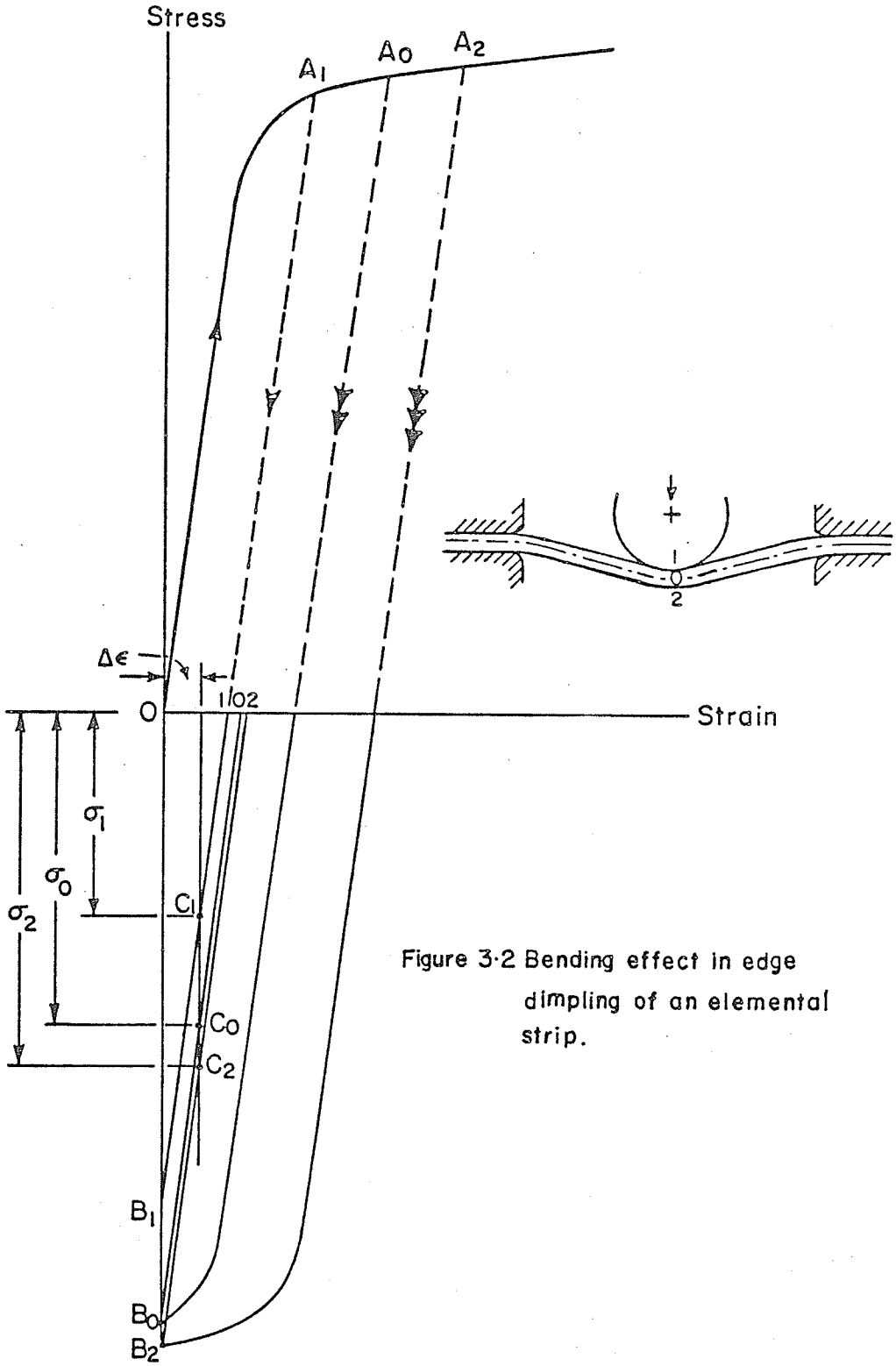

Figure 3·2 Bending effect in edge dimpling of an elemental strip.

is superimposed on the uniform stretch of the element. Therefore, points A0, A1, and A2 on the stress strain curve define the state of stress and strain after stretching. Subsequent flattening yields the state given by points B0, B1, and B2 which give the values of the MPRS at points 0, 1, and 2, respectively. The final state of stress after unclamping is determined by the amount of relaxation at each point due to elastic springback. For uniform relaxation throught the thickness, $\Delta\varepsilon$, the final state of residual stress is determined by points C0, C1, and C2. It can be seen that the effective value of residual compression, given by σ_1, is considerably lower than σ_0 and σ_2. It can also be seen that if the relaxation strain increases, the effective value of residual stress drops rapidly, and greater relaxation may result in residual tension at the concave side of the dimple. In the latter case the effect will be detrimental to fatigue strengthening.

The effect of bending decreases gradually as the amount of stretching increases. On the other hand, for small amounts of stretching, point 1 on the concave side may not experience any plasticity. Therefore, a situation of zero residual stress at one side and high residual compression on the other will cause the strip to bend to achieve a balance of stresses. This will greatly lower the effect of residual compression.

The bending effect may be made negligible by further dimpling the elemental strip in the opposite direction. This treatment is applicable to the whole edge dimple region as well and will be called the reversed edge dimpling procedure. This reversed procedure is illustrated in Figure 3.3 as applied to the elemental strip example. A point on the concave side during the first dimple will be on the convex side during

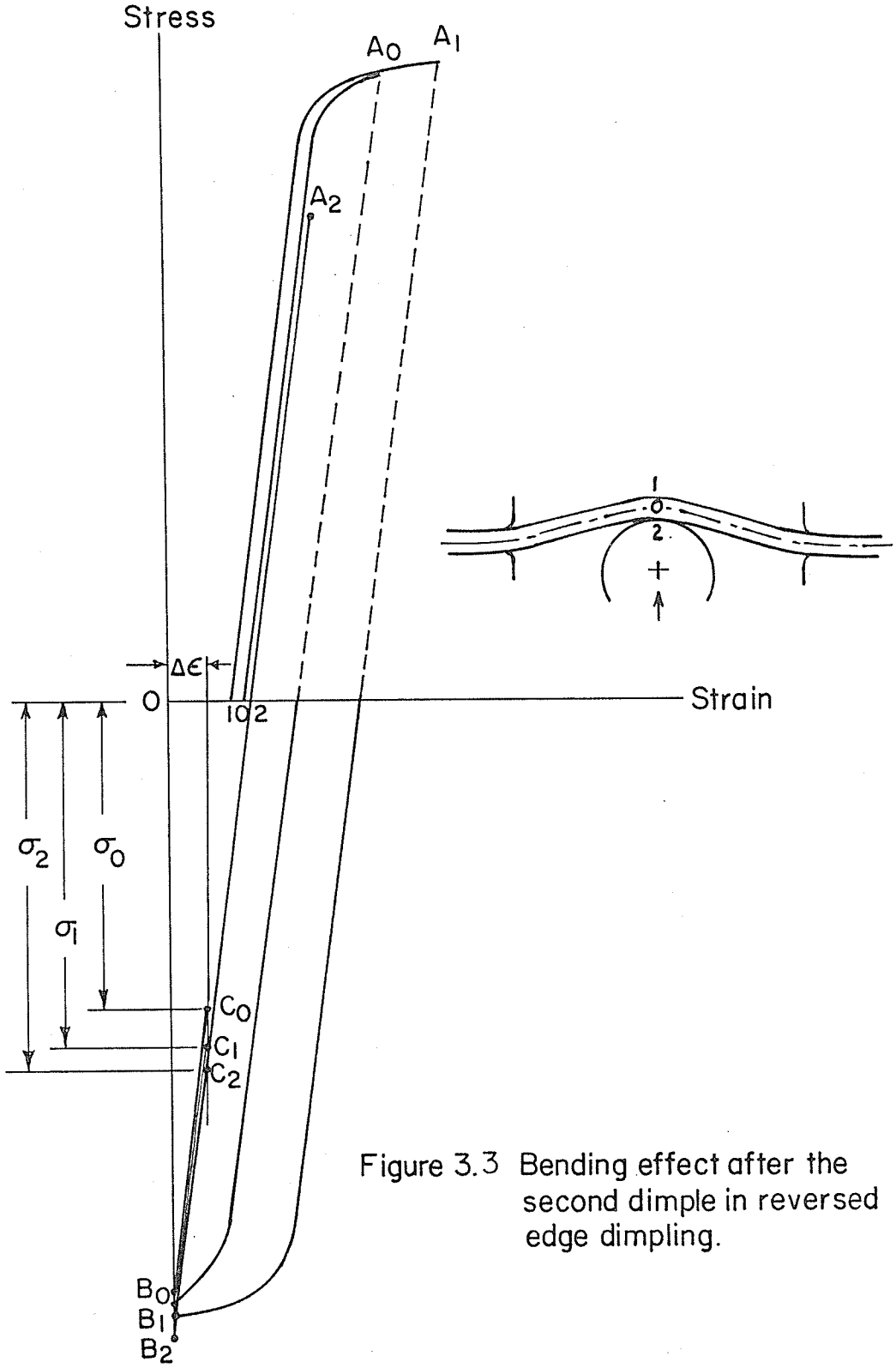

Figure 3.3 Bending effect after the second dimple in reversed edge dimpling.

the second dimple, and vice versa. The immediate result of the reversal of dimpling is to raise the lowest residual stress σ_1 to a value closer to σ_0 and σ_2 thus ensuring a higher effective residual compression and a more uniform residual stress distribution throught the thickness. It can be seen that the reversed edge dimpling procedure results in an effective residual stress which is closer to the mid-thickness residual stress. This is an advantage to the analysis as the mid-thickness residual stress may be used and the bending effects may, therefore, be neglected. Henceforth, the term edge dimpling will imply reversed edge dimpling.

3.2.2 DIMPLING APPARATUS

In order to perform the edge dimpling process described in the preceding section a special dimpling apparatus was designed and used. The dimpling apparatus is ullustrated in Figure 3.4. It consists of a base (1) on which the clamping jaws are constructed: a fixed jaw (2) and a movable jaw (3). The movable jaw may be tilted to permit the insertion of the specimen (4). The latter is located in position with an adjustable locator (5) and then clamped firmly by tightening the clamping screws (6). The apparatus is equipped with two contoured dimpling heads (7) that are replaceable. The heads are carried on a saddle (8) which is mounted on the dimpling ram (9). The ram slides in a T-slot cut in the base of the apparatus. The ram movement is performed with an operating handle (10) and the limits of the ram travel are controlled by two set-up screws (11) at both ends. The movement may also be monitored by an indicator and scale (12).

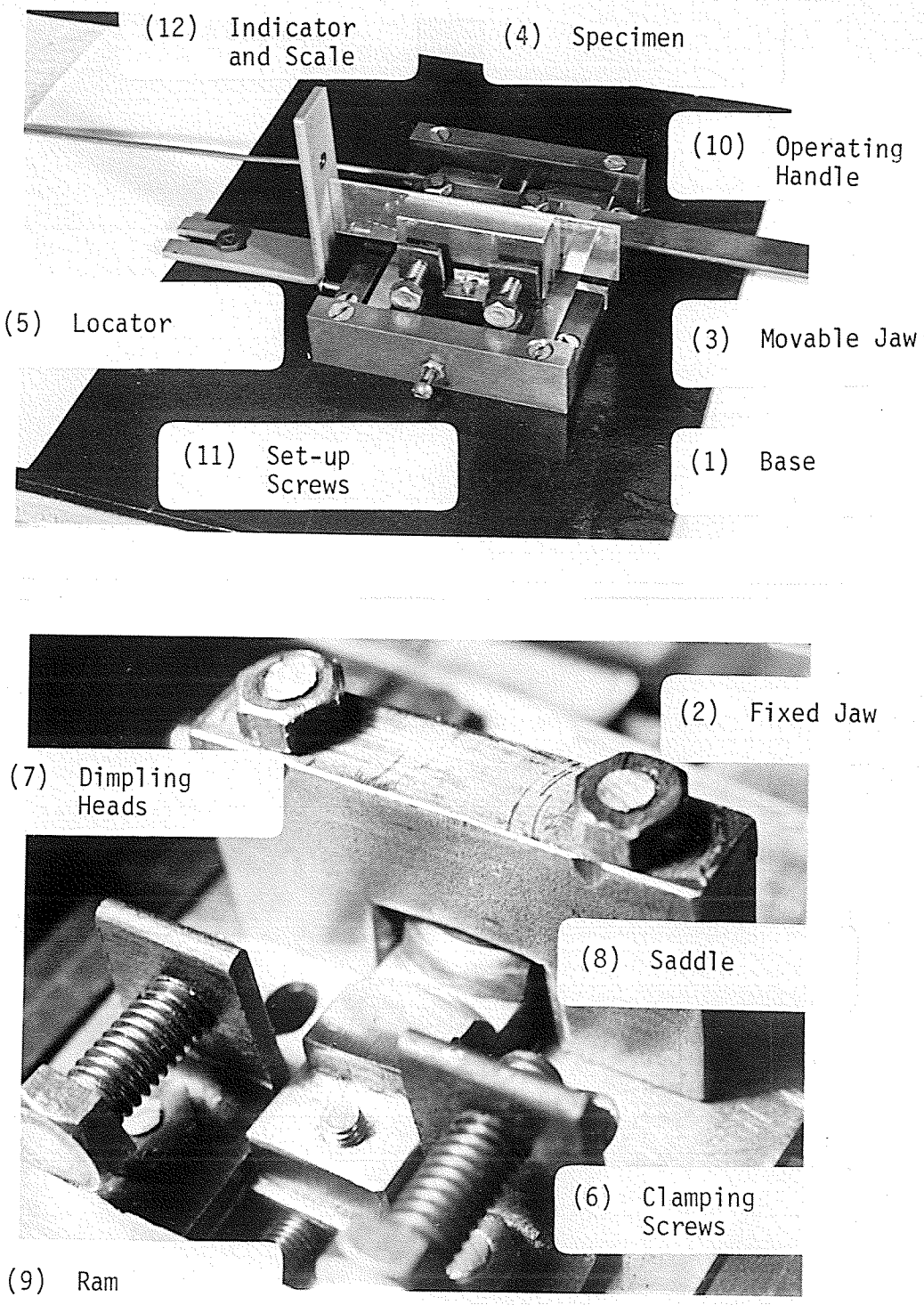

Figure 3.4 Edge Dimpling Apparatus

The steps of edge dimpling are illustrated in Figure 3.5 by a series of photographs which were taken after each step with the movable jaw removed.

3.2.3 DIMPLING PARAMETERS

The residual stress induced by edge dimpling is determined by two major factors. The first is the geometry of the dimpling apparatus and the extent of dimpling which determine the state of residual stress in a clamped specimen, i.e., the MPRS. The second is the amount of relaxation and redistribution of stress which takes place upon unclamping the specimen. This is a function of the relative shape and dimensions of the dimple area and the surrounding material that act as a constraint for relaxation of residual stresses. If the MPRS distribution in the dimpled area is known it is possible to determine the final residual stresses for a given geometry and dimensions. In this section the various parameters which characterize the edge dimpling procedure and determine the MPRS will be defined and the constituent relations of edge dimpling will be determined.

The basic non-dimensional parameters are defined as follows:

i. The dimpling-thickness ratio, R_t, which is the ratio of the extent of ram movement, d, to the material thickness, t;

$$R_t = d/t \qquad 3.1$$

ii. The dimpling-span ratio, R_b, which is the ratio of the extent of ram movment, d, to the span of the dimple area, 2b;

$$R_b = d/2b \qquad 3.2$$

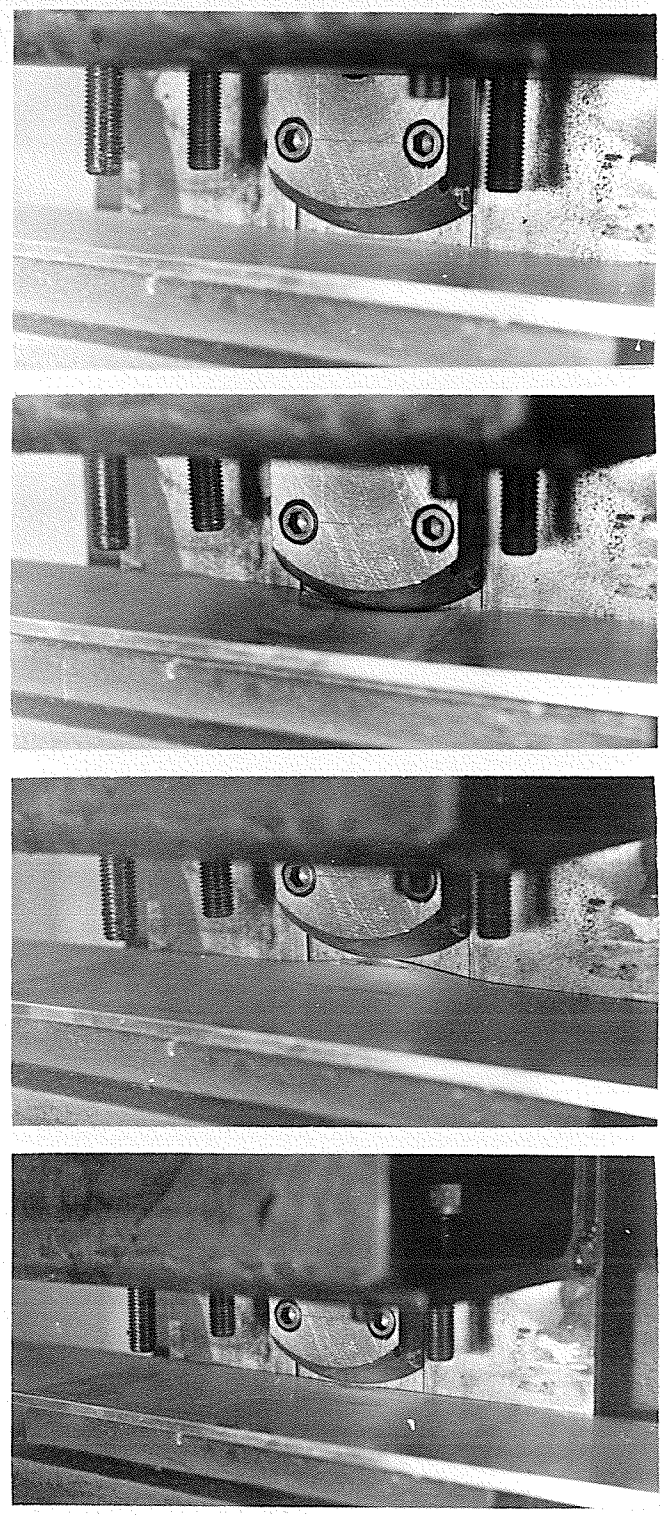

a. Specimen set-up in the apparatus.

b. First dimple.

c. Reversed dimple.

d. Specimen after straightening.

Figure 3.5 Illustration of the steps of edge dimpling.

Therefore, the two dimpling ratios are related by

$$R_t = (2b/t).R_b \qquad 3.3$$

iii. The dimpling constant, K, which relates the dimensions of the dimpling apparatus and the material thickness;

$$K = (r_1 + r_2 + t)/2b \qquad 3.4$$

where, r_1 is the radius of dimpling ram, and

r_2 is the radius of all fillets of the clamping jaws.

iv. The average (mid-thickness) edge strain, $\bar{\varepsilon}_e$; which is the maximum strain of the edge after stretching. It is a geometric parameter independent of the material properties.

The average edge strain may be determined in terms of the other parameters as follows. With reference to Figure 3.6, the mid-thickness length of half span, b, becomes b + Δb after stretching. That is

$$\begin{aligned} b + \Delta b &= \widehat{AB} + \overline{BC} + \widehat{CD} \\ &= [(r_1 + t/2).\theta] \\ &\quad + [b.\sec\theta - (r_1 + r_2 + t).\tan\theta] \\ &\quad + [(r_2 + t/2).\theta] \\ &= b.\sec\theta + (r_1 + r_2 + t).(\theta - \tan\theta) \qquad 3.5 \end{aligned}$$

Therefore, the average strain over b will be

$$\bar{\varepsilon}_e = \Delta b/b = (\sec\theta - 1) + [(r_1 + r_2 + t)/b].(\theta - \tan\theta) \qquad 3.6$$

Substituting K from Equation 3.4 into Equation 3.6:

$$\bar{\varepsilon}_e = (\sec\theta - 1) + 2\,K\,(\theta - \tan\theta) \qquad 3.7$$

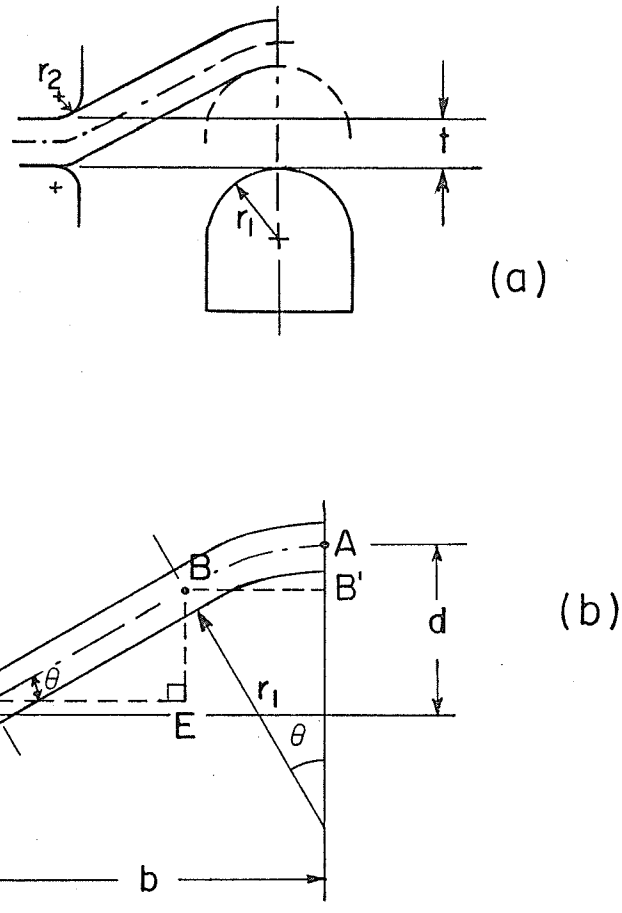

Figure 3.6 Geometry of edge dimple

Now, the angle θ may be found in terms of the dimpling parameters as follows:

$$
\begin{aligned}
d &= \overline{AB'} + \overline{BE} + \overline{C'D} \\
&= [(r_1 + t/2)(1 - \cos\theta)] \\
&\quad + [b.\tan\theta - (r_1 + r_2 + t).\sin\theta.\tan\theta] \\
&\quad + [(r_2 + t/2)(1 - \cos\theta)] \\
&= (r_1 + r_2 + t)(1 - \sec\theta) + b.\tan\theta \qquad 3.8
\end{aligned}
$$

Substituting Equation 3.8 into Equation 3.2, and using Equation 3.4, we obtain:

$$R_b = 1/2 \tan\theta - K.(\sec\theta - 1) \qquad 3.9$$

Therefore, the relation between the average edge strain and other dimpling parameters may be found from Equations 3.7 and 3.9. There is no simple relation between the dimpling parameters except for the case when $K \to 0$. In this case the span of dimpling becomes much greater than the other dimensions and Equations 3.7 and 3.9 may be reduced to one equation

$$\overline{\varepsilon}_e = \sqrt{1 + 4 R_b^2} - 1 \qquad 3.10$$

Substituting for values of θ in Equation 3.7 and 3.9 the relations between $\overline{\varepsilon}_e$ and R_b are determined for different values of K as plotted in Figure 3.7. It is evident that for a given dimpling ratio, the average edge strain is determined by the dimpling constant K regardless of the specific dimensions of the dimpling apparatus. Although a smaller dimpling constant means a smaller edge strain and subsequently a lower residual stress, it does indicate a lesser bending effect and, hence, assures

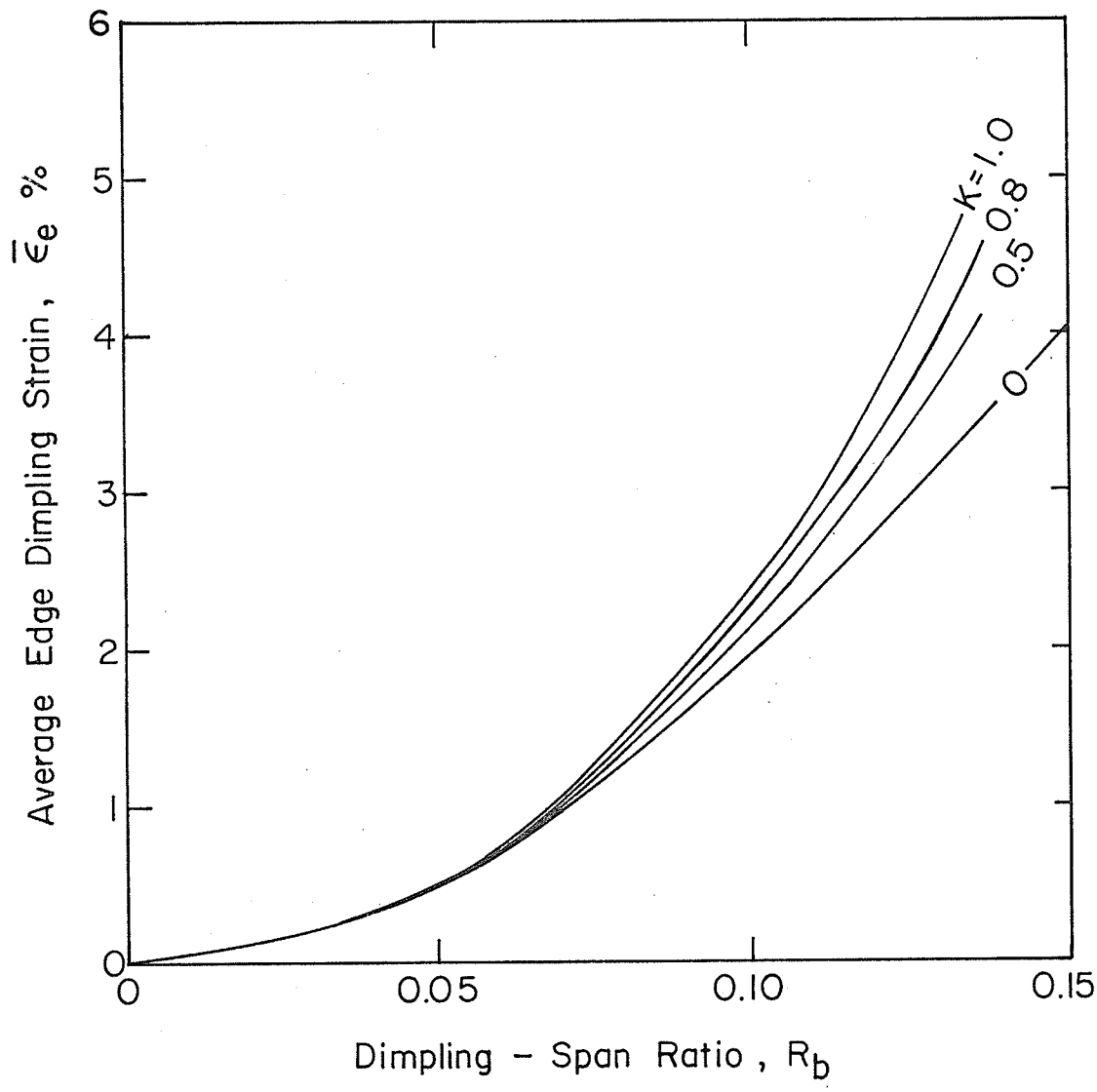

Figure 3.7 The average edge strain vs. dimpling ratio from various values of $0 \leq K \leq 1.0$

better uniformity of the final residual stresses. However, K cannot be reduced to zero because the aspect ratio 2b/t must always be kept below the critical ratio to buckling.

The average edge strain, $\bar{\varepsilon}_e$, is a characteristic edge dimpling parameter and is used in conjunction with the dimpling ram profile and material properties to determine the residual stresses induced by the process.

3.2.4 CHARACTERISTIC CURVE OF EDGE DIMPLING

The careful examination of the stress-strain relations of Figures 3.2 and 3.3 leads to the observation of a significant characteristic relation which exists between the average edge dimpling strain, $\bar{\varepsilon}$, and the MPRS or residual deformation of an elemental strip. This relation is illustrated in Figure 3.8. The relation varies within three characteristic regions. These are:

I. The elasticity region in which the dimpling strain does not exceed the yield strain and, hence, no residual stress is left in the material after dimpling.

II. The developing region in which the stress develops rapidly with increasing dimpling strain. This region exists for an average dimpling strain range from the yield strain up to approximately twice the yield strain. It is characterized by high sensitivity of stress to strain. A small change in strain will produce a large change in stress and, hence, lead to fatigue improvement with the inherent possibility of high scatter in the results.

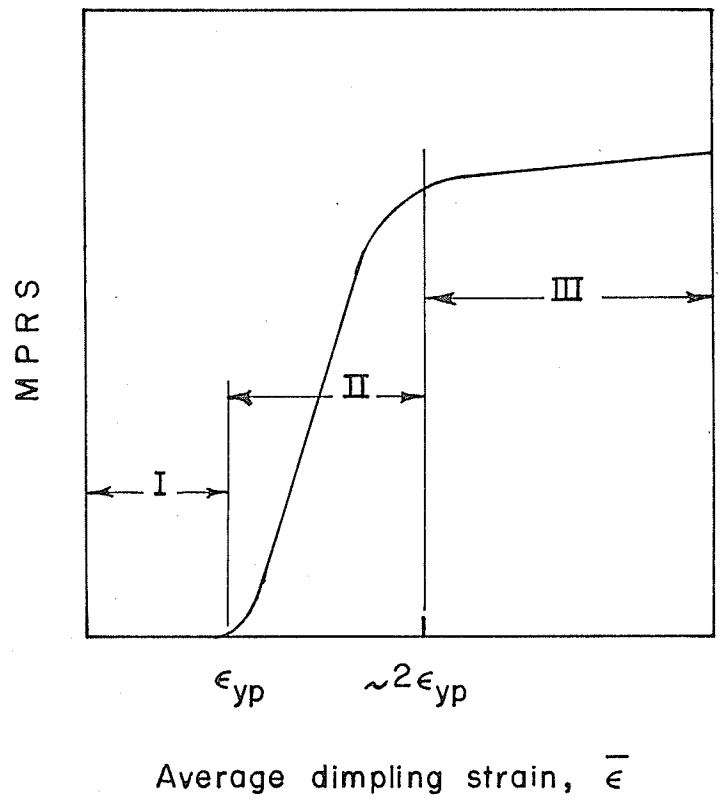

Figure 3.8 The characteristic dimpling curve.

THE UNIVERSITY OF MANITOBA LIBRARIES

III. The stability region in which the residual stress is stabilized at values close to the yield stress of the material. In other words, the permanent deformation will be close to the yield strain of the material. The residual stress will be relatively insensitive to dimpling strain variation as larger changes in $\bar{\varepsilon}$ become necessary to produce smaller changes in the stress. This presents a useful condition of maximum fatigue improvement with minimum scatter due to dimpling.

Therefore, the value of $\bar{\varepsilon}$ should always be in excess of twice the yield strain of the material, i.e., in the stability region. Although the characteristic curve should maintain a similar shape for all metals, it will have different slopes and inflection points depending on the shape of the stress-strain curve and the amount of Bauschinger effect that the material possesses at each strain value.

3.3 SUMMARY

The edge dimpling technique, as a method of edge treatment, is described. It consists of creating a misfit between a portion of the edge and the surrounding material, thus resulting in a residual compressive stress in the critical region to fatigue. The technique is capable of producing residual stresses which may be considered uniform throughout the material thickness. A specially designed apparatus is used to perform the edge dimpling procedure with variable parameters. It is found that there is a characteristic parameter which combines and relates the other geometric parameters of the technique. That is the average edge dimpling

strain. It must be maintained within the stability region to obtain a useful condition of maximum fatigue improvement with minimum scatter of results.

Before proceeding in the fatigue testing program it is desirable to determine the magnitude and distribution of the residual stress resulting from edge dimpling. Such information is necessary for the accurate assessment of the effect of edge dimpling on fatigue strength improvement. The analytic and experimental determination of residual stresses due to edge dimpling will be described in the following two chapters.

CHAPTER 4

ANALYTICAL DETERMINATION OF RESIDUAL STRESS DUE TO EDGE DIMPLING

4.1 INTRODUCTION

Timoshenko and Goodier [40] suggest that residual stresses may be obtained from the permanent plastic deformations of each element of the body. The general procedure assumes that the body is subdivided into a large number of small elements and that the permanent set for each is known. These deformations may be eliminated by applying certain body forces and surface tractions which satisfy the equations of equilibrium and the boundary conditions. By applying these forces the permanent set is removed so that the elements of the body fit one another and form a continuous body. It is then assumed that the elements of the body are joined together and the body and boundary forces are removed. Then evidently the initial stresses are obtained by superimposing the stresses prior to removal onto the stresses resulting from the removal of this system of imaginary forces. Thus, the problem is reduced to the usual system of equations of the theory of elasticity in which the magnitudes of the fictitious body and surface forces are completely determined if the permanent set is given.

There are two major difficulties that arise from this general procedure. These difficulties are associated with the determination of the permanent deformation and with the feasibility of the solution of the system of fictitious forces.

It is assumed that the permanent deformations for each of the elements are given, whereas, in most cases, due to the nature of the methods of setting up residual stresses, it is rather difficult, if not impossible, to determine such deformations analytically. This is particularly true for non-axisymmetric situations where the number of variables forms an insurmountable difficulty in the basic plasticity formulation of the problem, as indicated by Wang [41].

In case of edge dimpling it can be seen that the process involves stretching of the dimple area followed by flattening of the dimple shape. Both steps are accompanied by plastic bending in both longitudinal and transverse directions. If the permanent deformations are to be determined analytically two points, in addition to non-axial symmetry, have to be considered. The first is the friction forces acting on the contact surfaces which contribute to the residual stresses in the transverse and thickness directions. The second is the possibility of buckling during the flattening of the shell-type dimple. These factors lead to the exclusion of an analytical solution to the problem. However, it has been shown by Metha and Kobayashi [42] that numerical techniques such as the finite element may be employed to solve non-axisymmetric problems. The accuracy of the numerical solution depends on the number and nature of simplifying assumptions that have to be made and on the degree of complexity of shape, strain history, boundary conditions and the clear understanding of instability conditions.

Osadchuk [43] suggests that residual stresses may be determined starting from "certain a priori qualitative concepts with respect to the

character of the field of the residual deformations, while a quantitative description is found by comparison of the field of the residual stress, calculated on this basis, with the field of stresses obtained experimentally."

The method of solution used in the present work comprises the following:

- An approximate method to determine the distribution of residual deformation due to edge dimpling. Hence, the necessary fictitious forces to restore the original shape and dimensions of the dimple area may be determined.
- A numerical solution using the finite element method is used to determine the stresses resulting from the removal of that system of fictitious forces.
- The final state of residual stress is determined by superposing the solution of the stresses due to applying the fictitious forces to the large number of elemental strips onto the solution of stresses due to the removal of these forces which act on the entire body.

4.2 METHOD OF SOLUTION

4.2.1 ASSUMPTION OF FICTITIOUS FORCES

Imagine that the dimple area is separated from the whole plate leaving a space of the original dimensions. Furthermore, imagine that the dimple area is subdivided into a large number of free longitudinal elemental strips, as shown in Figure 4.1(a). Each strip undergoing the

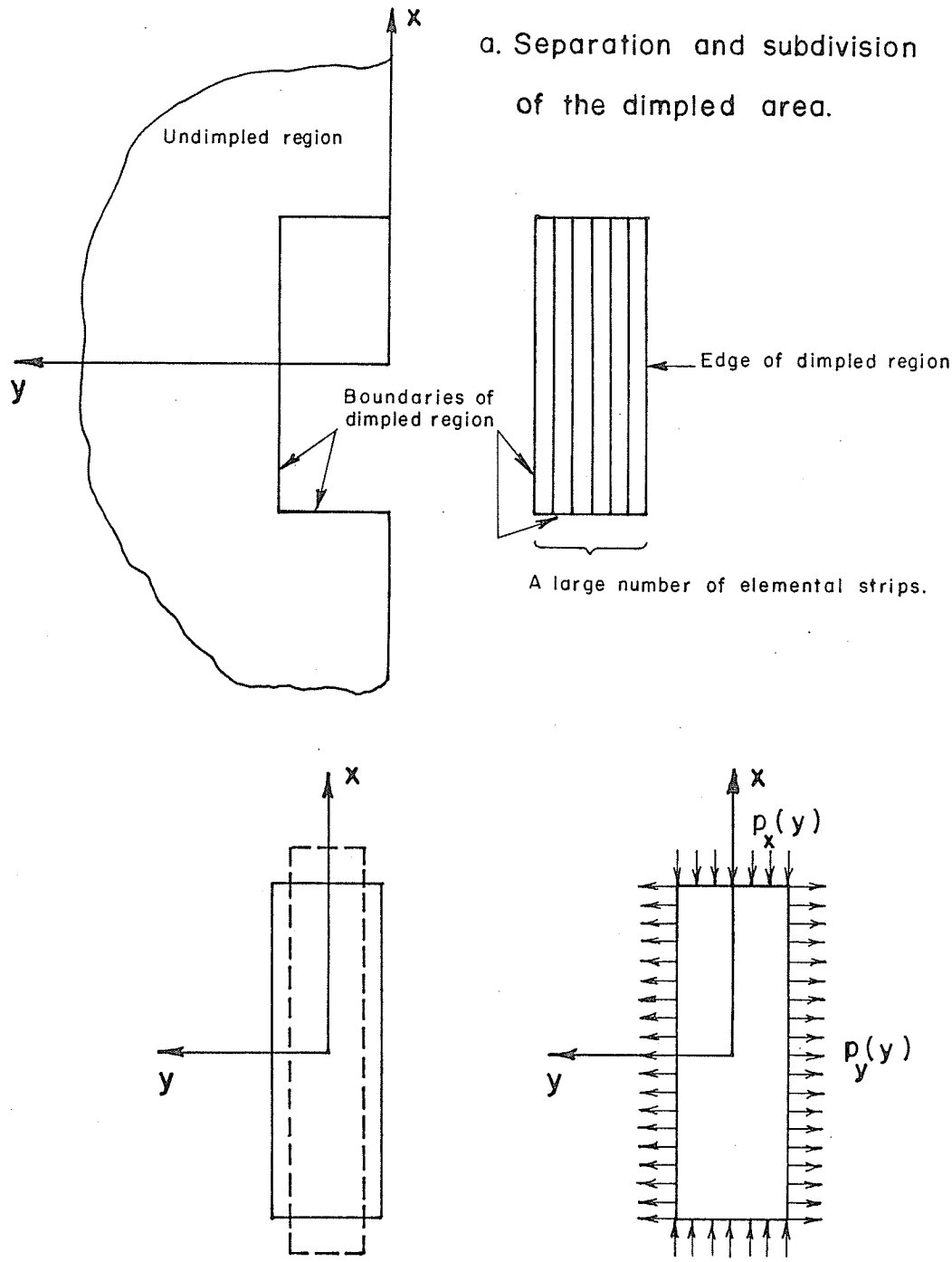

a. Separation and subdivision of the dimpled area.

b. Permanent deformation of an elemental strip $\epsilon_x^0(y)$, $\epsilon_y^0(y)$.

c. Applying boundary pressures $p_x(y)$, $p_y(y)$ to suppress the permanent set.

Figure 4.1 Subdivision of elemental strips.

dimpling process is assumed to have final dimensions as shown by the dotted line in Figure 4.1(b). Each elemental strip will have permanent strains $\varepsilon_x^0(y)$ and $\varepsilon_y^0(y)$ in the x- and y- directions, respectively. The amount of permanent deformations at any distance y depends on the dimpling head profile and the dimpling strain. Therefore, each element will have different dimensions and will not fit one another in the original space. It is sufficient to ensure fitting of the elements (in the original space of the dimple area) to suppress the deformation by applying the necessary boundary forces. This is to apply normal pressures p_x and p_y in the x- and y- directions, respectively, at the boundaries of the strip such that

$$\begin{aligned} p_x(y) &= -[E/(1-\nu^2)]\cdot[\varepsilon_x^0(y) + \nu\cdot\varepsilon_y^0(y)] \\ p_y(y) &= -[E/(1-\nu^2)]\cdot[\varepsilon_y^0(y) + \nu\cdot\varepsilon_x^0(y)] \end{aligned} \qquad 4.1$$

Equations 4.1 give the necessary boundary pressures to suppress the residual deformations of an elemental strip at any distance y from the edge.

The application of such pressures, as shown in Figure 4.1(c), will eliminate the planar residual deformations and ensure that the elemental strips may be joined together to form one integral body having the original dimensions of the dimpled area. At this point, it should be mentioned that the changes of thickness in the dimple region (thinning) will be neglected since the stresses in the direction of the thickness at the boundaries of the dimple region may be considered too small to influence the analysis. Note that these stresses (in the thickness direction) will predominate only around the boundaries of the dimpled region.

As $p_y(y)$ changes in the y- direction two adjacent elements will have two difference boundary pressures. When the elements are joined together a differential pressure will remain to act on the interfaces between each two elements. To satisfy the conditions of equilibrium as applied to the dimpled area this differential pressure gradient must have been created by an imaginary body force $B_y(y)$ per unit volume acting in the direction opposite to the boundary pressure at the edge and given by

$$B_y(y) = dp_y(y)/dy \qquad 4.2$$

The next step of the solution will be the determination of the permanent deformations $\varepsilon_x^0(y)$ and $\varepsilon_y^0(y)$ in terms of the various parameters of edge dimpling.

4.2.2 DISTRIBUTION OF RESIDUAL DEFORMATION

The permanent deformations of an elemental strip at a distance y from the edge of a plate undergoing edge dimpling are determined if the following are known:

a. The stress-strain curve of the material.

b. The Bauschinger effect of the material.

c. The amount of average dimpling strain.

It is often convenient to consider a bi-linear stress-strain relation [44], as shown in Figure 4.2, in which the stress up to the yield point is determined by

$$\sigma = E \cdot \varepsilon \qquad 4.3$$

where ε is the strain and E is the elasticity modulus of the material.

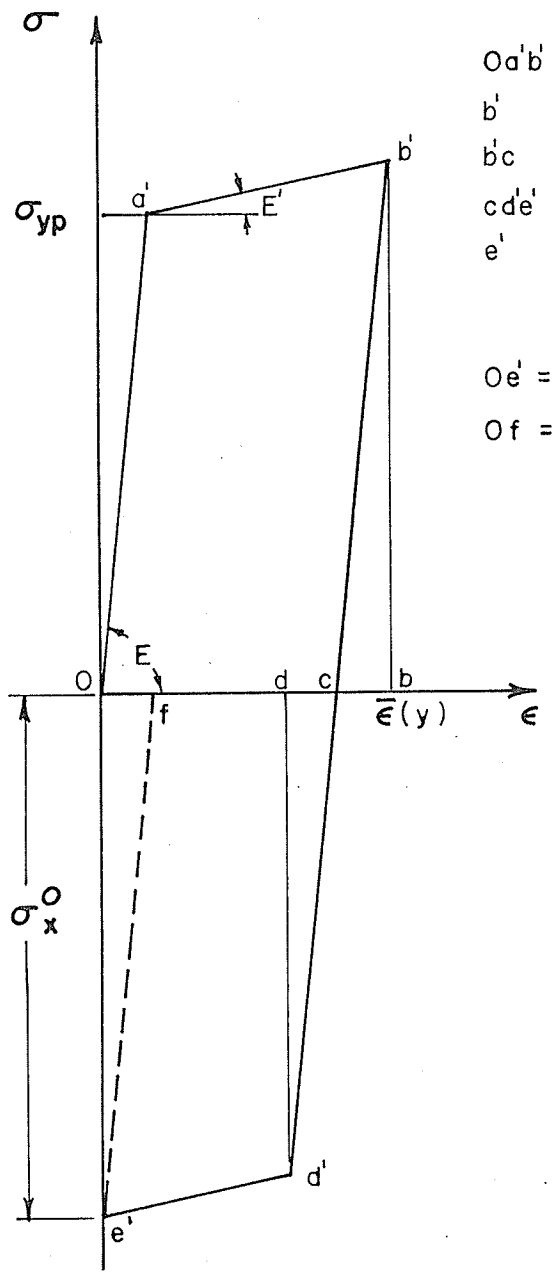

Oa'b' Stretching.

b' End of stretching.

b'c Release of stretching load.

cd'e' Compression to zero strain.

e' End of compression.

Oe' = MPRS

Of = Equivalent residual strain.

Figure 4.2 Edge dimpling procedure represented by idealized stress-strain relations.

Once the yield stress is exceeded the stress is determined by

$$\sigma = \sigma_{yp} + E' \cdot (\varepsilon - \varepsilon_{yp}) \qquad 4.4$$

where σ_{yp} and ε_{yp} are the yield strength and strain; respectively, and E' is a plastic modulus much smaller than the elastic modulus, E .

Due to the Bauschinger effect, the elastic strength in compression is lowered by a certain amount, usually depending on the strain prior to load reversal, $\bar{\varepsilon}$. The Bauschinger stress, σ_B , is defined as the difference between the forward yield strength, σ_F , and the absolute value of the reverse yield strength, σ_R [45]. Therefore, if the Bauschinger stress is known the reverse yield point can be calculated. This relation may be written

$$\sigma_B = \sigma_F - |\sigma_R| \qquad 4.5$$

This relation may be rearranged in the form

$$|\sigma_R| = (1 - \gamma) \cdot \sigma_F \qquad 4.6$$

where $\gamma = \sigma_B/\sigma_F$ is the Bauschinger effect parameter which is a function of $\bar{\varepsilon}$.

With reference to Figure 4.2 which represents the edge dimpling process, the MPRS in an elemental strip, and hence the permanent deformation, may be calculated in terms of $\bar{\varepsilon}$, γ and the material constants E , E' and σ_{yp}:

$$\sigma_x^0 = - E \cdot \varepsilon_x^0 = - |\sigma_{d'} + E' \cdot \overline{do}| \qquad 4.7$$

But using Equation 4.6:

$$|\sigma_{d'}| = (1 - \gamma) \cdot \sigma_{b'} \qquad 4.8$$

From Figure 4.2

$$\overline{do} = \bar{\varepsilon} - \overline{bd} = \bar{\varepsilon} - (1/E)\cdot(\sigma_{b'} + |\sigma_{d'}|) \qquad 4.9$$

Substituting Equation 4.8 into 4.9

$$\overline{do} = \bar{\varepsilon} - (1/E)\cdot(2 - \gamma)\cdot\sigma_{b'}. \qquad 4.10$$

Substituting Equations 4.8 and 4.10 into 4.7:

$$\sigma_x^0 = - E\cdot\varepsilon_x^0 = - |(1 - \gamma)\cdot\sigma_{b'} + E'\cdot\bar{\varepsilon} - (E'/E)\ (2 - \gamma)\cdot\sigma_{b'}|$$

$$= - |E'\cdot\bar{\varepsilon} + [(1-\gamma) - (E'/E)\cdot(2-\gamma)]\cdot\sigma_{b'}| \qquad 4.11$$

But

$$\sigma_{b'} = \sigma_{yp} + E'\cdot(\bar{\varepsilon} - \varepsilon_{yp}) \qquad 4.12$$

Therefore,

$$\sigma_x^0 = - E\cdot\varepsilon_x^0 = - |E'\cdot\bar{\varepsilon} + [(1-\gamma) - (E'/E)\cdot(2-\gamma)]\cdot$$

$$[\sigma_{yp} + E'\cdot(\bar{\varepsilon} - \varepsilon_{yp})]| \qquad 4.13$$

Equation 4.13 may be written in the form

$$\sigma_x^0 = - E\cdot\varepsilon_x^0 = - |[1-E'/E]\cdot[(1-\gamma) - (2-\gamma)\ (E'/E)]\cdot\sigma_{yp}$$

$$+ [1-E'/E]\cdot[2-\gamma]\cdot E'\cdot\bar{\varepsilon}| \qquad 4.14$$

and the residual deformation will be

$$\varepsilon_x^0 = [1-E'/E]\cdot[(1-\gamma) - (2-\gamma)\cdot(E'/E)]\cdot\varepsilon_{yp}$$

$$+ (E'/E)\cdot(1-E'/E)\cdot(2-\gamma)\cdot\bar{\varepsilon} \qquad 4.15$$

The expressions of Equation 4.14 or 4.15 may be evaluated for different values of γ and $\bar{\varepsilon}$ for a given material. It should be noted that these relations are only valid if $\bar{\varepsilon}$ is such that $\overline{do} \geq 0$, i.e., the MPRS in the strip is not less than $\sigma_{d'}$. Substituting $\sigma_x^0 = \sigma_{d'}$ in Equation 4.14 obtain the lower limit of $\bar{\varepsilon}$ to be

$$\bar{\varepsilon} \geq \frac{\sigma_{yp}}{E}\ \frac{(2-\gamma)(1-E'/E)}{1-(2-\gamma)(E'/E)} \qquad 4.16$$

For values of $\bar{\varepsilon} \leq \varepsilon_{yp}$ there will be no plastic deformation and, hence, no permanent set or residual stress. For the range of strain

$$\varepsilon_{yp} \leq \varepsilon \leq \frac{\sigma_{yp}}{E} \; \frac{(2-\gamma)(1-E'/E)}{1-(2-\gamma)(E'/E)} \qquad 4.17$$

and following the same procedure it can easily be shown that

$$\sigma_x^0 = - E \cdot \varepsilon_x^0 = - E(1-E'/E)(\bar{\varepsilon} - \varepsilon_{yp}) \qquad 4.18$$

and

$$\varepsilon_x^0 = (1-E'/E)\ (\bar{\varepsilon} - \varepsilon_{yp}) \qquad 4.19$$

Using Equations 4.14 through 4.19 the characteristic dimpling curve for 2024-T3 alclad aluminum alloy material may be determined as shown in Figure 4.3. The three regions of edge dimpling are designated by I, II and III. It appears that to gain high and reproducible residual stress the average dimpling strain must be in the third region, i.e., greater than approximately twice the yield strain. This limit is recommended for the average edge strain, $\bar{\varepsilon}_e$, as interior elements will have smaller dimpling strains. However, bearing in mind the shape of the actual stress-strain relation, the non-idealized characteristic curve would be curved at the points of slope change. This is shown by the dotted line in Figure 4.3. Therefore, the boundaries of the three regions of the characteristic curve are not exactly defined. In this case the average edge strain may be taken as a minimum of three times ε_{yp} to obtain stable residual stress at the edge. In the following analysis, the characteristic curve based on the idealized stress - strain relation will be used.

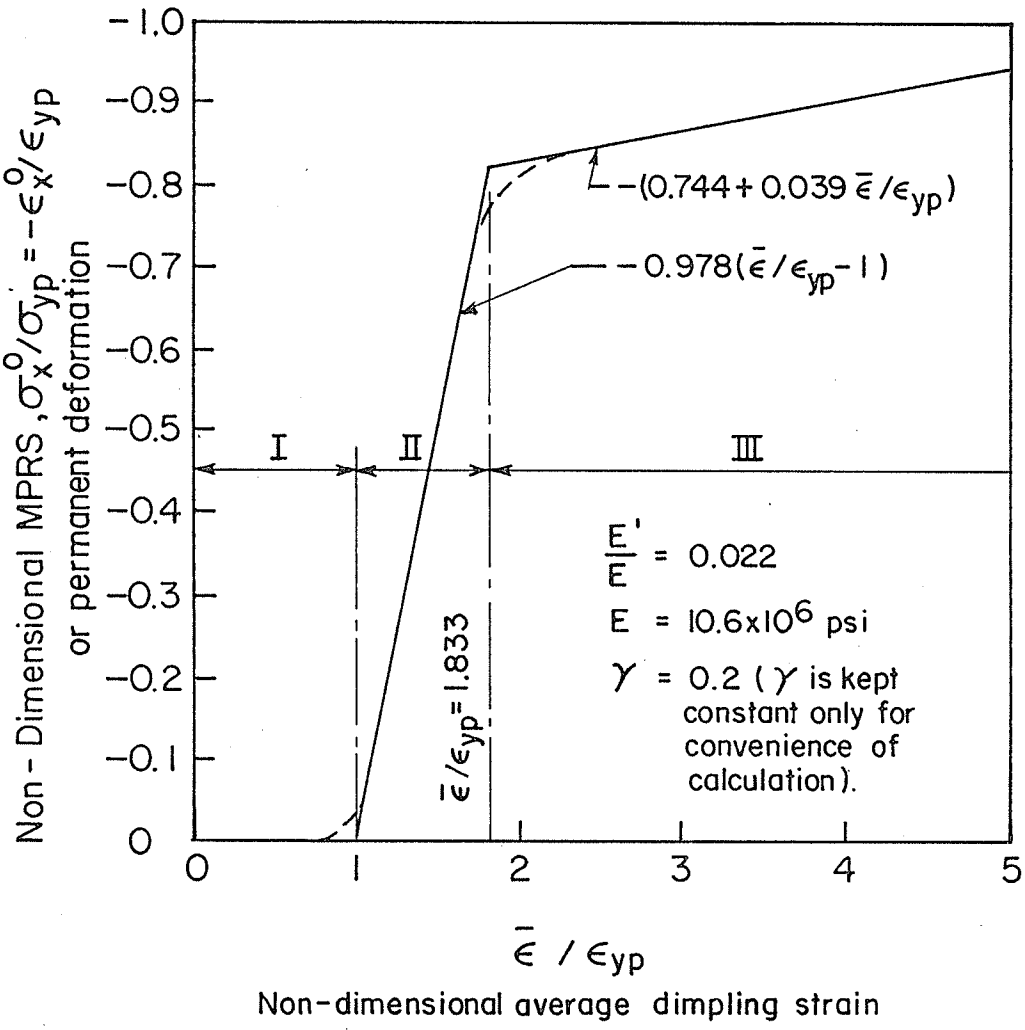

Figure 4.3 Characteristic curve of edge dimpling for 2024-T3 Aluminum Alloy material.

To calculate the permanent strain in the transverse direction of the elemental strip the total volume change due to dimpling has to be considered. Without details of the transverse strain history during dimpling of the strip, the final volume (as the element is left free from external forces causing any elastic strain) should be equal to the initial volume, i.e., the volume does not change. In terms of the principal strains this implies that the sum of residual strains in the longitudinal, transverse and thickness directions must vanish. Therefore,

$$\varepsilon_y^0 = -0.5\,\varepsilon_x^0 \qquad 4.20$$

The next step will be to determine the residual strain distribution in the dimple area. This requires knowledge of the profile of the dimpling head; shown in Figure 4.4. For any point at a distance y from the edge the dimpling depth, d, will be reduced as y increases until the contact between the dimpling head and the specimen is lost at a distance y_{max} determined from the geometry of Figure 4.4

$$y_{max} = \sqrt{r_3^2 - (r_3 - d)^2} \qquad 4.21$$

Therefore, the effective ram movement (the dimpling depth), d', at any distance $y < y_{max}$ will be given by

$$d'(y) = d - r_3\left(1 - \sqrt{1 - (y/r_3)^2}\right) \qquad 4.22$$

The dimpling-span ratio and the dimpling constant at any distance y are then given by

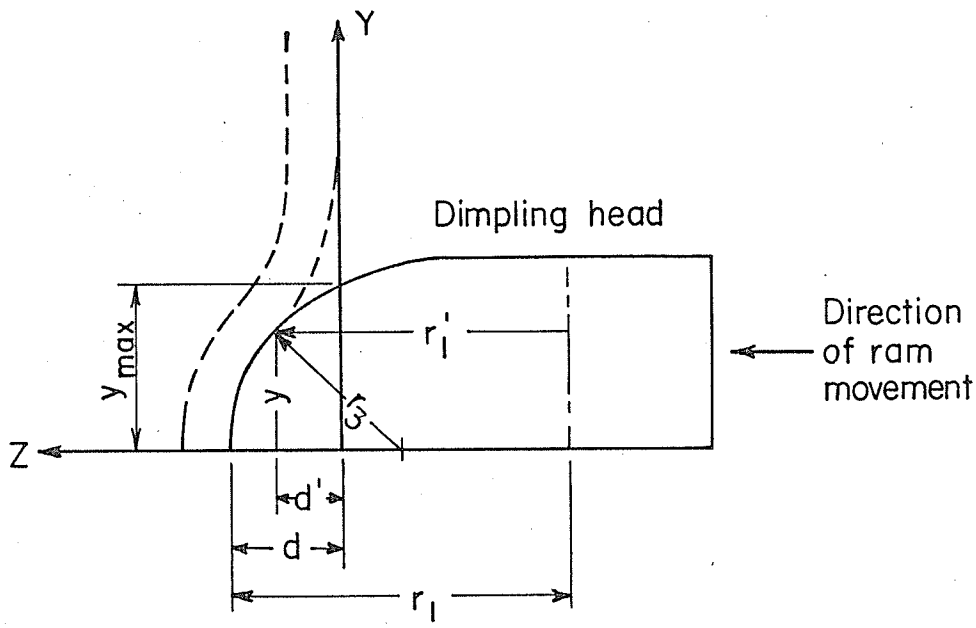

Figure 4.4 Dimpling head profile

$$R_b'(y) = d'/2b = d/2b - r_3/2b\cdot(1 - \sqrt{1 - (y/r_3)^2})$$

$$K'(y) = \frac{r_1' + r_2 + t}{2b} \qquad 4.23$$

$$= \frac{r_1 + r_2 + t}{2b} - \frac{r_3}{2b}(1 - \sqrt{1 - (y/r_3)^2}$$

Therefore,

$$R_b'(y) = R_b - \Delta(y)$$

$$K'(y) = K - \Delta(y) \qquad 4.24$$

where

R_b , K are the dimpling-span ratio and the dimpling constant of the apparatus, respectively, and

$\Delta(y)$ is a correction factor given by

$$\Delta(y) = \frac{r_3}{2b}[1 - \sqrt{1 - (y/r_3)^2}\,] \qquad 4.25$$

Using the corrected values of R_b' and K', the values of the average strain at any distance y , $\bar{\varepsilon}(y)$, may be determined from Figure 3.7 or Equations 3.7 and 3.9. For the geometry of the dimpling head given in Figure 4.4 and for an average edge strain of 2 percent the distribution of the average dimpling strain, $\bar{\varepsilon}$, is given in Figure 4.5.

The solid curve of Figure 4.5 holds fairly well for the points where the contact between the specimen and the dimpling head is maintained. It was observed that the contact is lost at some distance less than the

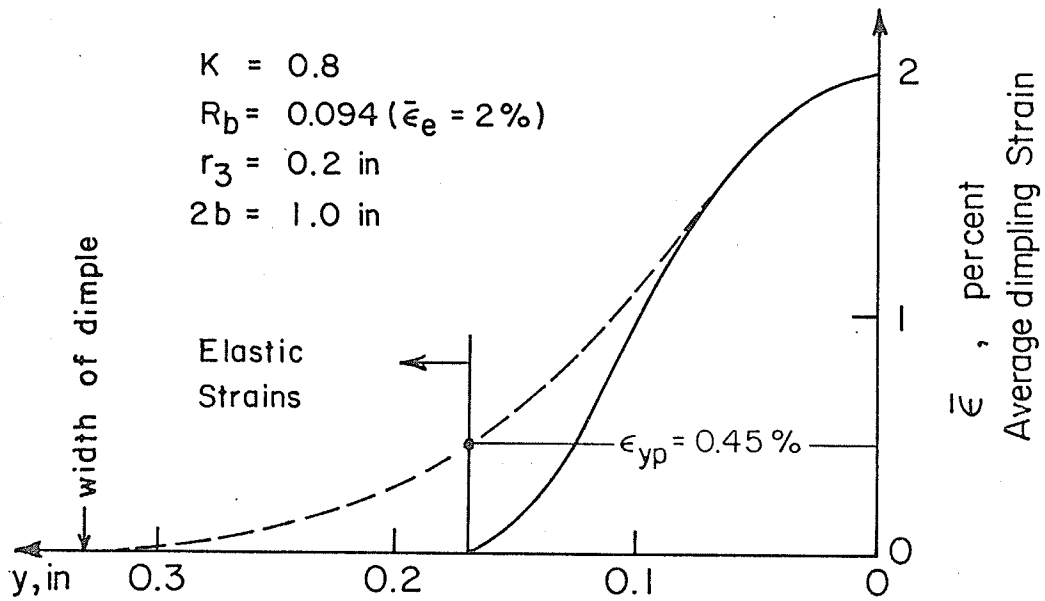

Figure 4.5 Values of the characteristic parameter $\bar{\epsilon}$ for the given conditions.

maximum expected value y_{max} . The material curves as shown by the dotted lines in Figure 4.4. This curvature tends to increase the average dimpling strain on the rest of the dimple area up to the full width of the edge dimple. Due to this curvature a correction must be made and the actual $\bar{\varepsilon}$-y curve may be qualitatively represented by the dotted line in Figure 4.5. In fact, most of the deviation occurs in the characteristic region of elasticity and, therefore, will have no reflection on the residual strain distribution. The remaining portion will practically produce permanent residual deformation but mostly within the characteristic region of development. The effect of this deviation will primarily reflect on the magnitude and location of the stresses in the interior region away from the edge.

Using the results of Figure 4.5 in conjunction with the characteristic curve of Figure 4.3, the residual deformation of an elemental strip at any distance y from the edge of the dimpled area may be determined. The results are given in Figure 4.6 for 2024-T3 alclad aluminum alloy material. Notice that this distribution is derived from an idealized stress-strain relation. The actual stress-strain relation may produce the modification illustrated by the dotted line in the same figure.

Substituting Equation 4.20 into Equation 4.1 obtain

$$p_x(y) = - [(1-\nu/2)/(1-\nu^2)]\cdot E\cdot\varepsilon_x^0(y)$$

$$p_y(y) = + [(1/2-\nu)/(1-\nu^2)]\cdot E\cdot\varepsilon_x^0(y) \qquad 4.26$$

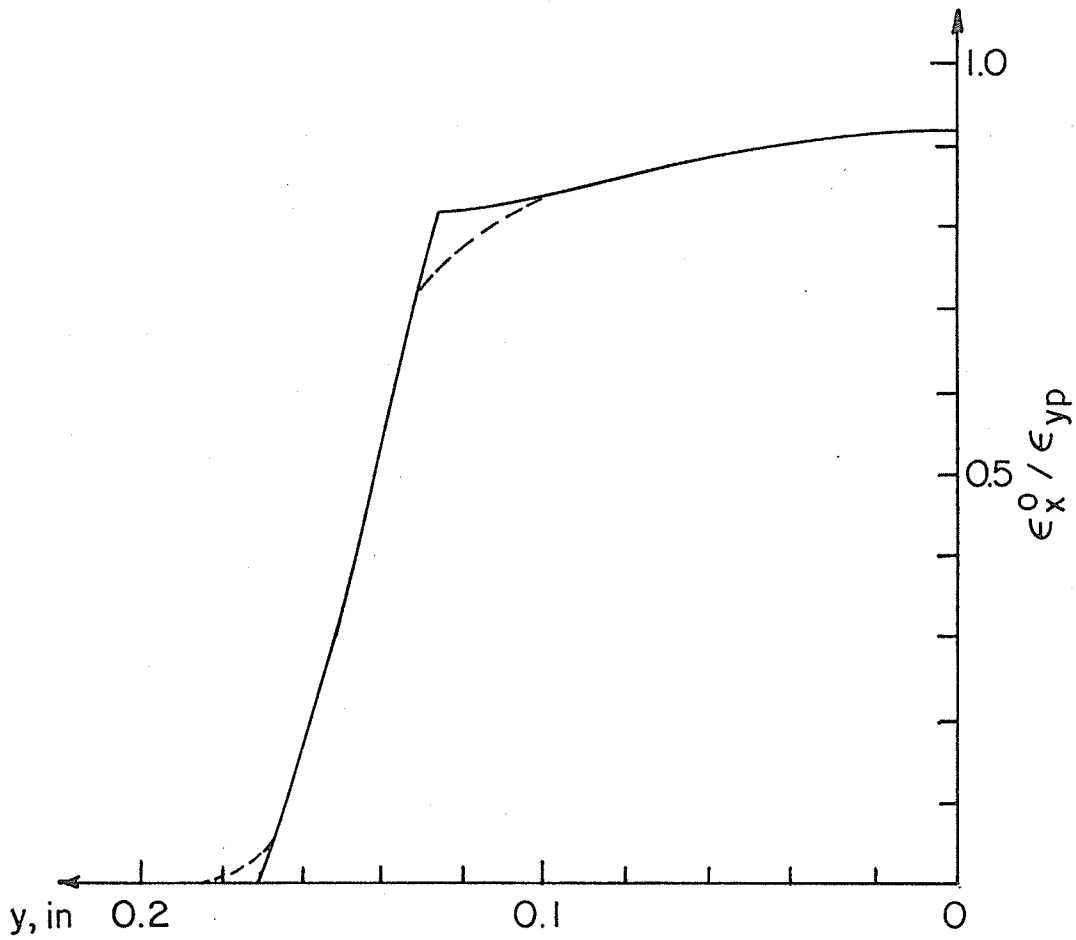

Figure 4.6 The distribution of $\epsilon_x^o(y)$

Equations 4.26 may be expressed in the non-dimensional form:

$$p_x(y)/\sigma_{yp} = -\ [(1-\nu/2)/(1-\nu^2)]\cdot E\cdot\varepsilon_x^0(y)/\sigma_{yp}$$
$$p_y(y)/\sigma_{yp} = +\ [(1/2-\nu)/(1-\nu^2)]\cdot E\cdot\varepsilon_x^0(y)/\sigma_{yp} \qquad 4.27$$

Using the distribution of $\varepsilon_x^0(y)$ as given in Figure 4.6 in conjunction with Equations 4.27, the necessary boundary pressures are determined and given in Figure 4.7.

In conclusion the procedure of determining $\varepsilon_x^0(y)$ may be summarized in the following steps:

1. Find the stress-strain properties of the material.
2. Using Equations 4.14 through 4.19 determine the characteristic curve of edge dimpling and plot the results as shown in the right top quarter of Figure 4.8.
3. Find the shape and dimensions of the dimpling head. For the selected ram movement calculate:
   a. the average edge strain, $\bar{\varepsilon}_e$,
   b. the average dimpling strain, $\bar{\varepsilon}(y)$, at any distance y from the edge.

   This may be done using Equation 4.24 and 4.25 and either Figure 3.7 or Equations 3.7 and 3.9. Note that the upper limit of $y = y_{max}$ can be determined from Equation 4.21. Therefore, the values of the characteristic parameter are determined and may be plotted as shown in the right bottom quarter of Figure 4.8.

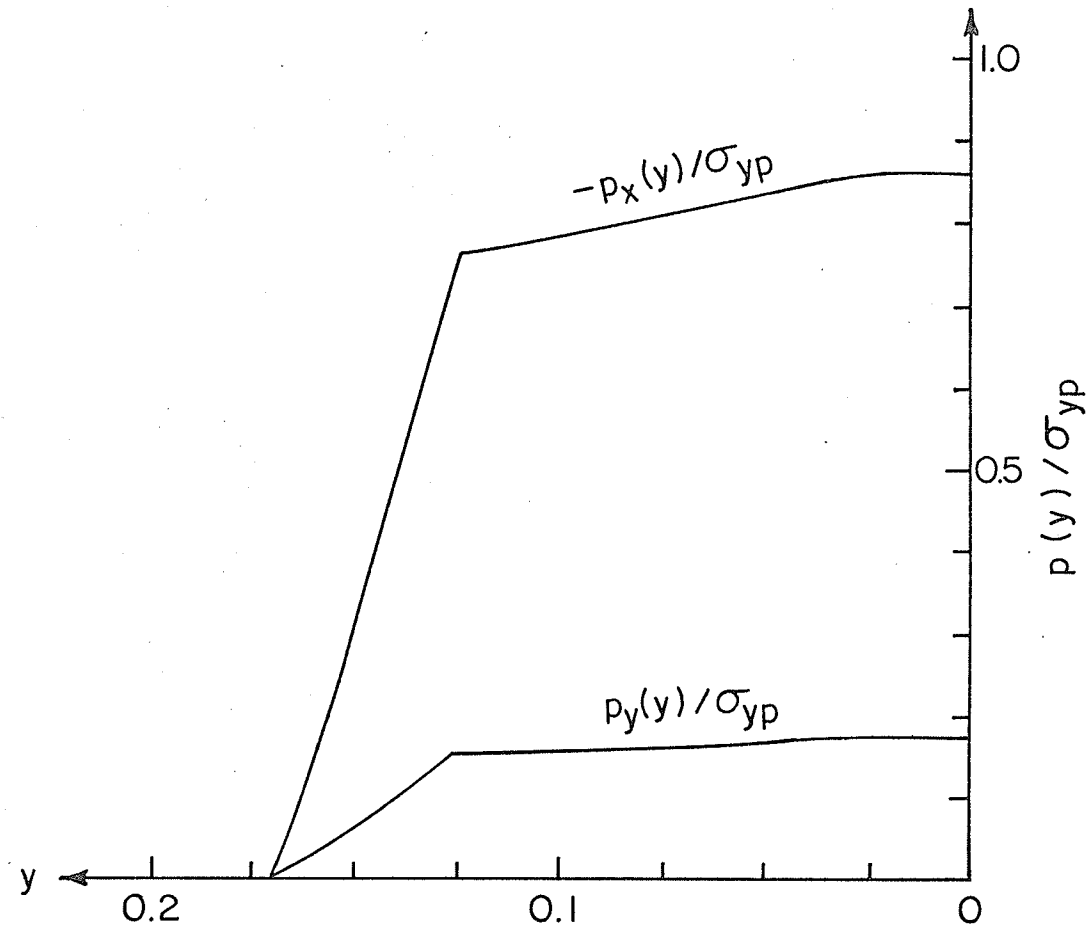

Figure 4.7 The necessary boundary pressure to suppress an elemental strip at a distance y from the edge to its original planar dimensions.

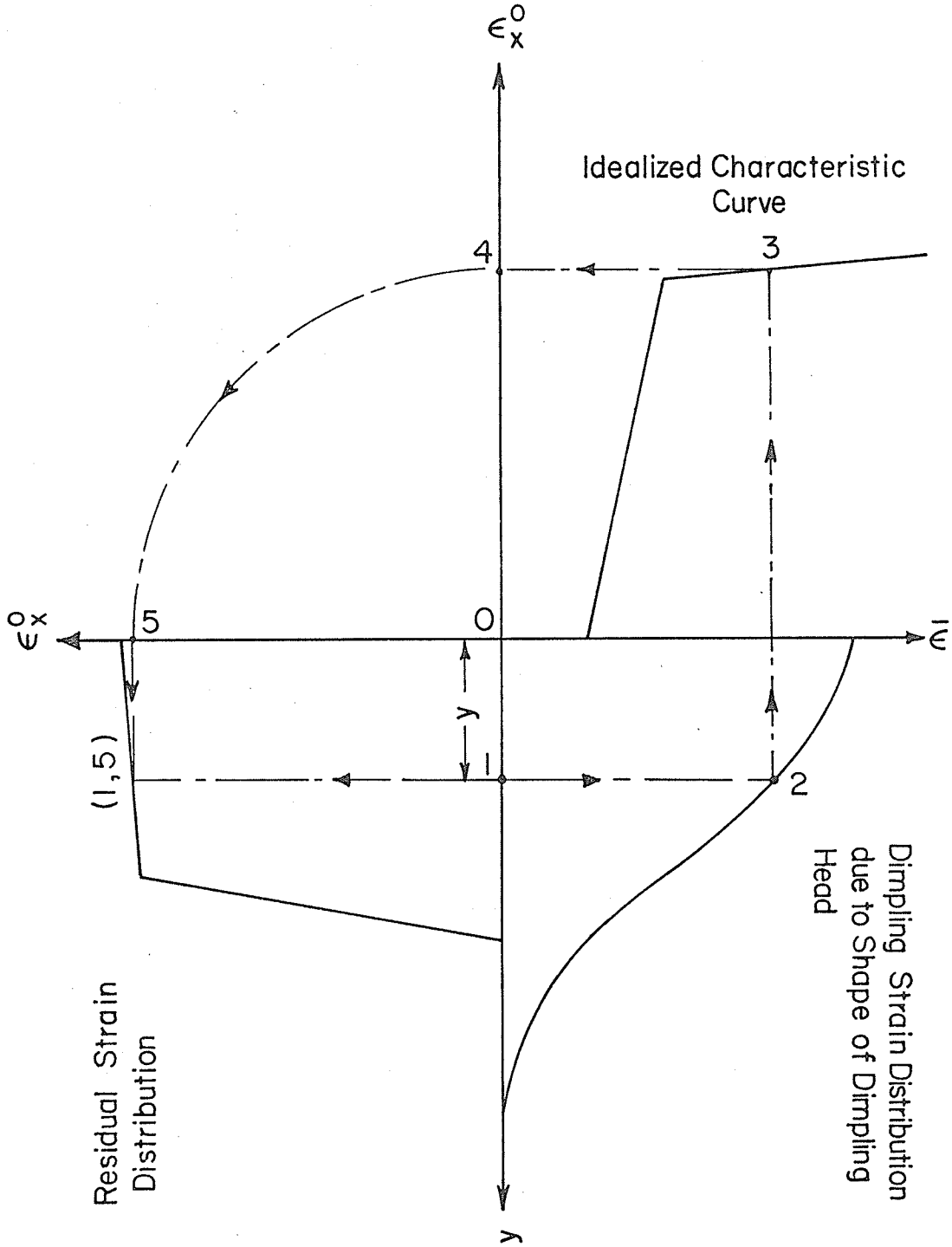

Figure 4.8 Summary of procedure of determining the residual strain distribution, $\epsilon_x^o(y)$.

4. To determine the distribution of residual deformation $\varepsilon_x^0(y)$ a graphical method may be used, as illustrated in Figure 4.8. Follow the chain dotted line starting from point 1 for a given value of y. For this value the corresponding average dimpling strain is determined at point 2. Drawing a line parallel to the y-axis to intersect the idealized characteristic curve at point 3, the corresponding residual strain ε_x^0 is determined. Projecting point 3 on the ε_x^0-axis point 4 is found, and by rotating point 4 a right angle in the counter clockwise direction point 5 is found. The data point having the coordinates $\overline{01}$ and $\overline{05}$ in the ε^0-y coordinate system determines a point on the residual strain distribution curve. The curve may be determined for any combination of the characteristic curve and dimpling strain distribution.

4.2.3 REMOVAL OF FICTITIOUS FORCES

The combination of body force $B_y(y)$ and the boundary forces $p_x(y)$ and $p_y(y)$ is shown in Figure 4.9(a). It can be seen that the clamping system may only exert the boundary pressure $p_x(y)$ but the free edge of the dimpled area is subjected to an imaginary pressure $p_y(0)$ in addition to the fictitious body force $B_y(y)$ which is not exerted by the clamping system. To visualize the state of stress in the clamped situation, i.e., the MPRS distribution over the entire dimpled region, it is necessary to remove the fictitious body and boundary forces in the y-direction. However, this step of solution may be by-passed as it does not affect the final result. The solution of the problem may be

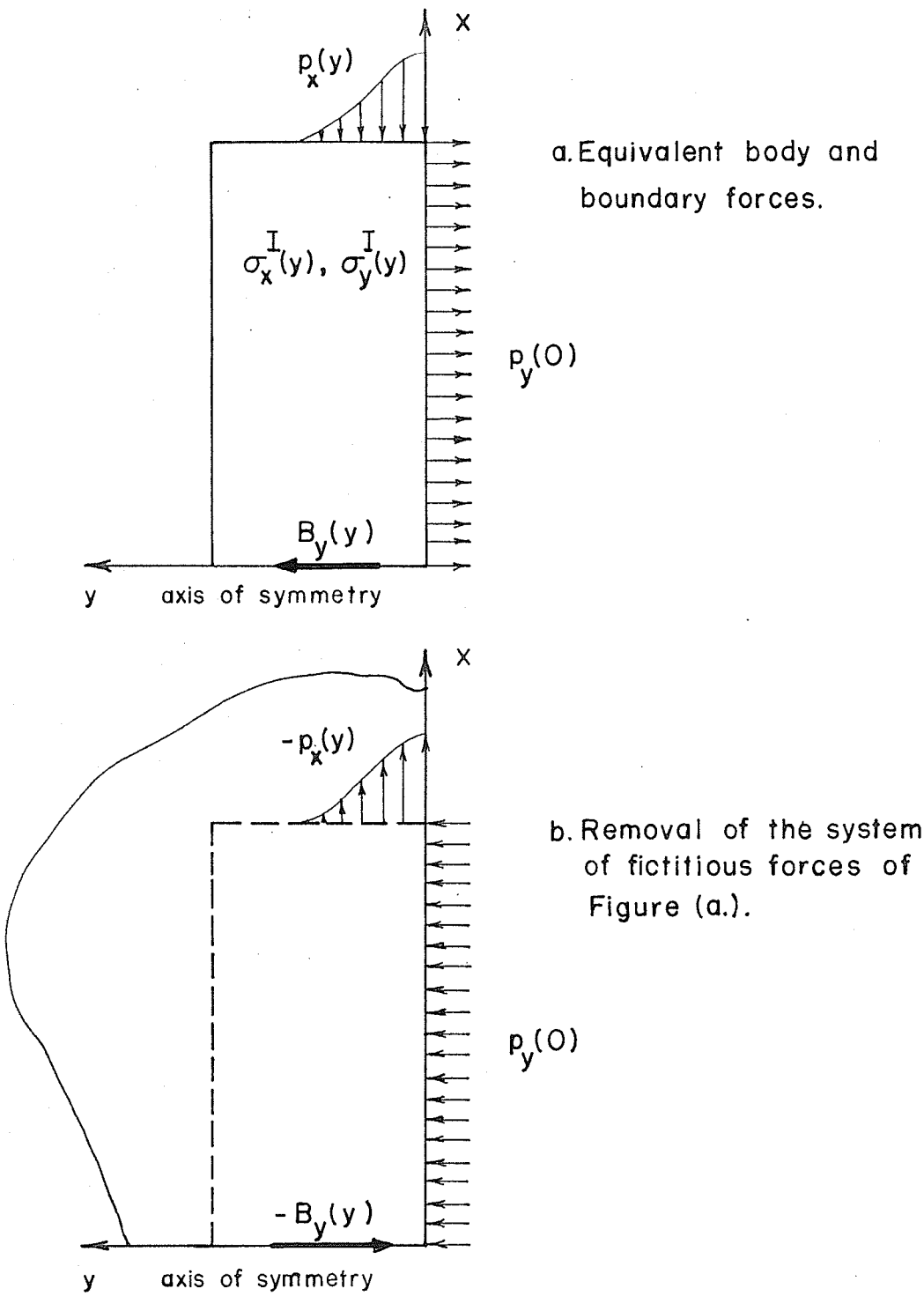

a. Equivalent body and boundary forces.

b. Removal of the system of fictitious forces of Figure (a.).

Figure 4.9 The elemental strips joined together in one integral body.

accomplished by removing the fictitious system of body and boundary forces. This is achieved by applying a system of body and boundary forces equal in magnitude but opposite in direction, as illustrated in Figure 4.9(b). The stresses produced by the removal-system of forces may be determined numerically by the finite element method. An exact analytical solution is not available in this case. However, it can be shown, mathematically, that the finite element solution converges to the exact solution as the number of elements is increased and, therefore, any desired degree of accuracy may be obtained [46].

The plate specimen is subdivided into a number of rectangular finite elements interconnected by nodes. Because of symmetry, only one half of the plate need be considered. The finite element mesh is illustrated in Figure 4.10. The element and node numbers except for the boundaries are omitted for clarity of illustration. The displacements of nodes 1 to 18 are restricted in the x-direction due to symmetry and node number 18 is fixed. The system of forces shown in Figure 4.9(b) is calculated and the necessary boundary conditions are applied to the proper elements. The body force $B_y(y)$ is substituted by the equivalent pressure at the interfaces between elements. A total of 170 elements and 198 nodes are used.

A finite element computer program [101] which performs linear plane stress analysis is used. Input data included the elastic properties of 2024-T3 alclad aluminum alloy material, node point coordinates and load or displacement, element data, and boundary pressures.

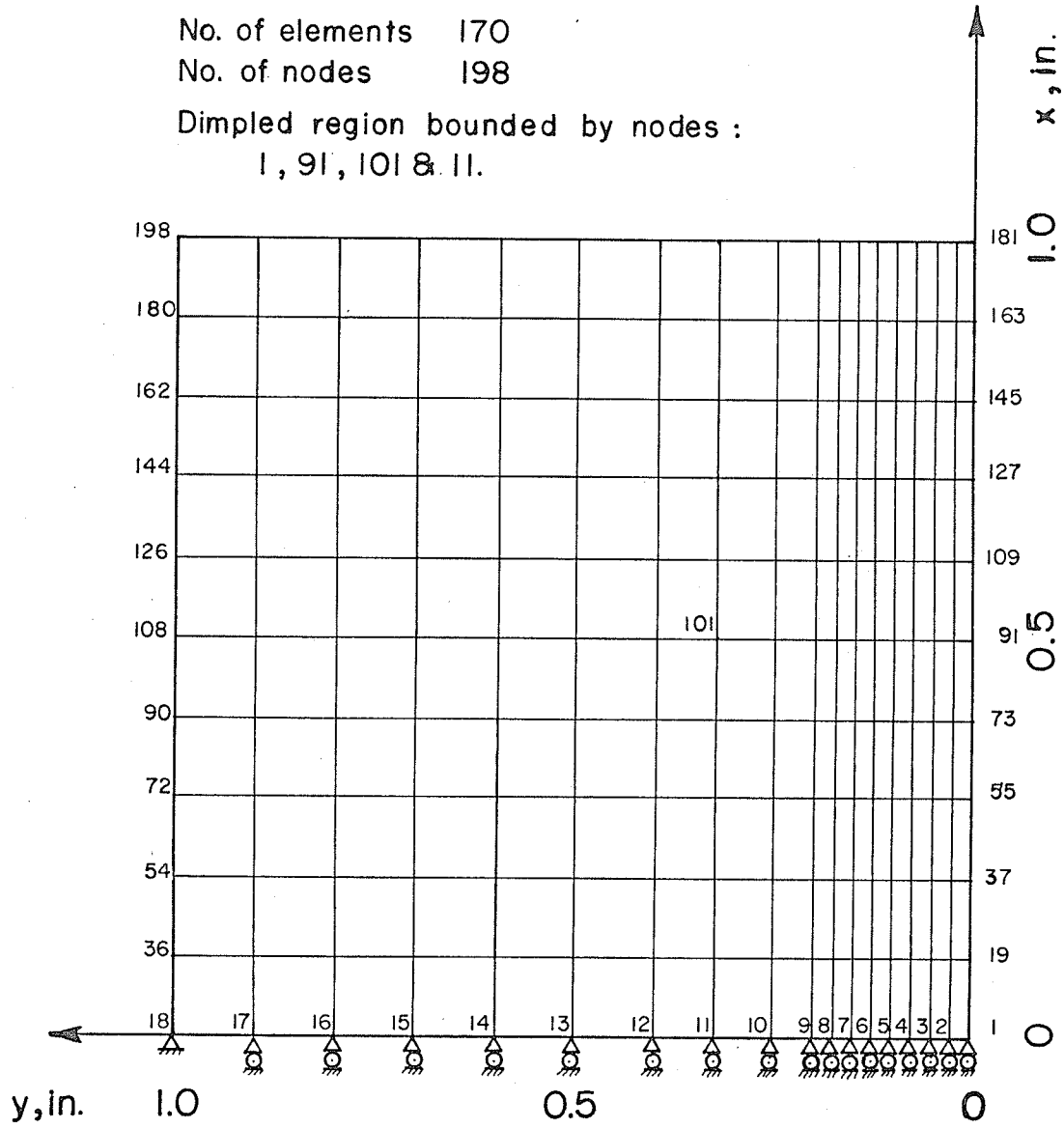

Figure 4.10 Finite element mesh for for edge-dimpled specimens.

Output is obtained for the stresses at the elements. The longitudinal stress in the x-direction, the transverse stress in the y-direction and the shear stress distributions may be determined at any distance from the axis of symmetry (x = 0) or any distance from the edge (y = 0). At x = 0.05 in., the shear stress component is found negligible, therefore, the stress distribution at the axis of symmetry is considered to be the same. Figure 4.11 shows the stress distribution at the axis of symmetry due to the removal of the fictitious system of body and boundary forces.

4.2.4 RESIDUAL STRESS DISTRIBUTION

The final residual stress distribution is the algebraic sum of two systems of stress. The first is the stress due to applying the fictitious forces to suppress the permanent strain of each elemental strip. This solution is given by

$$\sigma_x^I = p_x(y)$$
$$\sigma_y^I = p_y(y) \qquad 4.28$$

The second is the stress created by the removal of the system of fictitious forces. These stresses $\sigma_x^{II}(x,y)$, $\sigma_y^{II}(x,y)$ and $\sigma_{xy}^{II}(x,y)$ are determined numerically. Therefore, the final residual stresses will be symmetrical around x = 0 and given by

$$\sigma_x^{RS}(x,y) = \sigma_x^I(y) + \sigma_x^{II}(x,y)$$
$$\sigma_y^{RS}(x,y) = \sigma_y^I(y) + \sigma_y^{II}(x,y) \qquad 4.29$$
$$\sigma_{xy}^{RS}(x,y) = \sigma_{xy}^{II}(x,y)$$

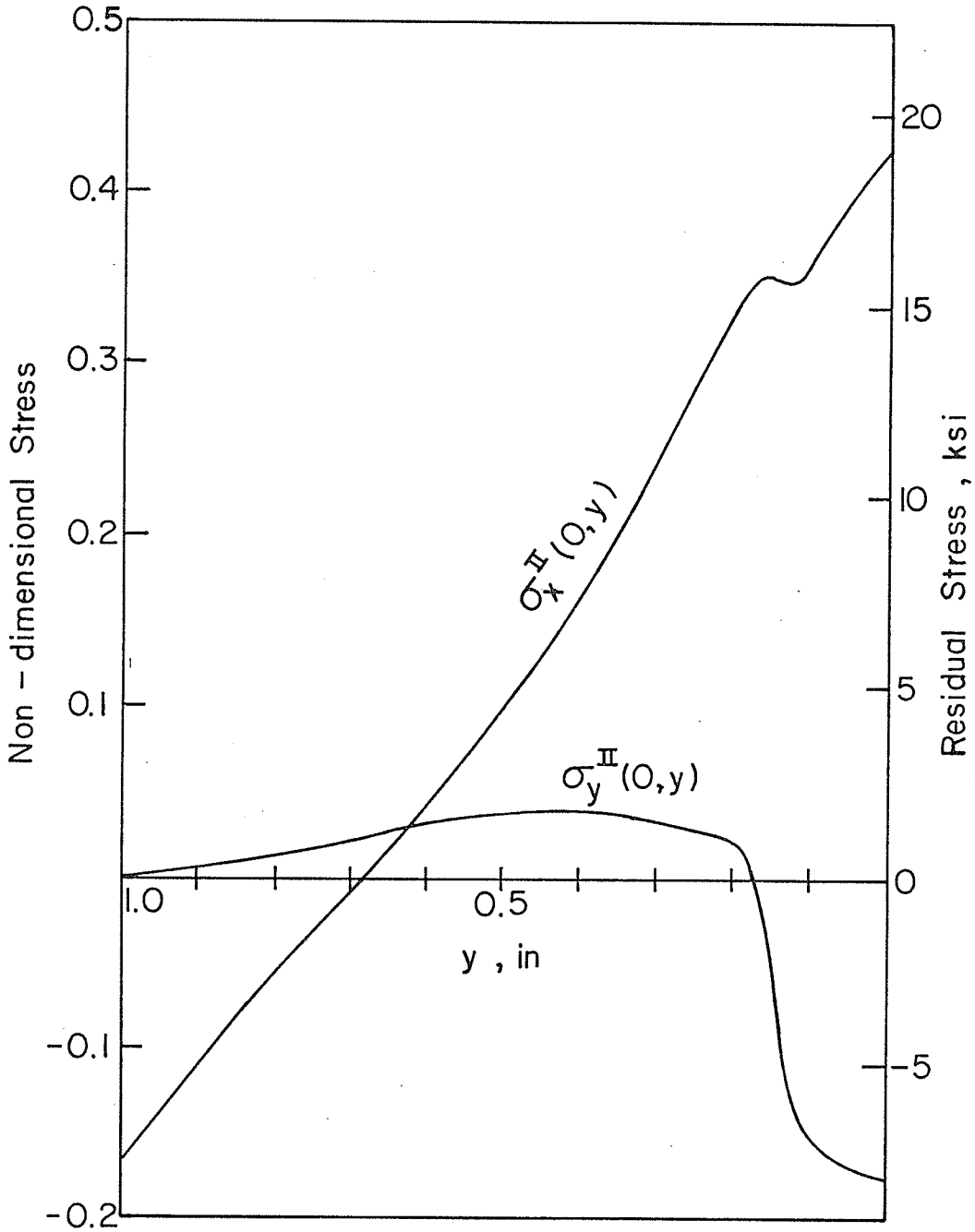

Figure 4.11 The stress created by the removal of fictitous forces.

Note that $\sigma_x^I(y)$ and $\sigma_y^I(y)$ vanish outside the dimple region. The solution given by Equations 4.29 is plotted in Figure 4.12 for x = 0.

The same solution may be obtained if the clamping forces and the MPRS distribution are known. The stress distribution due to unclamping is then superimposed on the MPRS to obtain the final residual stress distribution.

Before concluding this section, it should be noted that residual stresses in wider specimens will be higher in compression and lower in tension. For narrower specimens with the same dimpling conditions and width the opposite will occur. This fact is significant in practical situations as it appears that the consideration of the material surrounding the dimpled area is a major factor in determining the residual stresses. For most practical applications the ratio of the plate width to the width of dimple is expected to be far greater than the value of 3 employed in the present study.

4.3 EFFECT OF PRELOADING

A prior overload is called a preload. In fatigue testing a preload simulates gusts occurring in an early stage of the load spectrum. It has been indicated previously that preloading of unnotched specimens (prior to fatigue cycling) may produce a minor improvement in fatigue strength as a result of strain hardening. When a part having residual stresses is preloaded, localized yielding may occur as a result of the resultant stress exceeding the elastic limit. The resultant stress is the algebraic sum of residual stress and prestress. The localized

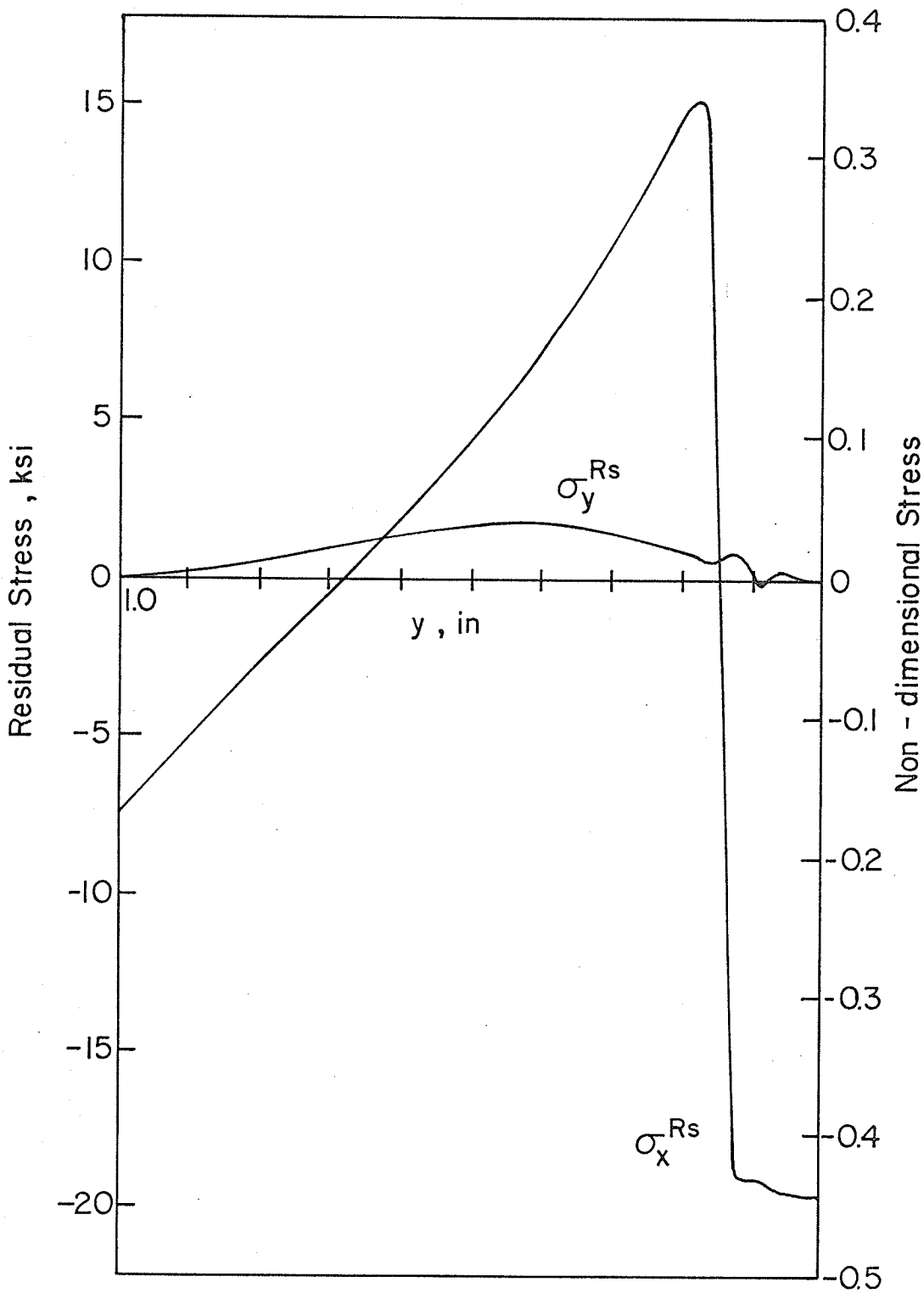

Figure 4.12 The analytical solution of residual stress (x=0)

yielding will occur in a region, the size of which is dependent on the amount of preload.

Figure 4.13 illustrates the effect of preloading on residual stress. Curve A is the residual stress distribution before preloading. Curve B is the resultant stress at small preloads. Upon removal of such a preload the original residual stresses will be restored to the original distribution of curve A. As the preload increases , the peak tensile stress reaches the yield stress, as represented by curve C. This is the limit after which inelastic deformation starts. It is determined by the difference between the yield stress and the peak of residual tension. For the present case, this limit is found at a prestress ratio of approximately 0.65. This limit has to be verified by experiment. As this limit is exceeded, localized plasticity occurs and the amount of plastic deformation is in proportion to the prestress, as illustrated by curves D and E. This will disturb the original equilibrium and result in a change of residual stresses. This change may, for small values of preload, cause an increase in the residual compression. However, high preloads will cause the spreading of the residual deformation along the specimen width which will result in reducing the residual stresses. The analytical or the numerical determination of residual stresses after preloading requires the definition of the newly created misfit zone and the stresses acting at its boundaries. Such a solution will be complicated by the non-axial symmetry and the biaxiality of residual stresses. Accordingly, the effect of preloading will be studied in terms of its effect on the fatigue strength improvement. A study of the subject is presented in Chapter 6.

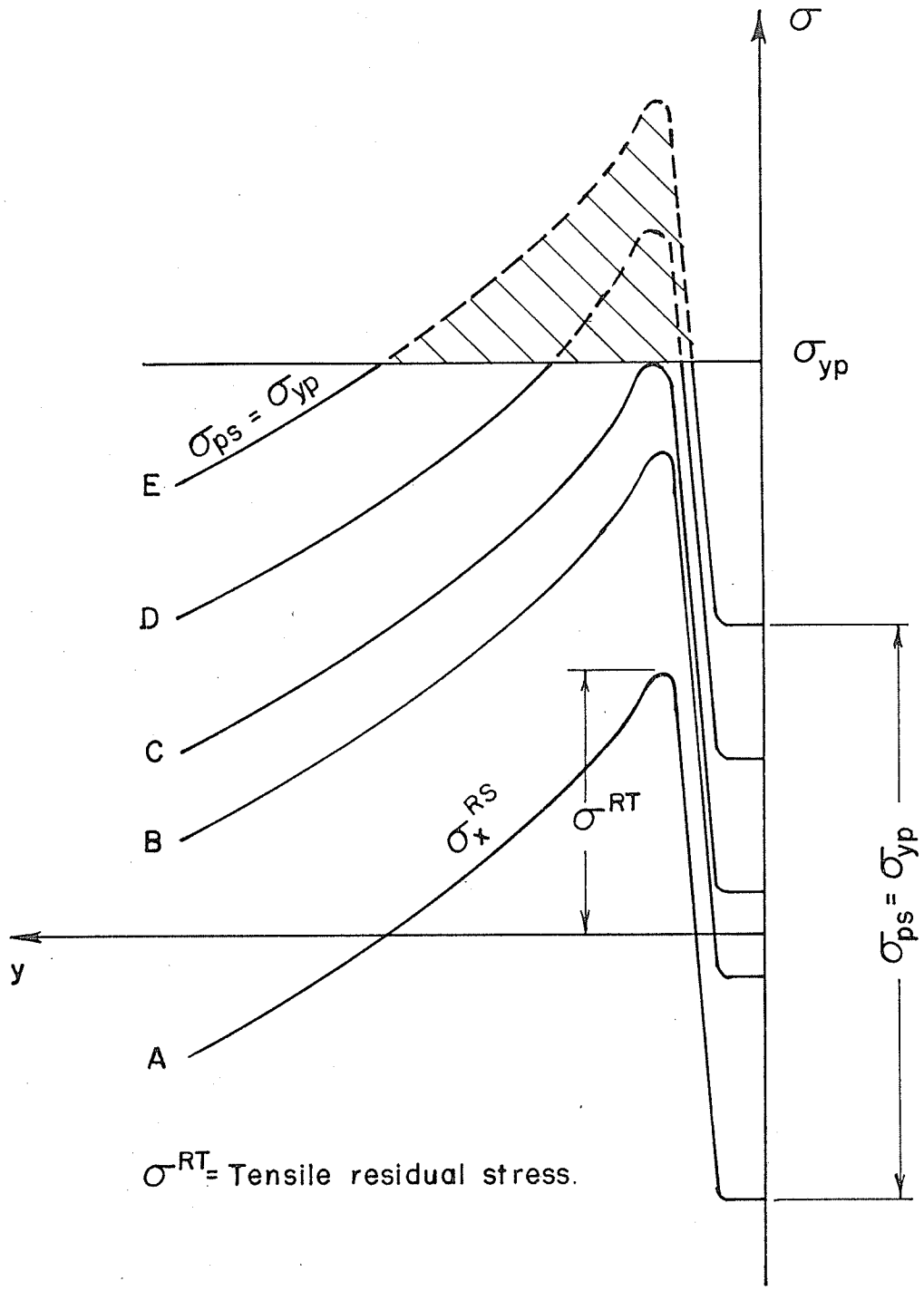

Figure 4.13 The effect of preloading of edge dimpled specimens.

4.4 SUMMARY

In this chapter residual stresses due to edge dimpling are determined analytically. The method employs an approximate procedure to determine the distribution of residual deformation based on the idealization of stress-strain relations. The finite element technique is used at some stage of the solution to determine the stress field produced by a system of body and boundary forces. The final residual stress distribution is determined for the given dimpling parameters. The results have yet to be verified by experimental measurement of residual stresses, which will be dealt with in the next chapter.

CHAPTER 5

THE MEASUREMENT OF RESIDUAL STRESSES

5.1 REVIEW OF RESIDUAL STRESS MEASURING TECHNIQUES

Various techniques have been used for the measurement of residual stresses. These techniques may be classified into destructive and non-destructive depending on whether the amount of damage made to the material can or cannot be tolerated. Non-destructive techniques, such as the X-ray technique, do not cause permanent damage to the material. On the other hand, destructive techniques, usually mechanical in nature, result in permanent damage and loss of the function of the part being tested. If the damage is tolerable, destructive techniques may be considered semi-destructive. In the following subsections the various techniques for measuring residual stresses will be reviewed.

5.1.1 NON-DESTRUCTIVE TECHNIQUES

Four non-destructive techniques will be discussed. These are: (i) the X-ray, (ii) the Ultrasonic, (iii) the Magnetic and (iv) the Indentation Techniques.

i. The X-ray technique is the most common of the non-destructive techniques. It is based on measuring the change in the crystal lattice spacing caused by the residual or applied stress at the surface of a specimen [47]. In general, Martin [48] has shown that the X-ray diffraction method is capable of yielding results which are reproducible to

within ±5000 psi. In a later experiment, Donachie and Norton [49] estimated the reproducibility of stress measurement in aluminum alloys to be within ±1000 psi. Although the technique is essentially non-destructive, it is a costly and time consuming method that requires complex equipment and highly skilled operators. The X-ray technique has been employed by many investigators in the measurement of residual stresses [4, 12, 21, 26, 27, 50, 51, 52].

ii. The ultrasonic technique, first proposed by Benson and Raelson in 1959 [53], is based on relating the changes in the characteristics of ultrasonic waves due to changes of physical or mechanical properties of the material produced by residual stresses [47]. The application of stress causes very small change in the wave velocity which cannot be easily measured. The complexity of the technique in addition to its expense and time requirements restrict its application to laboratory experiments. In 1973, Noronha, et al. [54] reported the development of a technique that measures the change of velocity of ultrasonic waves due to the application of stress. However, experimental results obtained on 4340 steel indicate a considerable deviation of ultrasonic measurements from X-ray measurements [47].

iii. A magnetic technique utilizes the phenomenon of magnetostriction which causes the dependence of magnetic properties of ferromagnetic materials on the state of stress [55]. This method requires considerable computation and may be regarded as qualitative rather than quantitative.

iv. Indentation methods relate the residual stress to the change of hardness which is determined from the changes of size and shape of the

indentation [56, 57]. This method, despite its simplicity, requires knowledge of the initial hardness of the material and special care in supporting the specimen during indentation. The major setback of this technique is the inherent lack of accuracy when measuring compressive or equibiaxial tensile residual stresses.

5.1.2 DESTRUCTIVE TECHNIQUES

The common principle of destructive techniques is that of the removal of a part of the material and measurement of the resulting changes in shape or dimensions. These measurements are used to calculate the average residual stress that was originally acting on the removed part. It is imperative to note that the removal of layers or parts of the material unbalances the equilibrium of forces and results in the redistribution of residual stresses. Such changes must be taken into account when a series of measurements are to be taken on one specimen. Destructive techniques, although destructive, are preferred to non-destructive methods wherever subsurface stresses are to be measured. They also are fast and less expensive. However, it should be noted that in most cases the examined specimen is no longer available for further exploration. The most common destructive techniques are: (i) Sachs', (ii) layer-removal, (iii) sectioning and (iv) hole-drilling techniques.

i. Sachs' technique was first introduced by Sachs [58] for measuring residual stresses in objects of rotational symmetry (both in geometry and stress field). Sachs' method or the boring-out method, as it is generally called, consists of measuring strains on the outer surface of a cylinder

while the bore is machined away which provides for accurate measurements of the stresses at the inner surface. An alternative procedure is to mount strain gages on the bore-hole wall and measure the strain as the outer diameter is turned down. The latter, known as Sachs' turning-down technique, provides accurate measurement of stresses at the outer surfaces. A combination of both techniques, developed by Bühler [59] permits accurate measurement at both surfaces. Further extension of Sachs' method to the measurement of antisymmetric stresses in round bars has been reported by Lambert [60]. A simplified procedure of calculation using graphical method was proposed by Weiss [61].

Several applications of Sachs' techniques to the measurement of residual stresses in cylinders [62], discs [63] and plates [33, 64] have been described. The results obtained by this technique, however, are poorly sensitive to the sudden changes in stress gradients and the accuracy of results is limited by the inherent stiffness of the tubular member on which strains are measured [48]. Sachs' technique is hampered by tedious machining requirements and is subjected to errors resulting from residual stresses and heat produced by machining.

ii. The layer-removal technique is similar to Sachs' technique but it is not bound by the object symmetry. It has been developed for measuring residual stress gradients in metal parts resulting from various manufacturing operations. It involves the removal of thin surface layers (of up to 0.0001 in.) and the simultaneous measurement of specimen deflection which accompanies the removal. Layers may be removed successively by fine grinding as reported by Rathbun and Coffin [12] or by milling as reported in determining residual stresses in plastics by

Golsby [65]. Layers may also be removed continuously by processes such as electrolytic polishing described by Letner [66] and Zapel [67] or by etching in a chemical solution as proposed by Weisman and Phillips [68] and Hospers and Vogelesang [69].

iii. The sectioning technique was first reported by Kalakoutsky in 1888 [70]. The basic principle of measurement is that internal stresses are relieved by cutting the specimen into smaller strips and, thus, by measuring the change in strain of the strips, residual stresses may be calculated. The selection of the locations for sectioning and partical sectioning was described by Tebedge et al. [71], Alpsten and Tall [72] and others [73]. This technique is best suited for large structural components as stresses induced by cutting or sawing become more serious in smaller sections. It also involves a great deal of accurate machining. The complexity of the method admits the introduction of errors that may offset the sensitivity and accuracy of measurements[48].

iv. The hole-drilling technique consists of drilling a hole in the material and measuring the resulting change of strain in the vicinity of the hole [74, 75, 76]. The conventional procedure consists of experimentally measuring the change of strain (the relaxation strain) for a given stress, strain gage-hole configuration, material and drilling procedure. From the measured relaxation strains relaxation coefficients are calculated and used to determine unknown residual stresses. Experiments have shown that certain features and requirements are associated with the technique. These are:

a. The measured stress must be uniform throughout the thickness.

Kelsey [77] showed that non-uniform stresses may result in estimates lower than the true values by up to 20 percent.

b. The hole depth should be specified to ensure full relaxation strain. This condition of optimum relaxation can be attained with a hole depth equal to the hole size as shown by Kelsey [77] and Tebedge et al. [73]. Meanwhile, Bathgate [78] suggests a hole depth of 0.5 the hole diameter.

c. The relaxation coefficients are found to be independent of the hole-gage assembly, if dimensional similitude is maintained within certain limits. Rendler and Vigness [79] determined these limits to be: a hole depth < the hole size, thickness > 4 times the hole size, and plate width > 8 times the hole size.

d. The rule of dimensional similitude was shown by Lake, et al. [80] to only apply for thick material. Therefore, a new calibration for each combination of hole-gage assembly and thickness becomes necessary, in the case of thin materials.

e. It has been shown by Kelsey [77] that uniaxial tensile and compressive relaxation coefficients are interchangeable. Uniaxial calibration coefficients may be used, applying the principle of superposition, to evaluate biaxial stresses. Several studies on biaxial stress fields have been reported by Cordiano and Salerno [81], Gupta [82], Bathgate [78] and Dini et al. [83].

f. Measurements are inherently limited to stresses within 1/3 of the elastic limit of the material as the stress concentration at the edge is 3. Beaney and Procter [84] suggest that the errors in

measuring stresses smaller than half the yield stress are negligible and as the stress approaches the yield point the error rises to approximately 10 percent.

v. Other techniques have been proposed by other investigators such as Schwaighofer [85], Vaidyanathan and Finnie [86]. A survey of some earlier techniques was reported by Tebedge et al. [73].

5.1.3 SUMMARY

As has been shown in this section, several methods are available for the measurement of residual stresses. These methods, either destructive or non-destructive, were proved to be of comparable accuracy and sensitivity [48]. In general, mechanical techniques have the advantage of being comparatively fast and less expensive. Some mechancial methods, such as the hole-drilling technique, may be regarded as semi-destructive if the amount of damage to the material can be tolerated. In the following sections a modified hole-drilling technique will be described, evaluated, and used in measuring residual stresses due to edge dimpling.

5.2 THE MODIFIED HOLE-DRILLING TECHNIQUE

In the present section a modification to the hole-drilling procedure is proposed in order to improve the practical value of the technique for measurement of residual stresses in thin plates. The modification is achieved by eliminating the need for calibrating each hole-gage assembly and by extending the range of measurement to stresses close to the yield strength.

5.2.1 THEORETICAL ANALYSIS

Kirsch's solution [40] for the stress distribution around a circular hole in a thin, wide, linearly elastic and isotropic plate subjected to uniaxial tension may be written:

$$\sigma_r = \frac{\sigma_x}{2}\{(1 - \frac{\lambda^2}{4}) + (1 - \lambda^2 + \frac{3}{16}\lambda^4)\cos 2\theta\}$$

$$\sigma_\theta = \frac{\sigma_x}{2}\{(1 + \frac{\lambda^2}{4}) - (1 + \frac{3}{16}\lambda^4)\cos 2\theta\} \qquad 5.1$$

$$\sigma_{r\theta} = -\frac{\sigma_x}{2}\{(1 + \frac{\lambda^2}{2} - \frac{3}{16}\lambda^4)\sin 2\theta\}$$

where: λ is the non-dimensional hole diameter defined by d/r (Figure 5.1), or it is the reciprocal of non-dimensional radius, r/d. These equations hold fairly well for plate widths of at least five times the hole diameter.

The strain distribution around the hole (after drilling), is given by:

$$\varepsilon_r = \frac{1}{E}(\sigma_r - \nu\sigma_\theta)$$

$$\varepsilon_\theta = \frac{1}{E}(\sigma_\theta - \nu\sigma_r) \qquad 5.2$$

while the strain distribution before drilling may be written:

$$\varepsilon_r^0 = \frac{\sigma_x}{E}(\cos^2\theta - \nu\sin^2\theta)$$

$$\varepsilon_\theta^0 = \frac{\sigma_x}{E}(\sin^2\theta - \nu\cos^2\theta) \qquad 5.3$$

Strain gages may be used to detect the change in strain resulting from drilling the hole. This change is defined as "relaxation strain" and will be denoted by ε_{Rr} and $\varepsilon_{R\theta}$ in the radial and tangential directions,

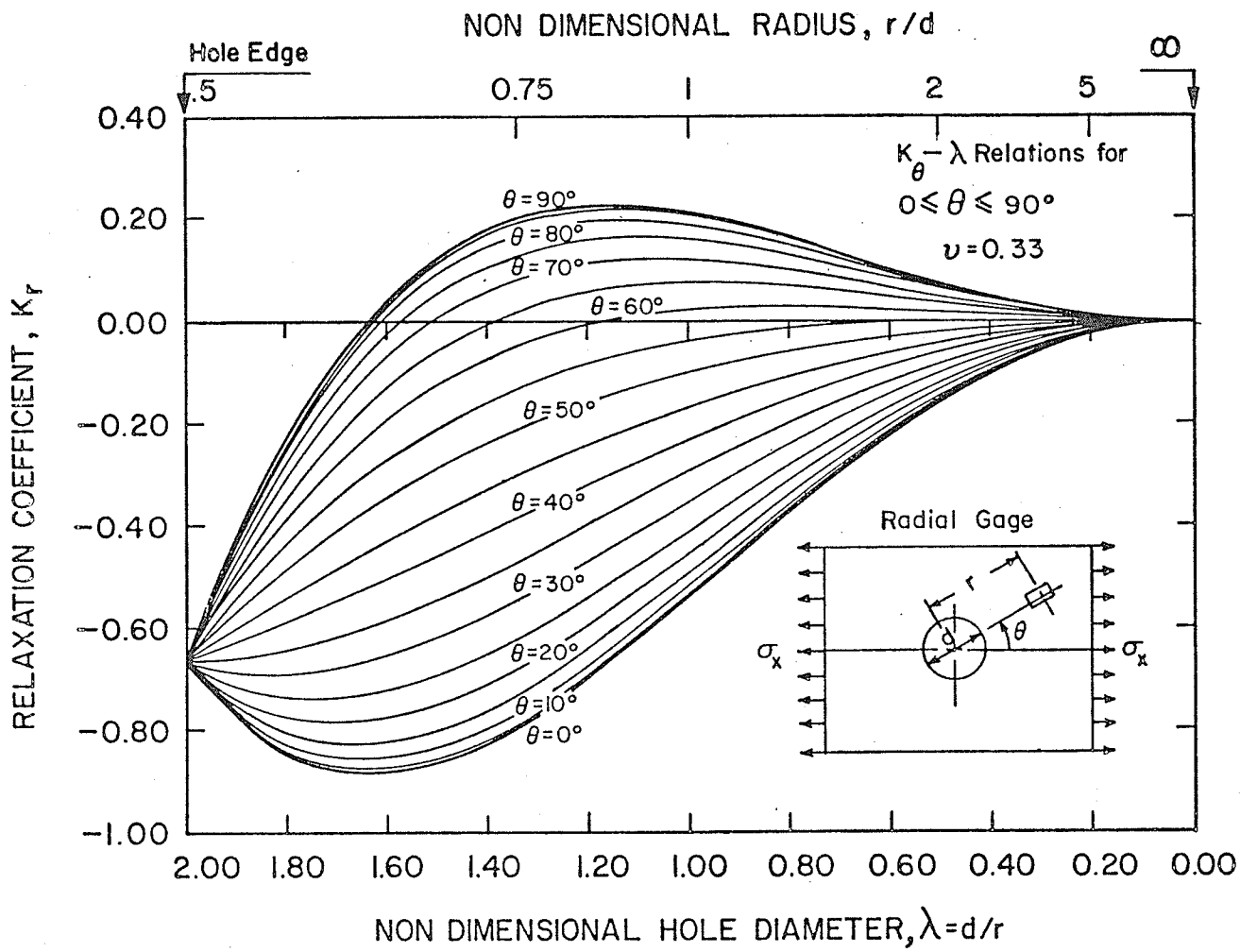

Figure 5·1 Values for the Radial Relaxation Coefficient

respectively. It should be noted that ε_{Rr} and $\varepsilon_{R\theta}$ are the net relaxation strains due to the stress (applied or residual). Relaxation strains are defined as:

$$\varepsilon_{Rr} = \varepsilon_r - \varepsilon_r^0$$
$$\varepsilon_{R\theta} = \varepsilon_\theta - \varepsilon_\theta^0 \qquad 5.4$$

Substitution of Equations 5.1, 5.2 and 5.3 into Equations 5.4 yields:

$$\varepsilon_{Rr} = K_r \frac{\sigma_x}{E}$$
$$\varepsilon_{R\theta} = K_\theta \frac{\sigma_x}{E} \qquad 5.5$$

where K_r and K_θ are defined as the relaxation coefficients at any angle θ, in the radial and tangential directions, respectively; and given by:

$$K_r = -\frac{(\nu + 1)}{8}\lambda^2 - \left(\frac{1}{2}\lambda^2 - \frac{3(\nu + 1)}{32}\lambda^4\right)\cos 2\theta$$
$$K_\theta = -\frac{(\nu + 1)}{8}\lambda^2 + \left(\frac{1}{2}\lambda^2 - \frac{3(\nu + 1)}{32}\lambda^4\right)\cos 2\theta \qquad 5.6$$

The relaxation coefficients are non-dimensional quantities which depend on the point of measurement (λ,θ) and Poisson's ratio of the material ν. For $\theta = 0^0$, the radial relaxation coefficient is practically independent of Poisson's ratio for $\lambda < 1.15$. In this case, K_r becomes universal for all elastic isotropic materials.

Figures 5.1 and 5.2 show the variation of K_r and K_θ with θ for aluminum alloys. The study of these figures suggests that the following

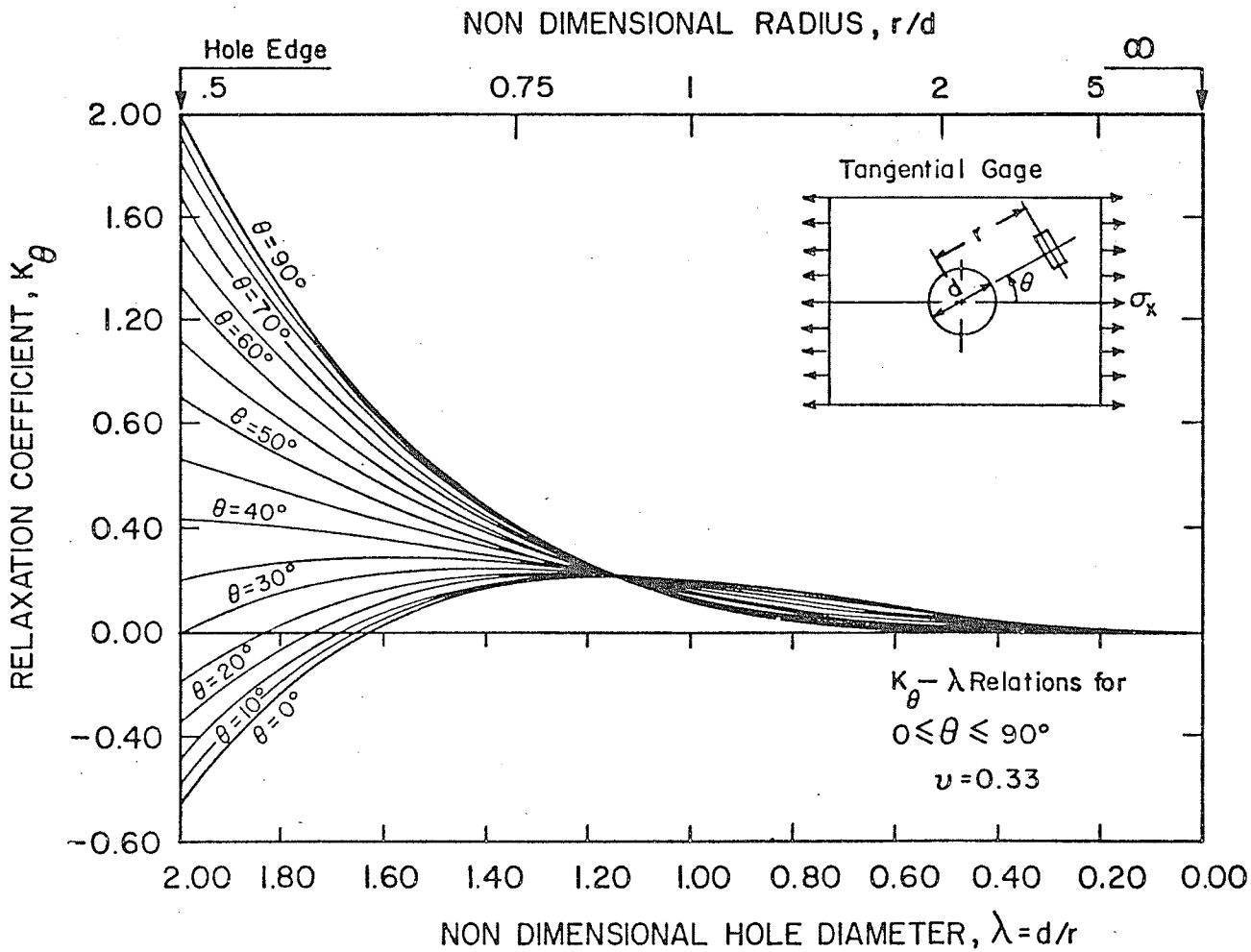

Figure 5·2 Values for the Tangential Relaxation Coefficient

points may be considered when laying out the hole-gage assembly:

a. Points of measurement (λ,θ) of maximum relaxation coefficient are recommended while those of minimal relaxation must be avoided.

b. In general, higher values of relaxation coefficients exist in the radial direction at $\theta = 0^{o}$. Therefore, radially oriented gages parallel to the stress offer the best measurement prospect. Although a tangential gage at 90° exhibits the maximum value of relaxation coefficient, its use is not advised. This is primarily due to the likelihood of large errors being caused by machining stresses. Unless a stress-free hole drilling technique becomes available it is recommended to use radial gages rather than tangential gages.

c. Higher values of λ are, generally, favourable for highest values of relaxation. As λ decreases, the relaxation coefficients decrease and the error in measurement becomes a considerable fraction of the measured relaxation strain.

d. A change of a few degrees in the orientation of a strain gage parallel or transverse to the stress is insignificant.

The foregoing discussion is, of course, applicable to the measuring of any general stress no matter how such stress condition is generated. It also is subject to certain practical considerations which will now be discussed.

5.2.2. PRACTICAL CONSIDERATIONS

It has been shown in Equations 5.5 that for a given strain gage-hole assembly and material the relaxation coefficient is fixed and the

stress is directly proportional to the relaxation strain. However, the measured strain relaxation is due not only to the applied stress but it also includes the contribution of some other effects. Therefore, the separation of the "net relaxation strain" due to the stress from the "measured or total relaxation strain" is necessary. The principal components of total strain, ε_T, for radial gages* are:

1. Net relaxation strain, $\varepsilon_{Rr} = \varepsilon_R$;
2. Relaxation strain due to drilling operation, ε_m;

and

3. Relaxation strain due to localized plastic flow, ε_p.

These strains are related by:

$$\varepsilon_T = \varepsilon_R + \varepsilon_m + \delta\ \varepsilon_p \qquad 5.7$$

where, $\delta = +1$ if $(\varepsilon_T - \varepsilon_m) > 0$ and $\delta = -1$ if $(\varepsilon_T - \varepsilon_m) < 0$. The reason for using the sign operator will be clarified in subsection (ii). Therefore the net relaxation strain to be used in Equations 5.5 will be:

$$\varepsilon_R = (\varepsilon_T - \varepsilon_m) - \delta\ \varepsilon_p \qquad 5.8$$

The relaxation strain components ε_m and ε_p will now discussed in more detail in subsections (i) and (ii), respectively.

i. The relaxation strain component ε_m results from machining residual stresses. Such stresses depend on the drilling conditions and are highly localized in the immediate vicinity of the hole. They drop rapidly as the distance from the hole edge increases. Therefore, the effect of machining

---

* Similar analysis may be made for tangential gages.

stresses may not be significant in a particular hole gage assembly but will certainly be significant in scaled-down, dimensionally-similar, hole-gage assemblies as the distance between the gage and the hole edge decreases. It is rarely necessary to scale-down in thick plates. This provides an explanation as to why the rule of dimensional similitude does not hold for thin materials.

The primary interest is not in measuring machining stresses but is in determining the location, r, at which the relaxation strain component, ε_m, is acceptably small. This can be done experimentally as described in Section 5.2.5(i). It should be mentioned that, due to axial symmetry, ε_m is independent of the orientation θ. In addition, machining stresses are independent of the stress to be measured, and hence ε_m should maintain the same sign regardless of the sign of ε_T as shown in Equation 5.7.

ii. The relaxation strain component ε_p is produced only if the stress field around the hole is disturbed by localized plastic flow. In uniaxial loading the stress concentration factor at the hole edge at $\theta = 90^o$ is 3 while at $\theta = 0^o$ it is -1. As the nominal stress exceeds 1/3 of the yield strength plastic flow will start at the hole edge at $\theta = 90^o$ and the elastic solution is no longer valid. However, it is always possible to determine the deviation of the elastic estimate from the true value of the stress. If the error is acceptable, the elastic solution may be practically used for determining stresses beyond 1/3 of the yield strength. Due to the nature of this localized plastic flow, its influence on transverse gages is expected to be greater than that on parallel gages.

Therefore, the relaxation strain ε_p will be a function of the relative location of the gage with respect to the location and magnitude of the maximum stress concentration factor. Hence, ε_p is a function of θ and will also vary with the biaxiality ratio, when measuring biaxial stresses.

It can be seen that ε_p will always increase the absolute value of the net relaxation strain regardless of its sign. For this reason it was necessary to introduce the sign operator δ in Equation 5.7. Thus, if the relaxation strain ε_p is neglected the measured stress, whether tensile or compressive, will always be overestimated. The presence of ε_p, being neglected, will lead to unrealistic and misleading results. This may be illustrated with the aid of Figure 5.3. Assume that a uniform stress $\sigma_x > 1/3\ \sigma_{yp}$ is measured by drilling a hole and recording the total relaxation strain $\overline{ac}$. If $\overline{ac}$ is considered entirely due to the existing stress, direct substitution in Equation 5.5 gives a stress $\sigma_x' = \overline{ac} \cdot E/K_r$. However, if $\varepsilon_p = \overline{bc}$ is considered, the true stress will be $\sigma_x = \overline{ab} \cdot E/K_r$ and the error in estimating will be equal to $\overline{bc}/\overline{ab}$, i.e., $\varepsilon_p/\varepsilon_R$. Correction for ε_p is required for stresses that are in excess of $1/3\ \sigma_{yp}$ or of a limit to be determined from experiments.

5.2.3 EXPERIMENTS

An experimental program was carried out to determine values of relaxation strain components ε_m and ε_p and to test the accuracy of the proposed hole-drilling procedure. The material used was aluminum alloy sheet of two different nominal thicknesses, as designated in Figure 5.4. Specimen dimensions and strain gage layout are also shown in the same

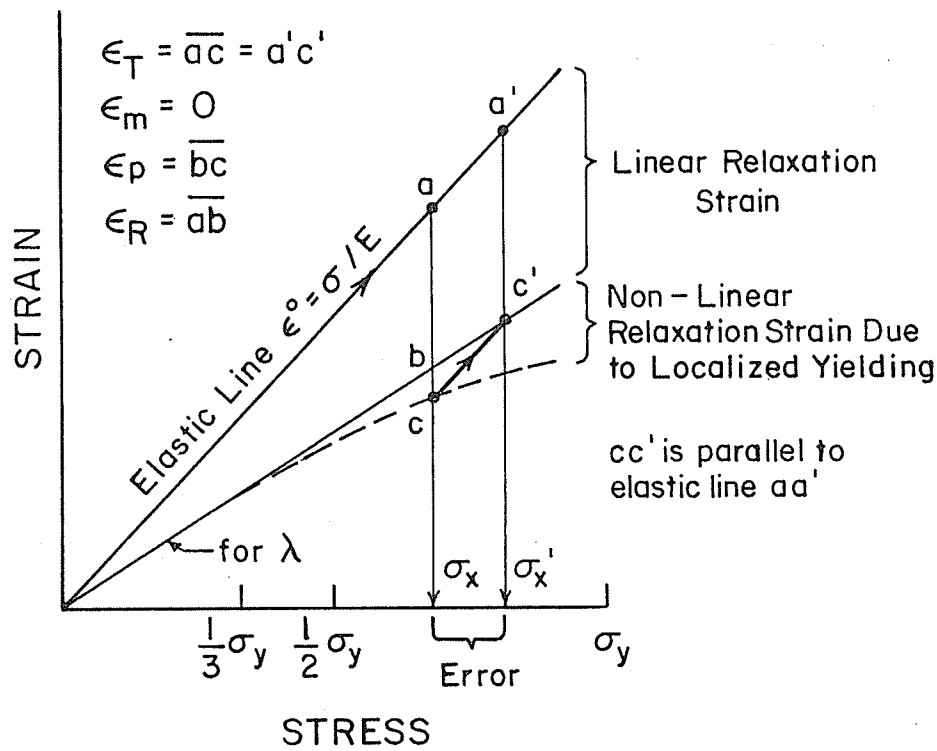

Figure 5·3 Error in Evaluating Stress Due to the Effect of Local Plastic Yielding.

Specimen	Thickness	r = Nominal	Maximum Hole Diam.	Material
I —+	0.125"(3.175mm)	0.236"(6.00mm)	0.25"(6.35mm)	2024 – T3
II —+	0.050"(1.27 mm)	0.285"(7.25 mm)	0.25"(6.35mm)	(1050 – Alum.)*

* Low strength aluminum alloy, σy = 18 Ksi (120 MPa)

—+ Strain Gages = MM, Type EA-13.050 AH-120 for Specimen I
SR-4, Type FAP-12-12 (FAP-6) for Specimen II

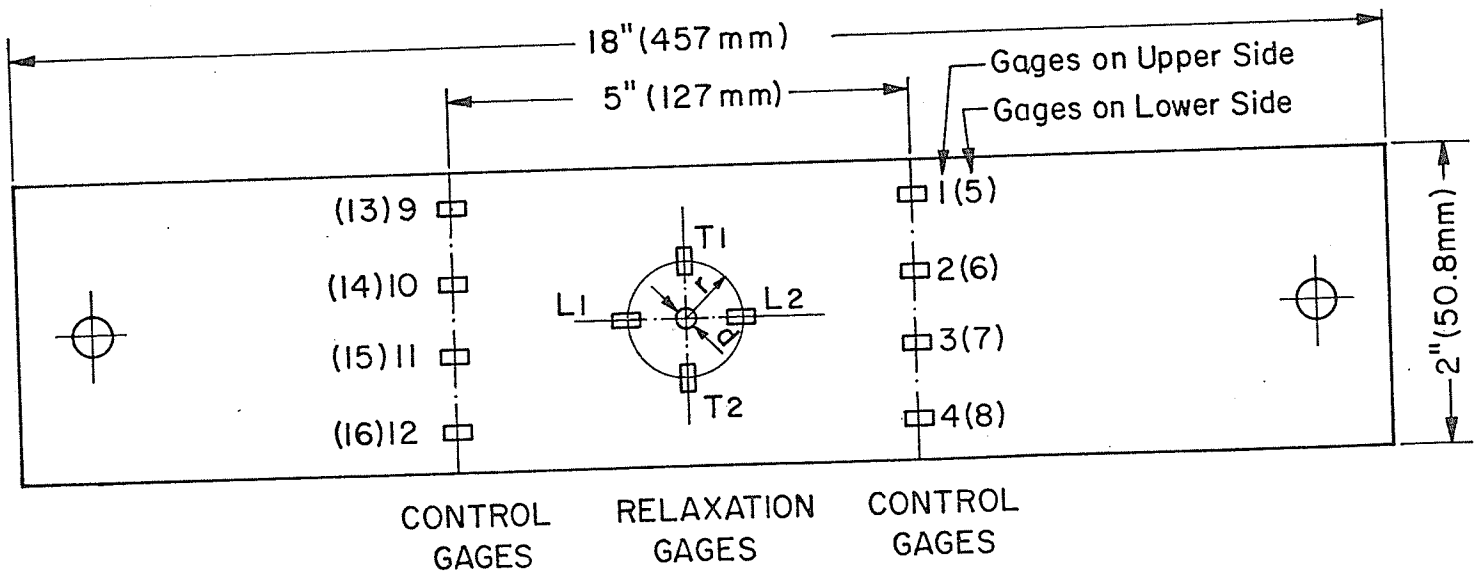

Figure 5.4 Test Specimen and Strain Gage Layout

figure. The strain gages were arranged in two groups - the control group and the relaxation group. The purpose of the control gage was to measure the magnitude of the uniform stress field as well as to assist in the detection and, if possible, elimination of any non-uniformity due to loading. The relaxation gages were used to measure the total strain relaxation. To assist in accurately locating the strain gages and to permit accurate drilling, a very small guide hole was first drilled at the specimen centre.

In the first experiment bending stresses were larger than desired (average of 6 percent of applied stress). Therefore, in the second experiment a different loading method was used wherein bending stresses were reduced (to an average of 3 percent) [87].

Testing consisted of primarily increasing the hole size by drilling and, at each increment of drilling, loading the specimen through a number of applied stress levels and recording the associated strain gage readings. A portable hand drill and sharp double-fluted H.S.S. drills were used in dry cutting the holes. It was felt that the requirement of a specially dressed end mill and a special milling guide are not justified in connection with thin materials. The effect of heat generation was small due to the large surface to volume ratio for thin plates. To avoid bending stresses that may result from drilling, specimens were backed with small blocks and low feeding rates were used. The use of a small guide hole kept the eccentricity error in hole location very small. This, backed by the small differences in readings of gages T1, T2 and L1, L2 (Figure 5.4) justified taking averages of those gage readings.

5.2.4 RESULTS

The results of experiments are given in Figures 5.5 and 5.6 for specimen I and in Figures 5.7 and 5.8 for specimen II.

5.2.5 DISCUSSION

The discussion of the results is presented in three subsections:

(i) Machining Effect.

(ii) Localized Plastic Flow Effect.

(iii) Recommended Values of λ.

i. Machining Effect:

The relaxation strain due to machining, ε_m, was determined by extrapolating the linear strain-stress relations to zero stress level and measuring the intercepts. Figure 5.9, determined from Figure 5.5, shows the variation of ε_m with the drilling clearance, c_d. The drilling clearance is the distance between the hole edge, where maximum machining stresses exist, and the near end of the gage matrix. Similar results could not be obtained from Figure 5.6, due to unknown error that reflects only on the intercepts. It should be mentioned that the highly localized nature of machining stresses together with the expected variability in their magnitude near the edge demands precise locations of the strain gages to be measured. Therefore, the parameter c_d is believed to be more adequate for this purpose.

It can be seen from Figure 5.9 that if the drilling clearance is kept greater than or equal to 0.16 in. (4.0 mm) the machining effect may

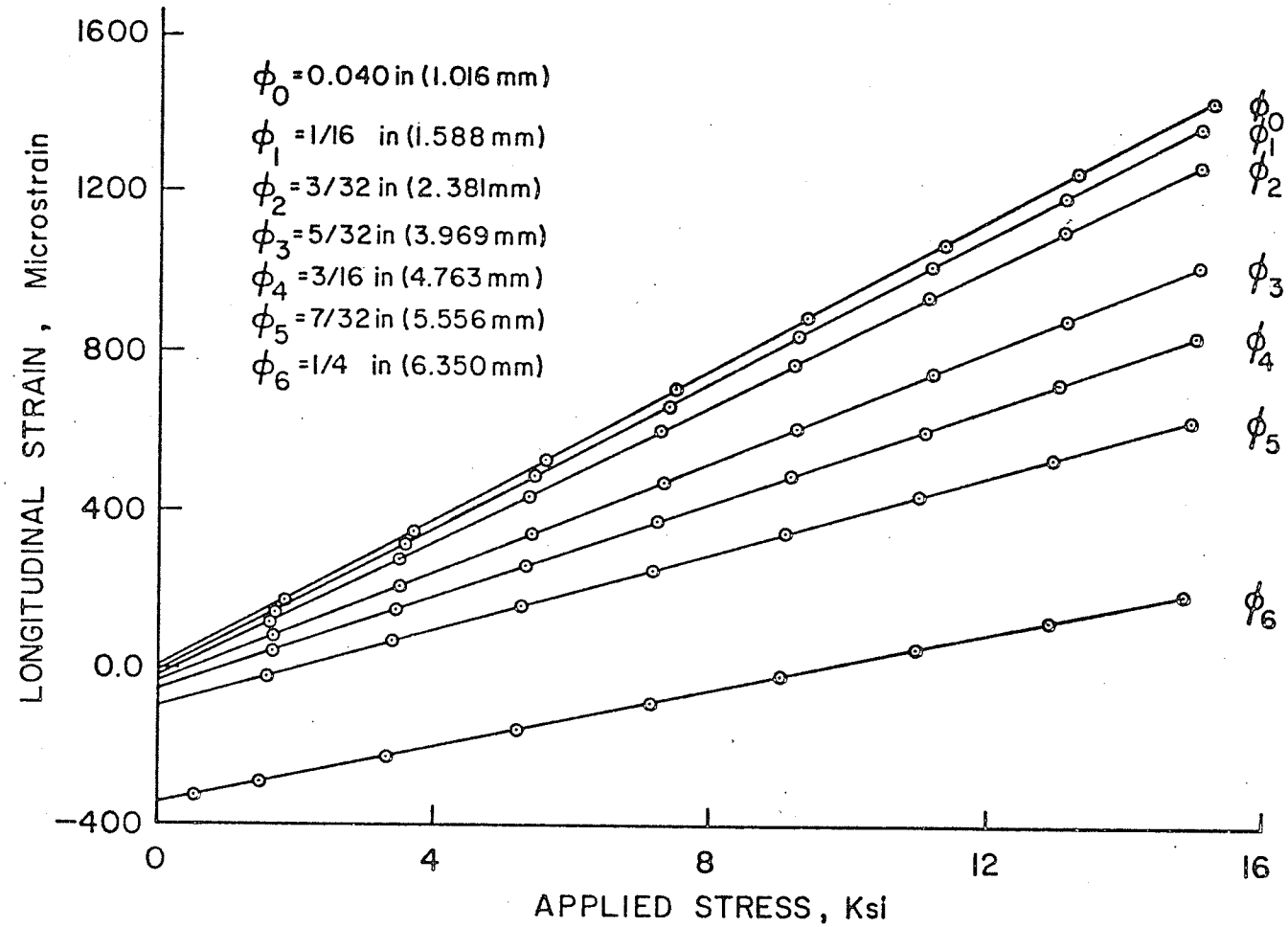

Figure 5.5 Results for longitudinal gages – Specimen I

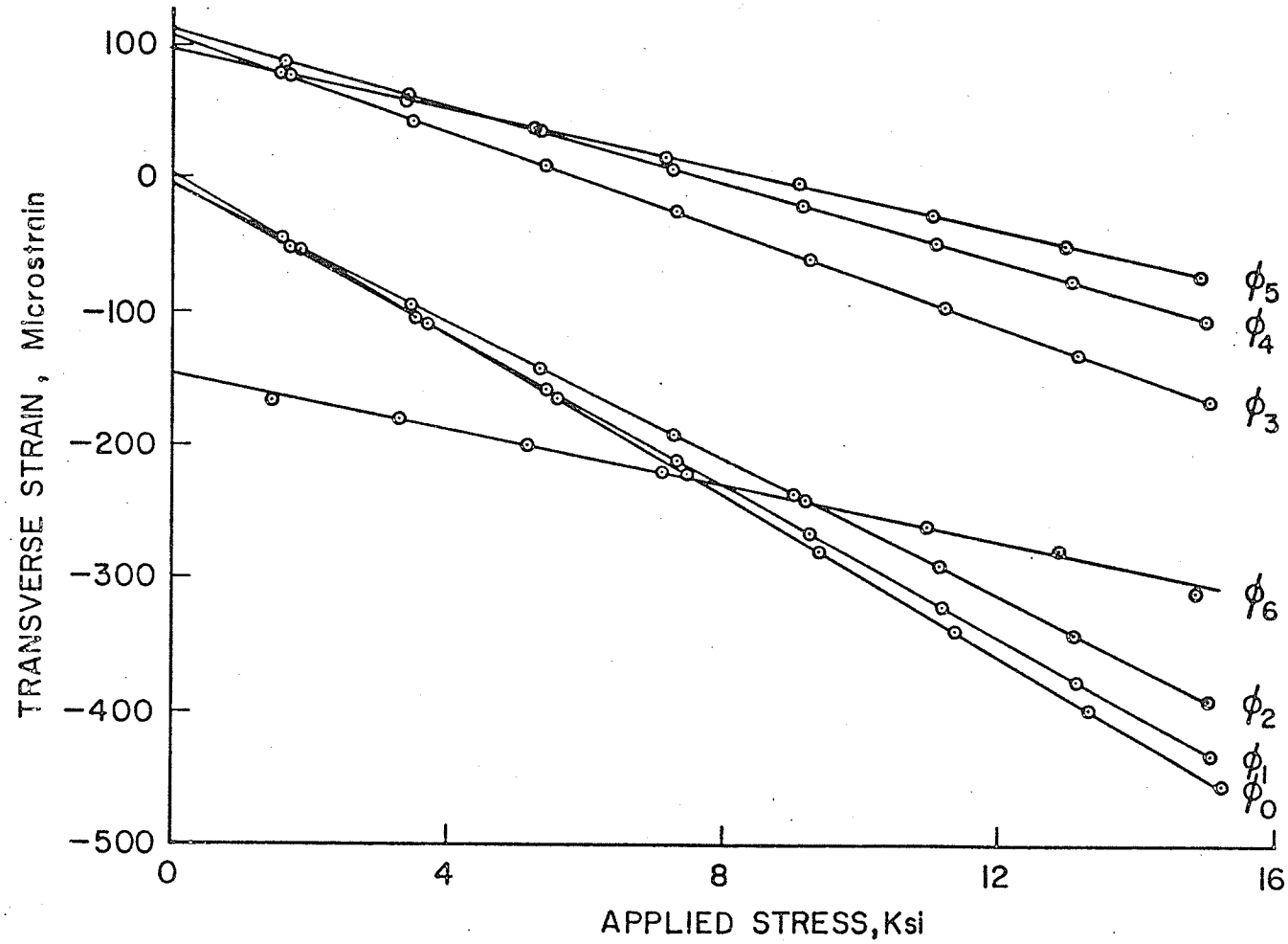

Figure 5.6 Results for transverse gages_ Specimen I

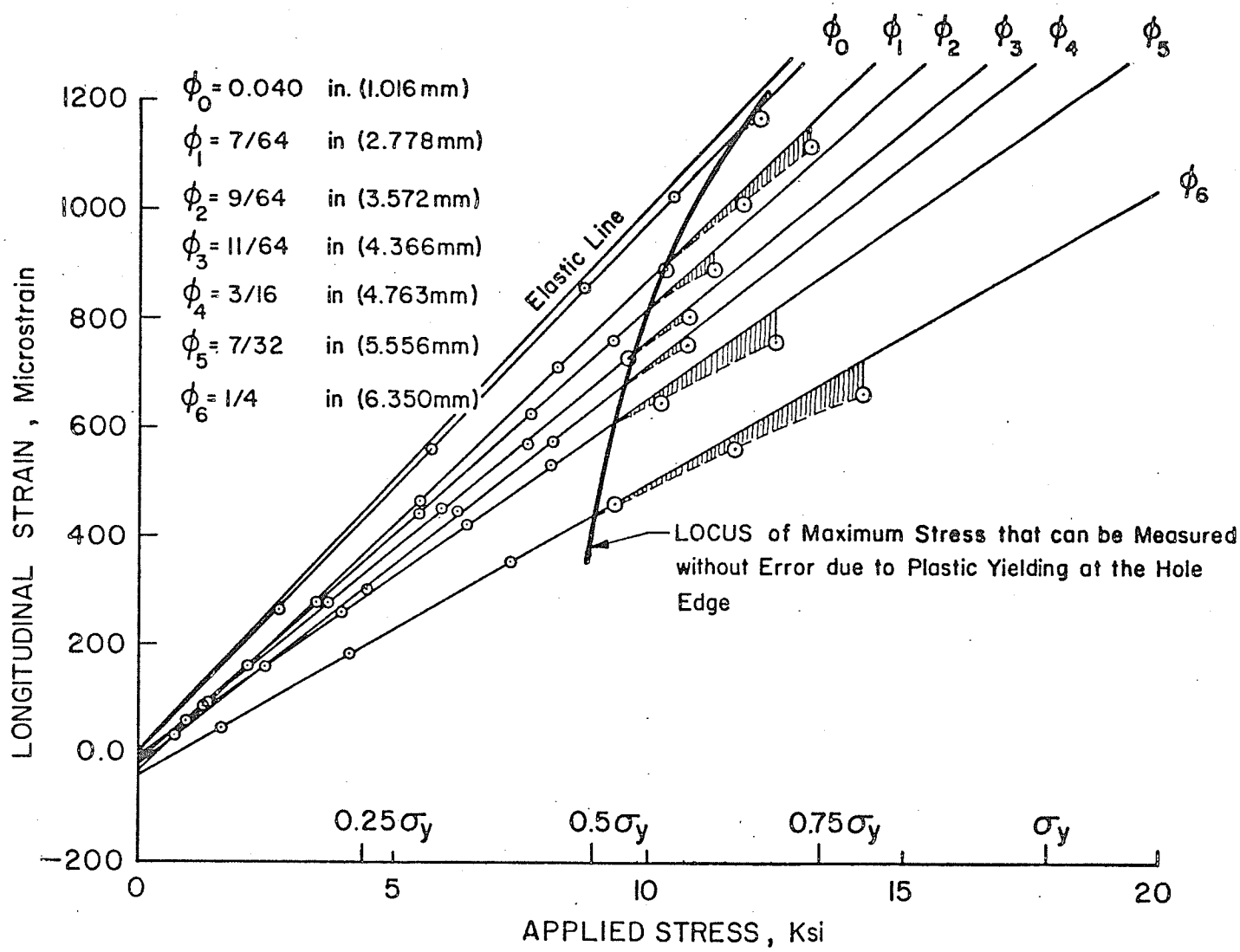

Figure 5.7 Results for longitudinal gages _ Specimen II

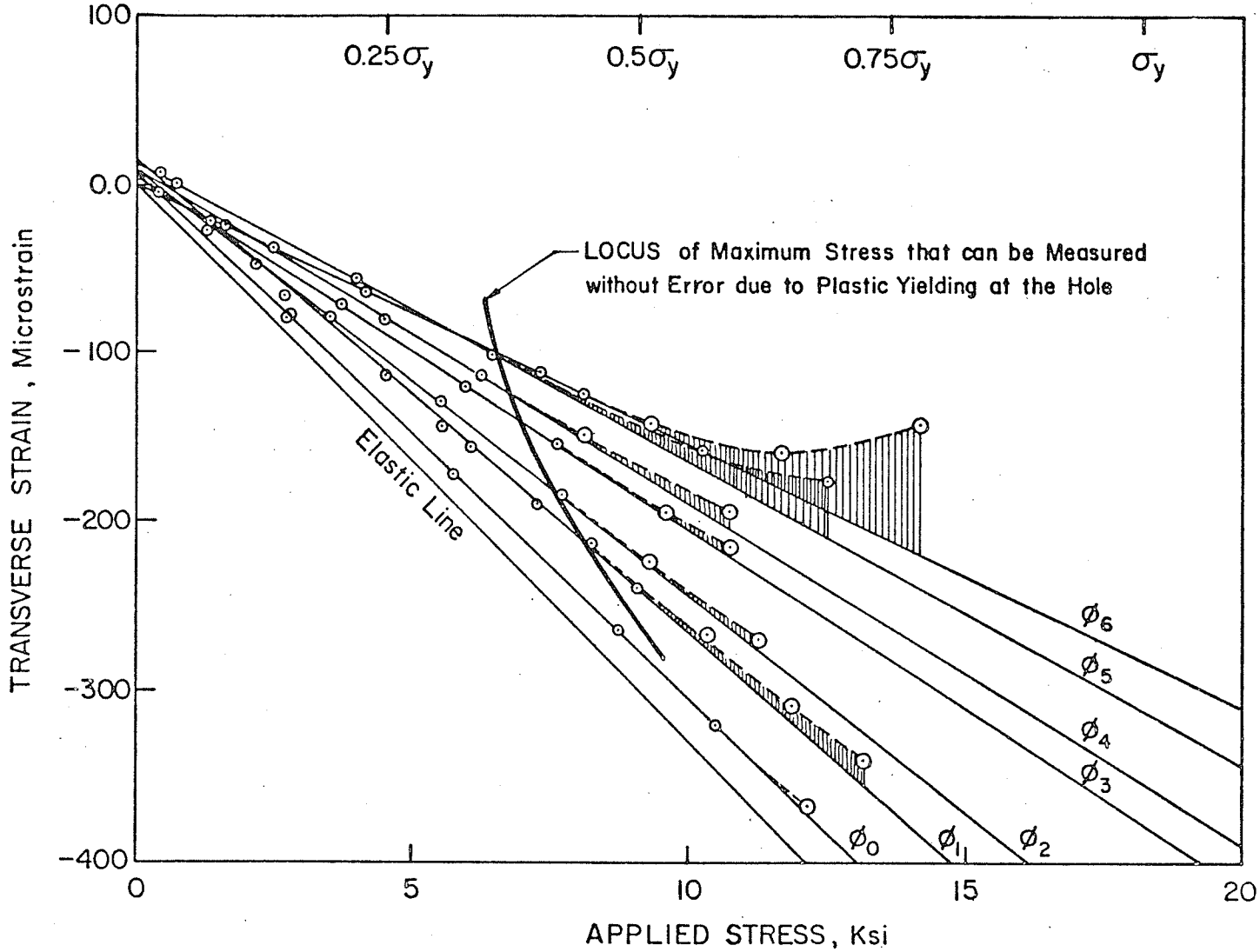

Figure 5.8 Results for transverse gages – Specimen II

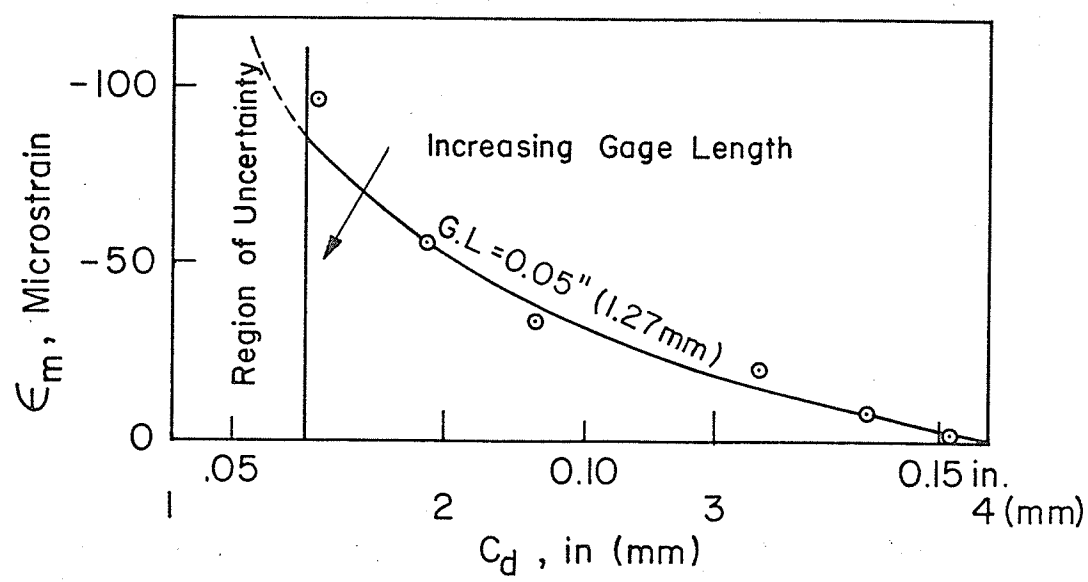

Figure 5.9 Values for the Relaxation Component Due to the Machining Stresses

be neglected ($\varepsilon_m = 0$). For smaller clearances the values of ε_m may be determined directly from the diagram. If gages with different gage length are used, c_d may be replaced by

$$c_d' = c_d + \frac{1}{2}(GL - 0.05) \text{ , in.}$$

or

$$c_d' = c_d + \frac{1}{2}(GL - 1.27) \text{ , mm} \qquad 5.9$$

where GL is the gage length. This is valid if the machining stress distribution over the gage length could be assumed linear.

Experiments on specimen II made use of the foregoing results. c_d was equal to 0.153 in. (3.88 mm) when the largest size hole was drilled and since a gage length of 0.12 in. (3.0 mm) was used, the maching effect ε_m will be negligible.

The value of the parameter λ may be calculated once the drilling clearance, the gage length to be used and the hole size are selected. Therefore,

$$\lambda = d/[c_d + \frac{1}{2} d + \frac{1}{2} GL] \qquad 5.10$$

ii. Localized Plastic Flow Effect:

Having eliminated the effect of machining stresses in experiment II, only the effect of localized plastic deformation remains to be studied. An examination of the results of Figures 5.7 and 5.8 suggests the following:

a. As the stress exceeds a certain value, the strain-stress relations

generally deviate from linearity, causing the absolute value of relaxation strain to increase. The "critical stress" at which the deviation starts is dependent on the hole size and strain gage location, or more conveniently, c_d. The locus of the "critical stress" that can be measured without error due to localized plastic yielding at the hole edge is shown, in both figures, to be a function of the gage orientation, i.e., the angle θ. It may be seen that these loci are asymptotic to 1/2 and 1/3 the yield strength in the parallel and transverse directions, respectively.

b. The interpretation of the experimental results may proceed from the principles enunciated in Figure 5.3. Thus, it may easily be determined that, in Figure 5.8, a stress of 0.75 σ_{yp} may be overestimated by as much as 30 percent (if $\lambda = 0.9$). The trend of deviation predicts that the error will drastically increase as the stress approaches the yield strength. Parallel gages, Figure 5.7, show a corresponding error of approximately 10 percent. Therefore, transverse gages are not recommended in measurements of stresses higher than one third the yield strength of the material.

c. Figure 5.10 is constructed from the results of Figure 5.7. Each curve represents the true value of stress σ_x and determines the corresponding relaxation component ε_p for values of c_d. The critical stress, that can be measured without error, i.e., $\varepsilon_p = 0$, may be determined at different values of c_d by interpolation between the given intercepts. A similar set of curves can be constructed for transverse gages or gages at any angle.

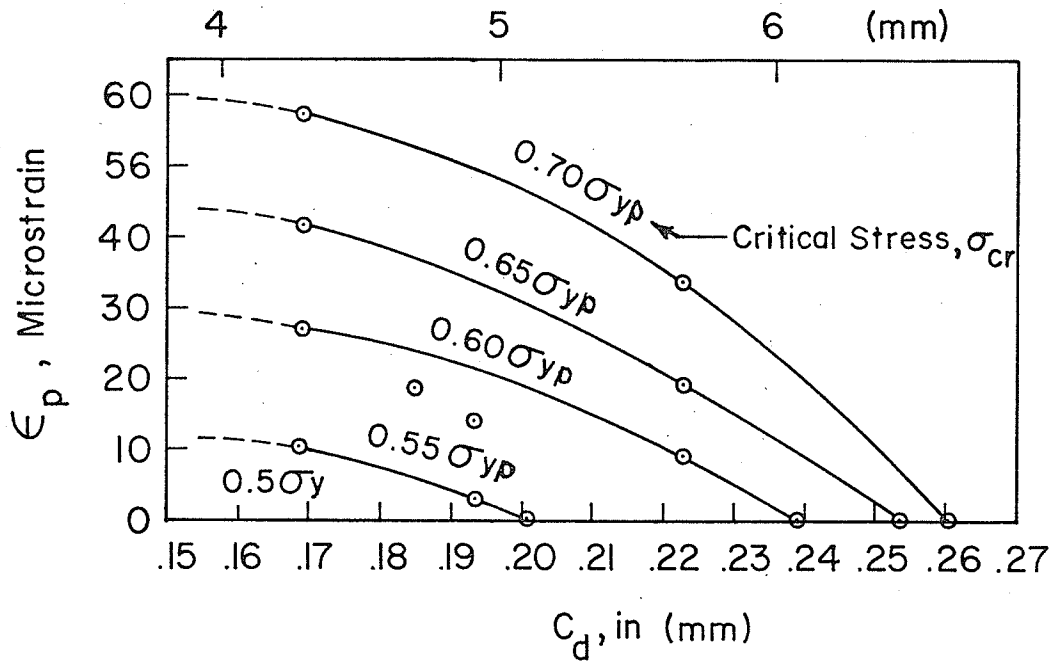

Figure 5.10 Values of ϵ_p for a Radial Gage at $\theta = 0$

d. When measuring stresses in excess of half the yield strength of the material, as c_d increases, λ decreases and the error due to plastic yielding decreases too. On the other hand, the relaxation coefficients become smaller. Therefore, the reduction of λ does not offer a practical solution to the problem and a compromise is necessary.

iii. Recommended Values of λ:

After correcting for the drilling and plastic flow effects, the relations between the strain and stress may be represented by a set of straight lines, one line for each value of the parameter λ. The strain relaxation is determined by subtracting the initial strain, determined by the elastic line at any stress level. Therefore, the values of the relaxation coefficients can be determined by direct substitution in Equation 5.5. The experimental relaxation coefficients were determined for radial and tangential gages and compared to the theoretical values at different values of λ. The comparison was sought in terms of the error in evaluating the stress when using the theoretical value of K_r. The results for both specimens are shown in Figure 5.11, from which it can be seen that values of λ of less than 0.5 are not recommended as error exceeds ±10 percent. However, it can be observed that the errors in the results of specimen I are generally higher than those of specimen II. This increase in error may be attributed to the observed non-uniformity of bending stresses. An uncancelled bending stress will virtually alter the slope of the strain-stress line, resulting in a corresponding error in the experimental value of K_r. It follows that a

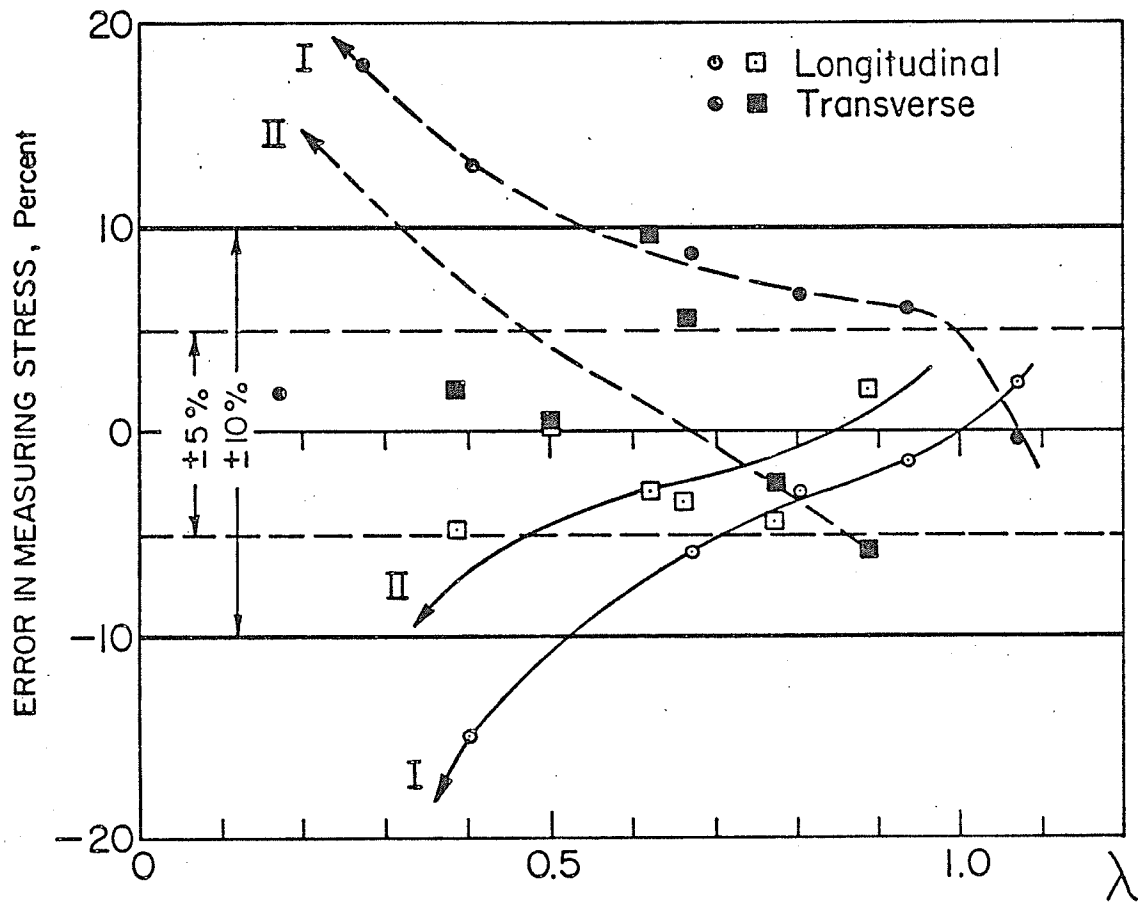

Figure 5.11 The Percentage Error in Determining the Stress as a Function of λ.

less conservative limit for an error of ±5 percent would be $\lambda = 0.5$. Extrapolation indicates that the upper limit of λ is approximately 1.2.

It may also be noted that the parallel gages have a slightly better accuracy than transverse gages. This difference may be due to the transverse sensitivity of electrical resistance strain gages. Several studies were conducted to assess the effect of transverse sensitivity on the evaluated strain gage measurement [88, 89, 90, 91]. Wu's results [88], in particular, indicate that a transverse sensitivity coefficient of 2-3 percent, which is a common value for smaller strain gages, may produce an error of up to 9 percent in the measured value of Poisson's ratio of aluminum alloys. In a later investigation, Beaney [90] has shown that the error in the numerically larger principal stress calculated from a strain gage rosette or from a pair of gages can be of the order of 1.3 times the cross sensitivity of gages. Therefore, that type of error will certainly lead to some difference between readings obtained by parallel and transverse gages. This may explain the slightly better accuracy of parallel gages. In view of the slight deviation that was observed it was felt that the effect of transverse sensitivity may not be taken into account.

The values of λ may be selected to reduce the error to an insignificant value. However, it has to be a compromise based on the error in measuring the stress and the correction values. Considering a total error of 2 percent which corresponds to 1000 psi in 50 ksi, it appears that for aluminum alloys, the hole-drilling technique is comparable in precision with the X-ray or other techniques.

5.2.6 SUMMARY

The modified hole-drilling procedure improves the practical value of the technique which extends the measurement to thin plates as well as thicker plates. The procedure for radial gages may be summarized in the following points:

1. Calculate the parameter $\lambda = d/r$.
2. Calculate the relaxation coefficient K_r from the first of Equations 5.6.
3. Using $c_d = r - (d + GL)/2$ and the gage length calculate c_d from Equation 5.9 and determine ε_m from Figure 5.9.
4. Set $\varepsilon_p = 0$.
5. Correct the measured strain relaxation ε_T according to Equation 5.8.
6. Using Equation 5.5 estimate the stress from

$$\sigma_x = \varepsilon_R \cdot E/K_r(\lambda,\theta) \qquad 5.11$$

7. If the estimated stress exceeds half the yield strength (for $\theta = 0^o$) use Figure 5.10 to find the value of the correction strain ε_p and then repeat steps 5 to 7 to obtain a better estimate of the stress. A number of iterations may be required in case of residual stresses approaching the yield strength.

This procedure is expected to yield measurements within ±5 percent. For instance, a stress of 30 ksi in aluminum may be measured to within ±1500 psi.

5.3 RESIDUAL STRESSES DUE TO EDGE DIMPLING

5.3.1 EXTENSION TO BIAXIAL STRESS MEASUREMENT

Several studies have been reported relating to the measurement of biaxial residual stresses by the hole drilling technique [78, 81, 82, 83]. The modified hole-drilling technique may also be used for this purpose although the relaxation coefficients are determined in a uniaxial stress field. The measured relaxation is a composite of that due to σ_x and σ_y.

Two distinct situations pertaining to biaxial stresses may exist depending on whether or not the principal directions are known: (i) unknown principal directions, and (ii) known principal directions.

i. If the principal directions are not known, it is necessary to use three strain gages (a rosette) to determine the stress field. With reference to Figure 5.12, each stress component will contribute to the net relaxation, ε_{Ri}:

$$\varepsilon_{Ri} = \frac{K_r(\lambda,\theta_i)}{E}\,\sigma_x + \frac{K_r(\lambda,90 - \theta_i)}{E}\,\sigma_y \qquad 5.12$$

where the subscript i = a, b, or c designates the strain gage location. Values of $K_r(\lambda,\theta)$ may be determined by Equation 5.6 in terms of θ_a, as θ_b and θ_c may be related to θ_a by the rosette angles. The simultaneous solution of Equations 5.12 will determine the values and orientation of principal stresses.

ii. If the directions of principal stresses are known, generally two strain gages will suffice to determine the stress field. Three different

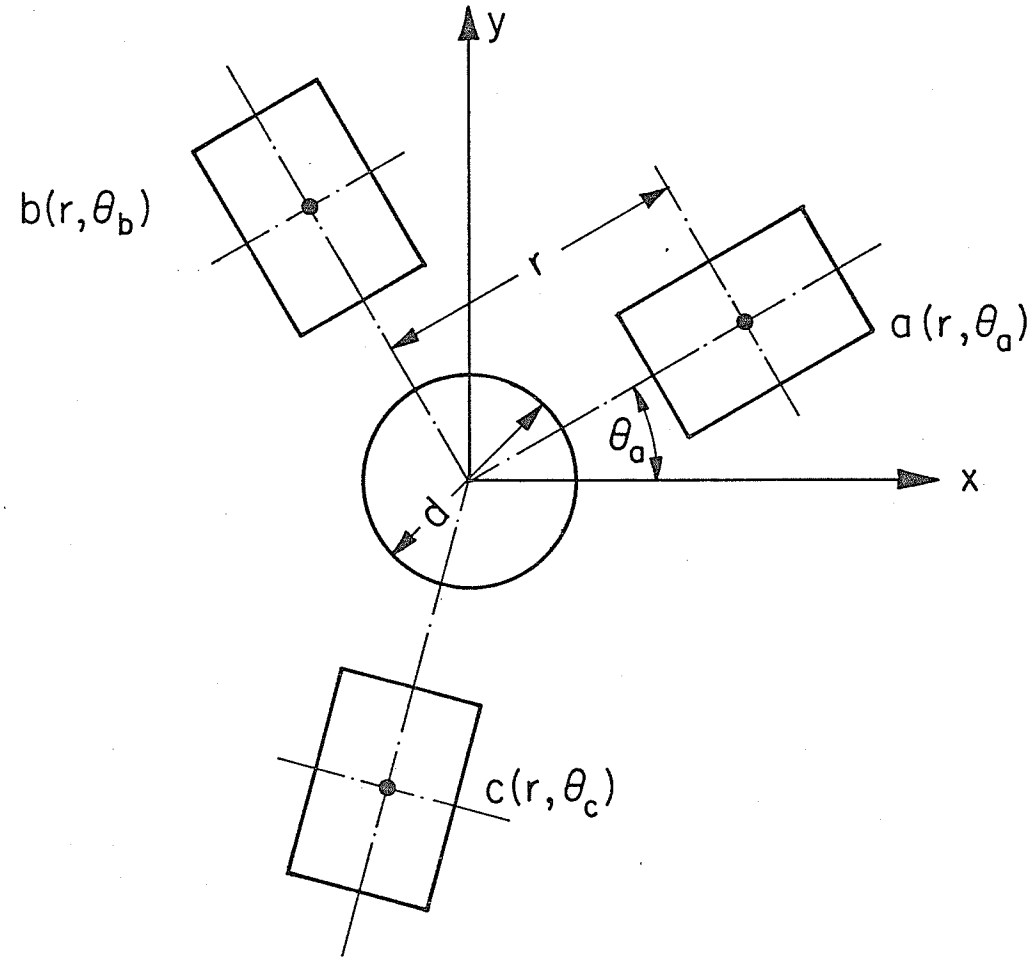

Figure 5.12 Strain gage arrangement for measuring bi-axial stresses

approaches may be followed:

a. Two gages located at right angle ($\theta = 0^o$ and $\theta = 90^o$), i.e., along the principal directions will indicate the strain relaxations

$$\varepsilon_{Rx} = \frac{K_r(\lambda,0)}{E}\sigma_x + \frac{K_r(\lambda,90^o)}{E}\sigma_y$$

$$\varepsilon_{Ry} = \frac{K_r(\lambda,0)}{E}\sigma_y + \frac{K_r(\lambda,90^o)}{E}\sigma_x \qquad 5.13$$

b. Two gages in line along $\theta = 0^o$. This arrangement may be used whenever it is not possible to place strain gages in the y-direction. The two strain gages, placed at different radii r_a and r_b, will yield relaxations:

$$\varepsilon_{Ra} = \frac{K_r(\lambda_a,0^o)}{E}\sigma_x + \frac{K_r(\lambda_a,90^o)}{E}\sigma_y$$

$$\varepsilon_{Rb} = \frac{K_r(\lambda_b,0^o)}{E}\sigma_x + \frac{K_r(\lambda_b,90^o)}{E}\sigma_y \qquad 5.14$$

Define a parameter $\alpha(\lambda)$ as the ratio of the relaxation coefficients at any value of λ:

$$\alpha(\lambda) = K_r(\lambda,90^o)/K_r(\lambda,0^o) \qquad 5.15$$

Substituting Equations 5.15 into 5.14

$$\varepsilon_{Ra} = \frac{K_r(\lambda_a,0^o)}{E}[\sigma_x + \alpha(\lambda_a)\cdot\sigma_y]$$

$$\varepsilon_{Rb} = \frac{K_r(\lambda_b,0^o)}{E}[\sigma_x + \alpha(\lambda_b)\cdot\sigma_y] \qquad 5.16$$

To obtain a solution, $\alpha(\lambda_a)$ should be substantially different from $\alpha(\lambda_b)$. However, in the practical range of λ, $\alpha(\lambda)$ maintains approximately a constant value. This corollary can easily be concluded from Figure 5.1. Thus, to obtain reasonable results using this method, one gage has to be placed in the close vicinity of the edge where $\alpha(\lambda) > 0$ and the other where $\alpha(\lambda) < 0$. But due to high machining stresses this approach becomes impractical unless stress-free hole machining is employed. At the present time, methods of stress-free metal removal are difficult to adapt to the general run of machining procedures and exhibit some difficulties in control of the hole location, size and depth.

c. One gage at $\theta = 0^o$. In certain cases, the biaxiality of the stress field is known. That is

$$\sigma_y = \beta \cdot \sigma_x \qquad 5.17$$

where β is a ratio known from previous testing or approximate analysis of residual stresses. Substituting Equations 5.17 and 5.15 into the first of Equations 5.13,

$$\varepsilon_{Rx} = \frac{K_r(\lambda, 0^o)}{E} [1 + \beta \cdot \alpha(\lambda)] \cdot \sigma_x \qquad 5.18$$

Therefore, one strain relaxation reading at $(\lambda, 0^o)$ will suffice to determine the residual stress. This approach is preferred whenever a limited number of strain gages has to be mounted or whenever it is not possible to mount transverse strain gages.

In the current investigation, the principal directions are known, and the numerical solution of residual stresses due to edge dimpling provides some estimate of the biaxiality ratio at all points of measurements. As a result the latter approach will be used in determining the residual stresses due to edge dimpling.

5.3.2 ADDITIONAL CONSIDERATIONS

Before proceeding with the experimental solution, it is necessary to consider several constraints associated with the application of the modified hole-drilling technique to the measurement of uniaxial stresses. These are:

1. The plate width should be at least 5 times the hole diameter and the distance from the hole to the near edge should be at least 2.5 times the hole diameter.
2. There is only one hole in the plate.
3. The stress should be uniform.

Practically, it is inevitable that these limits will be violated particularly when sufficient measurements are required to determine the stress distribution in a finite plate. Therefore, it becomes necessary to establish some legitimate departures from the limitations. This necessitates consideration of the following prior to experimental solution:

i. The effect of hole location.

ii. The effect of interaction between holes.

iii. The effect of stress gradients.

i. THE EFFECT OF HOLE LOCATION

Savin [92] considered the case of a semi-infinite plate with a hole of diameter d at a distance D from the plate edge subjected to a uniform stress of p , as shown in Figure 5.13. The values of stress concentration coefficient defined as σ_x/p are given (in the table attached to Figure 5.13) for three different points O, A and B, at the plate edge, the near hole edge and the far hole edge, respectively. From a careful examination of these values it appears that there is only a critical region in the narrow section O-A at which the stress distribution is greatly disturbed (as compared to the case of a central hole). For small values of $D/d \leq 1$, the disturbance causes the stress concentration coefficients at A and B to differ by more than 9 percent. For higher values of D/d the difference is continually reduced to zero. For instance, at $D/d = 1.55$ the difference is only 3 percent and the stress concentration coefficient at B differs by only 2 percent from the nominal value of 3. This convergence indicates that the strain at point C in Figure 5.13 will be essentially the same as that of a central hole case. Peterson [93] reproduced results of Mindlin and Udeguti in the same case, which indicate that for values of D/d of approximately 1.5 or more the deviation from the centered hole is small. The problem of stresses at the edge of an excentrically located hole in a finite plate under tension was solved by Sjöström in 1950. His results [93] show that an excentric hole in a finite plate has a stress concentration coefficient at A which is closer to the infinite plate solution of 3. It may, therefore, be reasonable to

D/d	σ_x/p at Point:		
	O	A	B
0.59	−4.080	5.064	3.362
0.67	−1.956	4.366	3.266
0.77	−0.895	3.919	3.201
0.91	−0.269	3.609	3.152
1.08	+0.134	3.396	3.115
1.29	+0.405	3.254	3.087
1.55	+0.591	3.162	3.065
1.88	+0.721	3.103	3.048
∞	+1.000	3.000	3.000

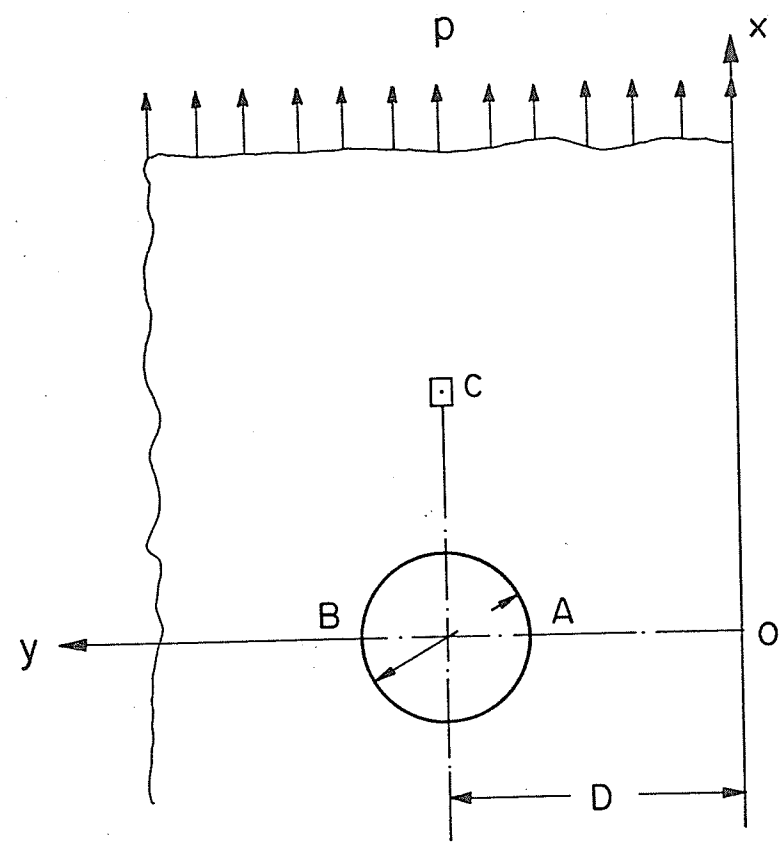

Figure 5.13 Effect of hole location, Savin [88]

keep the distance D to a minimum of 1.5d. In any case, no strain gages shall be placed in the narrow region O-A. Strain gages may be placed along the centreline y = d or in the region to the left as shown in Figure 5.13.

ii. THE EFFECT OF INTERACTION BETWEEN HOLES

The problem of a plate under uniaxial or biaxial stresses containing two circular holes of equal diameter, d, was discussed by Savin [93]. In the case of tensile stress p , as shown in Figure 5.14, it has been shown that the stress concentration factor changes with the change of the centre distance ratio $\gamma = C/d$, where C is the centre distance. Numerical values of stress concentration at points A and D are given in Figure 5.14. The results indicate that the major disturbance of stress occurs in the region between the two holes. It appears to be largely reduced for $\gamma > 5$ [93]. If transverse stress is small, it seems justifiable to assume that the disturbance of stress field along the line $y = \pm C/2$ due to the presence of the alternate hole is negligible. Therefore, the minimum centre distance between two holes may be taken as twice the hole size to ensure the independence of strain relaxations measured in the vicinities of each hole. In case of more than two holes, it becomes necessary to keep the centre distances as large as possible. The study of strain relaxation coefficients obtainable at various locations (r,θ) around a hole drilled in the stress field σ_x leads essentially to the same conclusion. Figure 5.15 shows a plot for the iso-relaxation lines, i.e., lines connecting all locations having the same radial

γ	σ_x/p at Point:	
	A	D
1.0	3.868	∞
1.5	3.151	3.264
2	3.066	3.020
3	3.020	2.992
5	3.004	2.997
8	3.001	2.999
∞	3.000	3.000

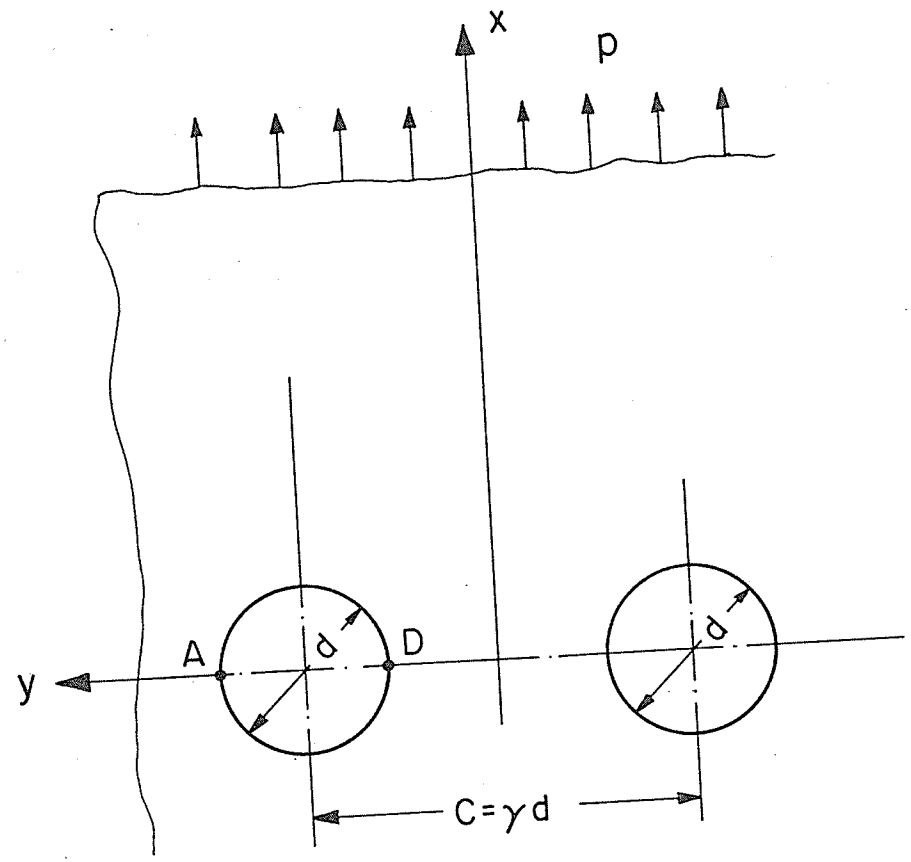

Figure 5.14 Interaction between two holes in a plate, Savin[88]

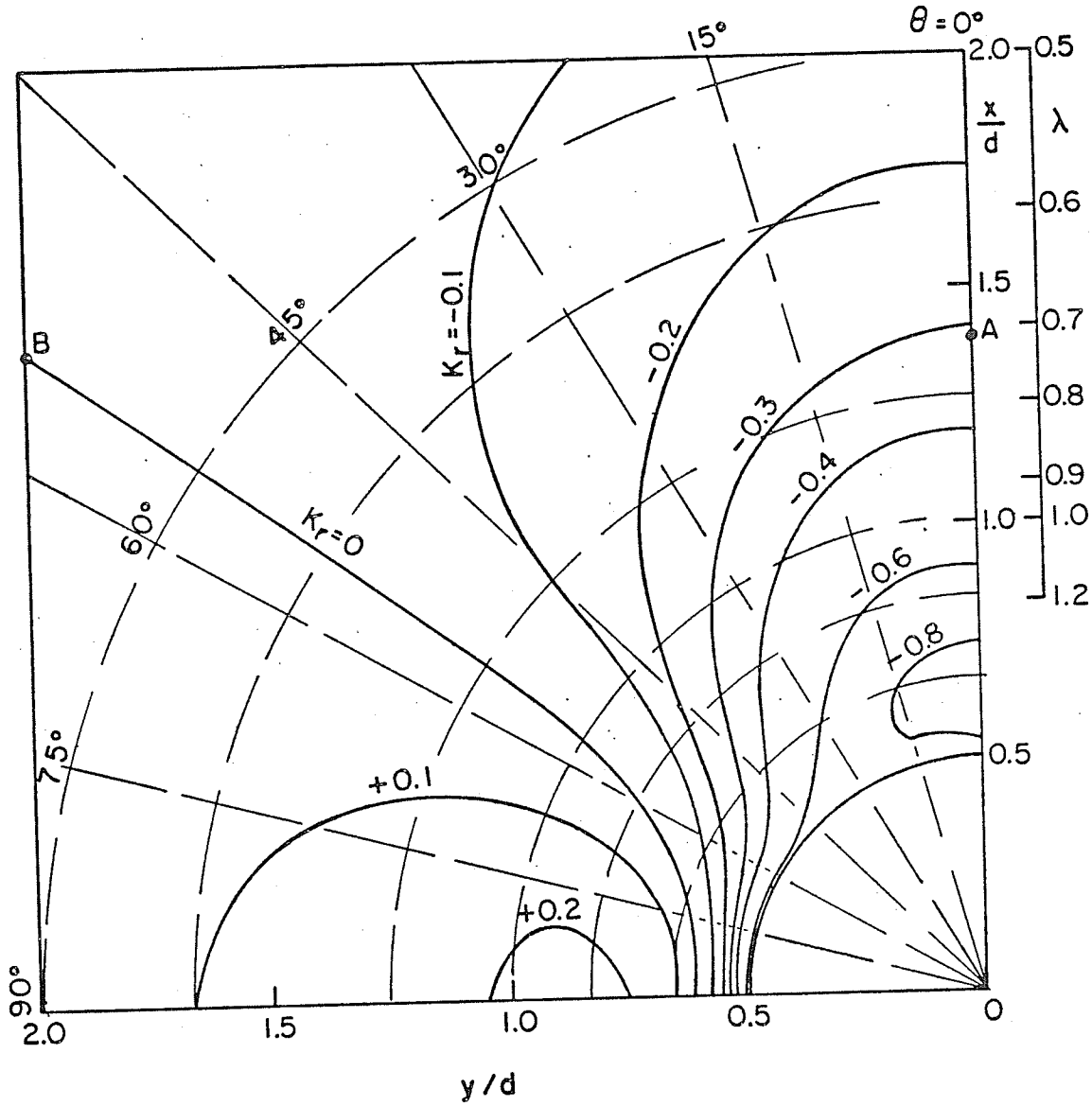

Figure 5.15 Iso-relaxation lines for a radial gage in the vicinity of a hole drilled at the origin O in the stress field σ_x.

relaxation coefficients. It is constructed from the data given in Figure 5.1. It can be seen that within the recommended range of λ, the highest relaxation is obtainable at zero angle with the direction of σ_x. For instance, consider point A where $\lambda = 0.72$ and $K_r(\lambda,0) = 0.312$. A radial gage placed at the same distance from the Y-axis but at greater radius from the hole centre will have a decreasing relaxation coefficient as y increases until it finally vanishes at point B, as shown in Figure 5.15. At point B, λ will drop to 0.21 and the angle will approximate 55°. If we consider a gage at B oriented to any direction, its relaxation coefficient will practically be zero. Therefore, a strain gage at B radially oriented towards a new origin O' will not be sensitive to the drilling of the hole at O. Conversely, the gage at A will not be sensitive to the drilling of a hole at O'. Since the sensitivity of the gage will not significantly change if the distance $\overline{AB}$ or $\overline{OO'}$ increases the minimum centre distance, $\overline{OO'}$, may be taken as 2d which will be sufficient to ensure independence of strain gage readings within the recommended range of λ. The iso-relaxation plot of Figure 5.15 may be used to determine iso-relaxation lines for any biaxiality ratio.

iii. THE EFFECT OF STRESS GRADIENTS

In a linearly-varying biaxial stress field, Cordiano and Salerno [81] have shown that the relaxation strain consists of three components. These components represent the uniform stress, the stress gradient and the shear stress at the point of measurement. If the stress varies only in the y-direction and measurements are taken in the

x-direction, the last two components disappear. Therefore, the effect of stress gradient is eliminated and the measured quantity will be the average value of stress at the hole centre. It follows that whenever it is reasonable to assume the uniformity of stress in one direction, the measurements may be made directly along this direction without regard to shear stress or stress gradient. In such cases, either two measurements along the same axis have to be taken or the biaxiality ratio has to be assumed. In case of nonlinear stress gradients, smaller strain gage-hole assemblies have to be used to make possible the assumption of linearity at the point of measurement.

5.3.3 EXPERIMENT

The experimental procedure for determining the residual stress distribution in edge-dimpled 2024-T3 aluminum alloy specimens is described. Since the measurement technique requires large specimens with enough space to permit a sufficient number of measurements to be taken, it was necessary to reproduce the same residual stresses in scaled-up specimens. This was easily done by scaling up the edge dimpling apparatus and material thickness while all the other non-dimensional parameters were maintained unchanged. Specimen dimensions and strain gage layout are shown in Figure 5.16. The hole and gage locations were selected in accordance with the general recommendations pertaining to the hole drilling technique [Section 5.2.5(iii)] and the considerations discussed in the preceding section [Section 5.3.2].

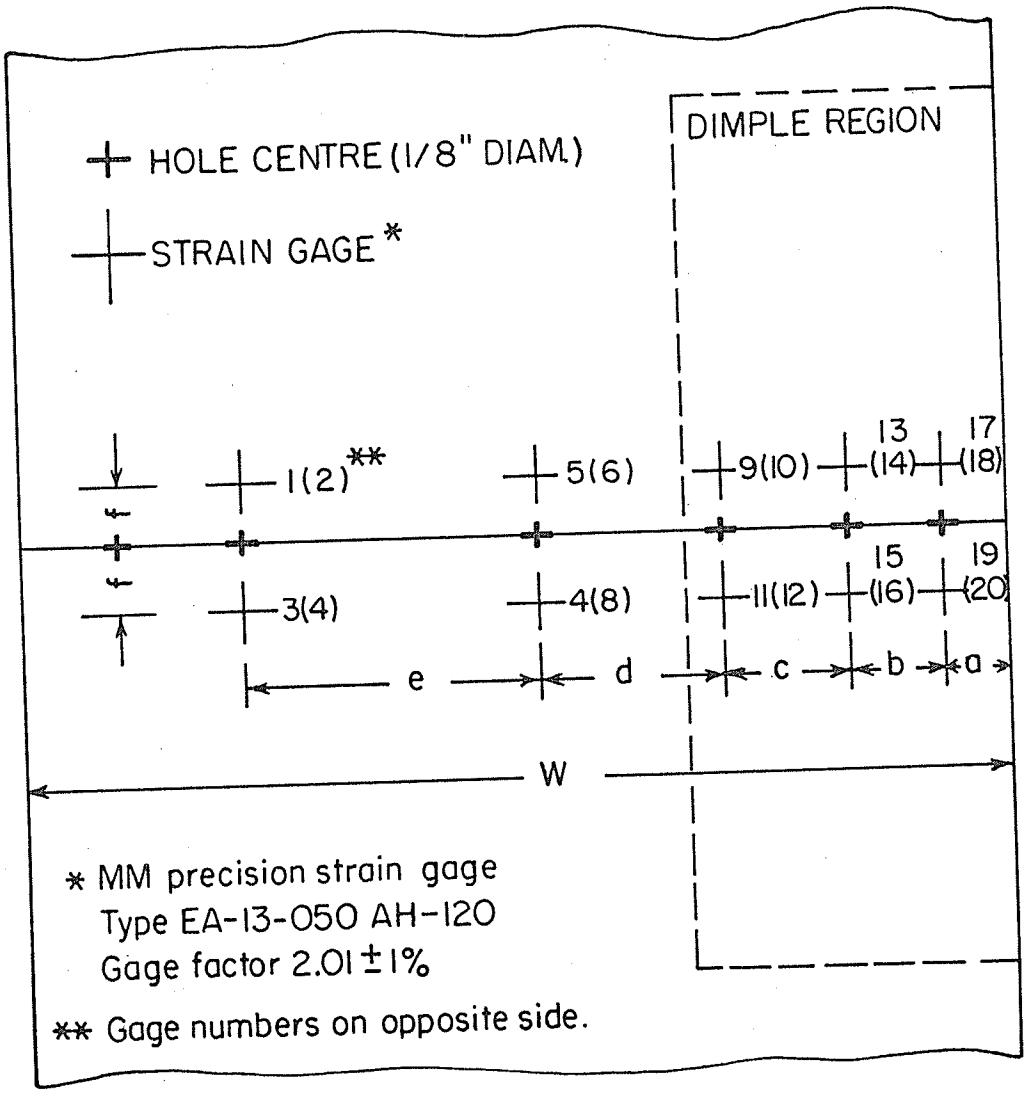

SPECIMEN		STRAIN GAGE LOCATIONS						HOLE SIZE	λ (NOMINAL)	C_d
		a	b	c	d	e	f			
O.D.S.	in.	5/32	1/4	5/16	7/16	3/4	5/32	1/8	0.79	0.07
	mm	4	6	8	11	19	4	3.2		1.8

Figure 5.16 Specimen and strain gage layout

Two drilling sequences may be utilized:

a. The inward drilling sequence (I.D.S.) in which the first hole is drilled at the farthest location from the dimpled region and then the drilling is continued towards and into the dimpled region.

b. The outward driling sequence (O.D.S.) in which drilling starts inside the dimpled region at the nearest location to the edge and then is sequentially continued in the other location.

It is found that correction for stress redistribution is easier if the O.D.S. is followed. Hence it is used as a basis for the determination of stresses. After each hole is drilled strain gage readings are recorded for all the hole locations. After the drilling is completed a travelling microscope is used to check the hole size and the eccentricity of drilling. It is found that the hole diameter is, on the average, 3 percent greater than the nominal size of the drill which is within the allowance of a medium accuracy drilling operation [94]. The distance between the hole centre and the strain gage centre is measured for each hole location. Any gage which, because of eccentric drilling, has a drilling clearance of less than the permitted value of 1.5 mm is not considered in the averaging of values for the particular hole.

5.3.4 RESULTS AND ANALYSIS

The measured relaxations of strain at each drilling step and for all hole locations are given in Table 5.1. Because of the placement of strain gages, and according to the discussion of section 5.3.2, the strain

TABLE 5.1

THE MEASURED RELAXATION STRAINS
FOR O.D.S. SPECIMEN
(MICROSTRAIN)

Hole Location	β	Drilling Sequence				
		5	4	3	2	1
1	-.41	+19	-3	+14	-7	106
2	0.30	-4	-4	+37	-66	-3
3	0.13	-33	+21	-308	0	-3
4	0.07	-54	-58	+18	-11	-2
5	0	+448	+28	+25	-16	0

+448 Relaxation of the remaining strain.

readings at a particular hole resulting from drilling at any other location are not true relaxation strains. They are due to stress redistribution resulting from drilling and must be corrected.

As a first step and neglecting the transverse stresses, the apparent stress changes may be calculated from Equation 5.11 as drilling takes place or from $E \cdot \Delta\varepsilon_x$ for changes of stress before drilling in the respective location. Values of the apparent stress are given in Table 5.2 with the estimates of the residual stress at the points of measurement. The residual stress, σ_x, at any hole location is estimated from

$$\sigma_x = \sigma'_x - \Sigma\Delta\sigma_x \qquad 5.19$$

where σ_x is the estimate of residual stress

σ'_x is the remaining residual stress at the time of drilling the hole

$\Sigma\Delta\sigma_x$ is the sum of changes of the residual stress due to redistribution of stress prior to drilling the hole, $\Delta\sigma_x = E \cdot \Delta\varepsilon_x$.

In a biaxial stress field (σ_x, σ_y), a change in stress of $\Delta\sigma_x$ and $\Delta\sigma_y$ results in a strain $\Delta\varepsilon_x$ as measured by the strain gages, given by:

$$\Delta\varepsilon_x = \frac{1}{E}\,[\Delta\sigma_x - \nu\,\Delta\sigma_y] \qquad 5.20$$

If we assume that the redistribution of stress is proportional to the stress, then:

$$\frac{\Delta\sigma_y}{\Delta\sigma_x} = \frac{\sigma_y}{\sigma_x} = \beta \qquad 5.21$$

TABLE 5.2

APPARENT STRESS CHANGES
AND RESIDUAL STRESSES, psi

Hole Location	Drilling Sequence					Residual Stress
	5	4	3	2	1	
1	+201	-32	+148	-74	-3,601	-3,844
2	-42	-42	+392	+2,186		+1,878
3	-350	+223	+11,297			+11,424
4	-572	+1,880				+2,452
5	-17,853					-17,853

$$\Delta\sigma_x = E \cdot \Delta\varepsilon_x$$

$$\boxed{\sigma'_x} = \frac{E\ \varepsilon_R}{K_r(\lambda,\theta)}$$

$$\sigma_x = \sigma'_x - \Sigma\Delta\sigma_x$$

and Equation 5.20 becomes

$$\Delta\sigma_x = E \cdot \Delta\varepsilon_x / (1 - \nu\beta) \qquad 5.22$$

The remaining stress, σ_x' , in a biaxial stress field is determined by substituting the net strain relaxation, ε_R, (as drilling takes place) and the biaxiality ratio into Equation 5.18. Therefore,

$$\sigma_x' = \frac{E \cdot \varepsilon_R}{K_r(\lambda,\theta)\ [1 + \beta \cdot \alpha(\lambda)]} \qquad 5.23$$

Values for the biaxiality ratio, β , were determined from the finite element solution of the problem discussed in Section 4.2.3. Values of β are given in the second column of Table 5.1. It was found that transverse residual stresses disappear in the vicinity of the edge and reach their maximum values outside the dimple region. The changes of stress and, hence, estimates of the residual stress are calculated with the biaxiality taken into account using Equations 5.22, 5.23 and 5.19. The results are given in Table 5.3. However, it can be seen that the influence of transverse stresses on measurements is insignificant.

An examination of column 3 of Table 5.3 which gives the changes of stress due to the drilling of the hole at location 5 indicates that the change of stress at any location is proportional to the residual stress except for location 4 where a very steep stress gradient exists. Therefore, it is reasonable to assume that a similar reduction of stress at the location of drilling has taken place during the action of drilling. This will, in turn, result in an error in estimating the residual stress

TABLE 5.3

CHANGES OF STRESS AND RESIDUAL STRESSES (psi)
WITH CONSIDERATION OF BIAXIALITY

Hole Location	β / $\alpha(\lambda)$	Drilling Sequence 5	4	3	2	1	Residual Stress
1	-0.41 / -0.492	+177	-28	+130	-65	-2,997	-3,211
2	0.30 / -0.446	-47	-47	+435	+2,524		+2,183
3	0.13 / -0.453	-366	+233	+12,004			+12,137
4	0.07 / -0.443	-586	+1,940				+2,526
5	0 / -0.457	+17,853					-17,853

$$\Delta\sigma_x = \frac{E \cdot \Delta\varepsilon_x}{(1 - \nu \cdot \beta)}$$

$$\boxed{\sigma'_x} = \frac{E \cdot \varepsilon_R}{K_r(\lambda,\theta)} \left\{\frac{1}{1 + \beta \cdot \alpha(\lambda)}\right\}$$

$$\sigma_x = \sigma'_x - \Sigma\Delta\sigma_x$$

at the location of drilling. To rectify this error assume that the remaining residual stress prior to drilling, σ_x' , drops by $\Delta\sigma_x'$ during drilling leaving a net residual stress σ_x'' given by

$$\sigma_x'' = \sigma_x' - \Delta\sigma_x' \qquad 5.24$$

Therefore, the relaxation strain will have two components; one is due to $\Delta\sigma_x'$ and the second is due to σ_x'' :

$$\varepsilon_R = \frac{\Delta\sigma_x'}{E} + \frac{\sigma_x'' \cdot K_r(\lambda,\theta)}{E} \qquad 5.25$$

Therefore,

$$\sigma_x'' = \frac{E \cdot \varepsilon_R}{K_r(\lambda,\theta)} + \frac{\Delta\sigma_x'}{K_r(\lambda,\theta)} \qquad 5.26$$

Using Equations 5.24 and 5.26, the true remaining stress before drilling the hole will be:

$$\sigma_x' = \frac{E \cdot \varepsilon_R}{K_r(\lambda,\theta)} + \Delta\sigma_x' \left[1 - \frac{1}{K_r(\lambda,\theta)}\right] \qquad 5.27$$

where $\Delta\sigma_x'$ is the drop in residual stress. It is evident that neglecting the second term of Equation 5.27 results in an error proportional to $\Delta\sigma_x'$. In biaxial stresses $K_r(\lambda,\theta)$ may be replaced by $K_r(\lambda,\theta)\cdot(1 + \beta\cdot\alpha(\lambda))$. The drop $\Delta\sigma_x'$ may be estimated from stress reduction at other locations. Table 5.4 gives the percentages of stress change. Assuming a drop $\Delta\sigma_x' = 0.03\ \sigma_x$ at the first hole location and substituting this into Equation 5.27 obtain $\sigma_x' = 20{,}400$ psi (136 MPa). In other locations it

TABLE 5.4

PERCENTAGE REDUCTION OF RESIDUAL STRESSES DUE TO THE REDISTRIBUTION

Hole Location	Drilling Sequence				
	1	2	3	4	5
1	-5.5	+0.9	-4.2	+2.2	?
2	-2.2	-2.2	+20.8	?	
3	-3.0	+2.0	?		
4	-23.2	?			
5	?				

seems that due to the redistribution of stress, the peak stresses swing right and left resulting in no clear trend of change. Therefore, the correction was not made except for the first hole location.

The final results are plotted in Figure 5.17 from which it may be deduced that the stress distribution is nearly balanced.

5.4 COMPARISON OF RESULTS

Comparison of experimental and analytical results is shown in Figure 5.17. The results indicate good agreement in the edge region which is the most critical to fatigue. It also indicates that the locations of peak tensile stress are almost identical. However, the peak values differ. This difference will directly influence the prestress limit at which inelastic deformation starts. It can be seen that this limit will drop from 0.65, the yield stress, to a figure in the vicinity of 0.5. Slight differences in the results are observed in the interior region. These differences may be attributed to the approximate nature of the analytic solution. The idealization of the stress-strain relations and its effect on the dimpling strain distribution, as illustrated in Figure 4.5, will reflect on the residual strain distribution. This in turn will most probably be the cause for this anomaly in the interior region. However, it should be indicated that the agreement is very reasonable in the edge region as the idealizaiton of the analytic solution is not likely to influence the edge residual stress.

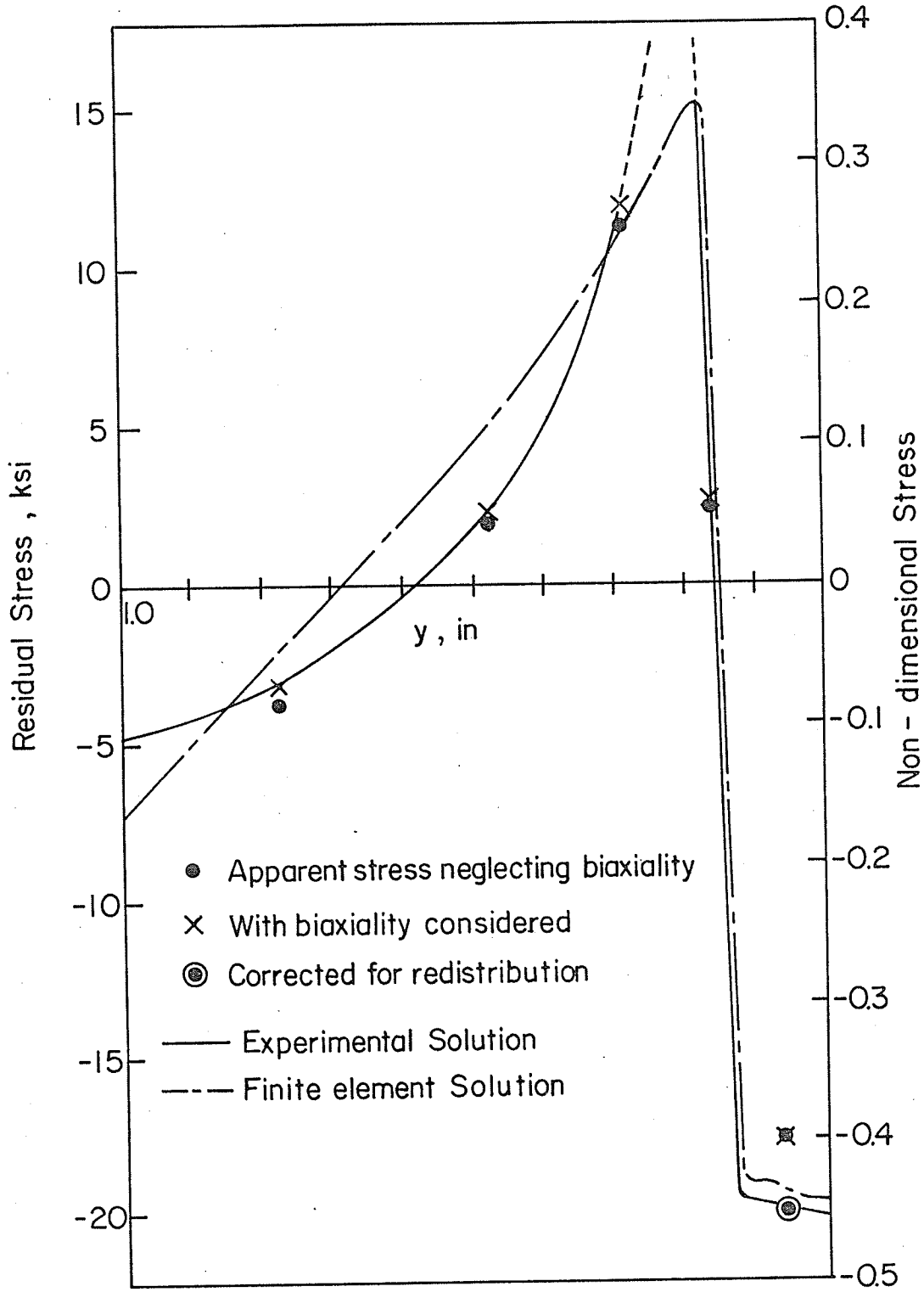

Figure 5.17 The residual stress distribution in edge-dimpled specimen.

5.5 SUMMARY

The study presented in this chapter describes a modified hole-drilling technique which eliminates the major disadvantages associated with the conventional hole-drilling procedure. The modified technique was employed to measure the residual stress distribution due to edge dimpling. Due to the nature of this distribution and the possibility of stress gradients in the thickness direction, the technique was used to determine the average residual stress in the specimen. The biaxiality of planar stresses did not seem to have a significant effect on the measurements. The experimentally determined residual stresses were found to be in good agreement with those obtained numerically by the finite element method. At this point, the residual stress distribution due to edge dimpling is determined quantitatively and qualitatively and in the following chapter we will proceed to the assessment of fatigue strength improvement and its relation to residual stress.

CHAPTER 6

EXPERIMENTAL FATIGUE TESTING PROGRAM

6.1 OBJECTIVES

An experimental program was carried out to assess the fatigue strength improvement by edge dimpling. The main objectives of the program were:

a. The optimization of the edge dimpling procedure. Since edge dimpling involves several parameters which control the magnitude and distribution of residual stresses and, hence, fatigue strength of the material, it is necessary to determine the best combination of parameters that is most beneficial. Therefore, it is desirable to find the optimum value, or range of values, of the average edge strain which gives the greatest fatigue strength improvement. It is assumed for the purpose of this dissertation that this optimum characteristic parameter is independent of the fatigue stress level. Once an optimum average edge strain is determined it will be fixed during the entire testing program.

b. The determination of fatigue strength improvement due to the optimum dimpling procedure. This is achieved by comparing the results of dimpled and undimpled specimens with S-N data obtained for plain specimens. The testing is intended to be in the high cycle region as the influence of residual stress in the low cycle range seems to decay due to gross plastic flow [95].

c. The study of the effect of preloading (prior overloading) on the fatigue strength improvement. This provides a simulation of gust loads in an actual load spectrum. The results are believed to reflect the effect of dimpling in actual service loading.

d. The correlation of fatigue improvement and residual stresses as determined in Chapters 4 and 5.

6.2 EXPERIMENTAL PROGRAM

6.2.1 TEST SPECIMENS

Preliminary fatigue testing using conventional dog-bone shaped specimens have shown that due to the strengthening effect of edge dimpling failures always occurred outside the test section (for instance, at the grips). Therefore, to obtain meaningful data, specimens had to be redesigned to cause failures to occur at a specific test section. It was necessary to notch the specimens at the middle section of the dimpled area where the largest residual stresses exist. Subsequently, notched specimens did not have to be of the conventional curved type and rectangular specimens were used. However, conventional specimens were used to obtain the control data for unnotched material. To assure that the comparison between specimens having different shape is still valid, comparative tests were performed using notched specimens of both types. The results are reported in Appendix A.1. It was concluded that there was no significant difference between notched specimens of both types.

Furthermore, it is believed that the fatigue strength improvement obtained in notched specimens is representative of improvement in unnotched specimens.

Accordingly, two different types of specimens were used. Details of shape and dimensions of each are given in Figure 6.1. Type-A specimens were used to obtain comparative data with and without dimpling in all preliminary and primary testing while type-B specimens were used only to determine reference data for plain specimens. Specimens were made of 2024-T3 alclad aluminum alloy. The nominal chemical composition and mechanical properties of this material are given in Table 6.1. Specimens were oriented in the rolling direction and were machined in batches under similar machining conditions to minimize the effects of variability in machining on the results.

6.2.2 TEST EQUIPMENT

All fatigue testing was performed on a Sonntag-Baldwin fatigue testing machine model SF-1.U at a test frequency of 1800 load cycles per minute (30 Hz). The machine is a single rotating weight type and has a capacity of 1000 ± 1000 pounds. Figure 6.2 is a view of the testing machine loaded with a type-B specimen. Closer view of the clamping system is shown in Figure 6.3. It whould be mentioned that the holes in the clamping area of specimens type-B are used only for clamping purposes and all of the load is transmitted through friction between the grips and the specimen.

in.	mm.	in.	mm.
0.050	1.27	1	25.4
3/4	19.05	2	50.8
1-5/16	33.34	3	76.2
1-1/2	38.10	5	127.0
		6	152.4

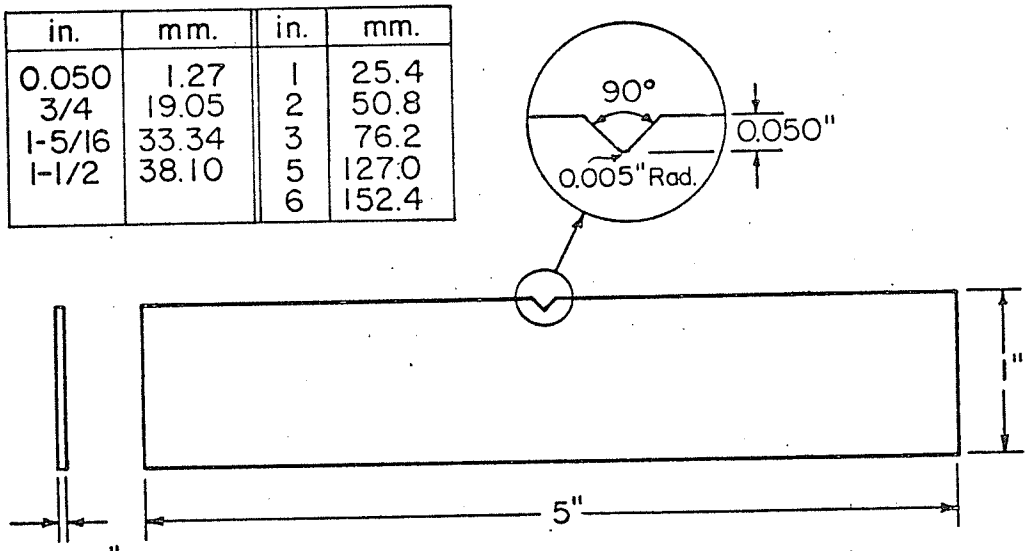

(a) Type-A Rectangular Specimens (with 90° notch)

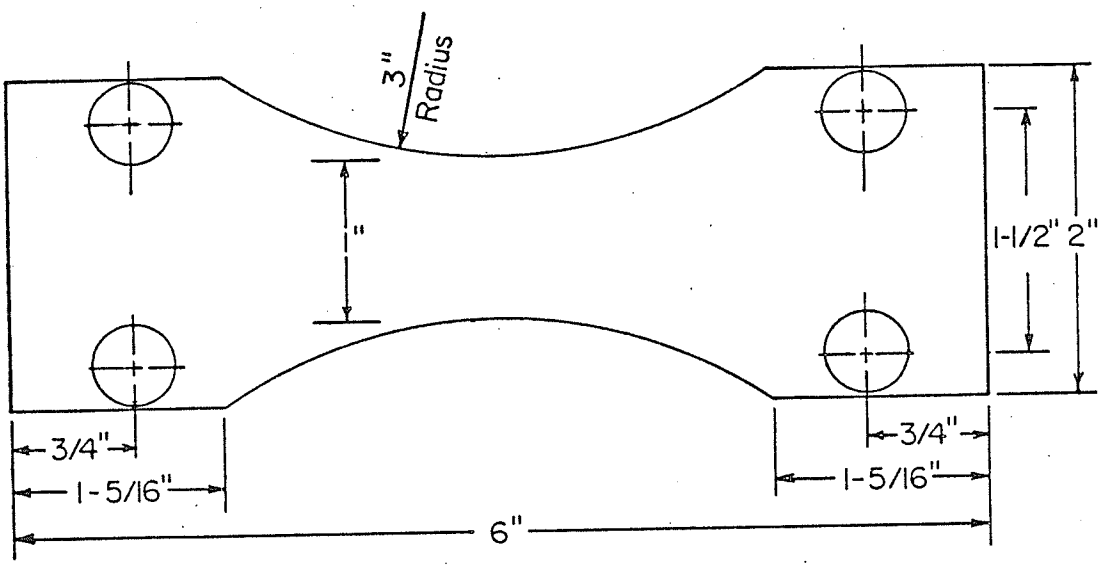

(b) Type-B Curved Control Specimens (Plain)

Figure 6.1 Types of Fatigue Specimens: shape and size.

TABLE 6.1

NOMINAL CHEMICAL AND MECHANICAL PROPERTIES OF

2024-T3 ALCLAD ALUMINUM ALLOY SHEET

Ref. Metals Handbook, ASM Part 1, Ed. 8.

Nominal Chemical Properties

Cu	4.5%
Mg	1.5%
Mn	0.6%

Nominal Mechanical Properties

Ultimate Tensile Strength	65,000 psi. (450 MPa)
Yield Strength	45,000 psi. (312 MPa)
Hardness (Rockwell E)	90-100
% Elongation (2 in. G.L.)	18
Modulus of Elasticity	10.6×10^6 psi. (7.3×10^4 MPa)

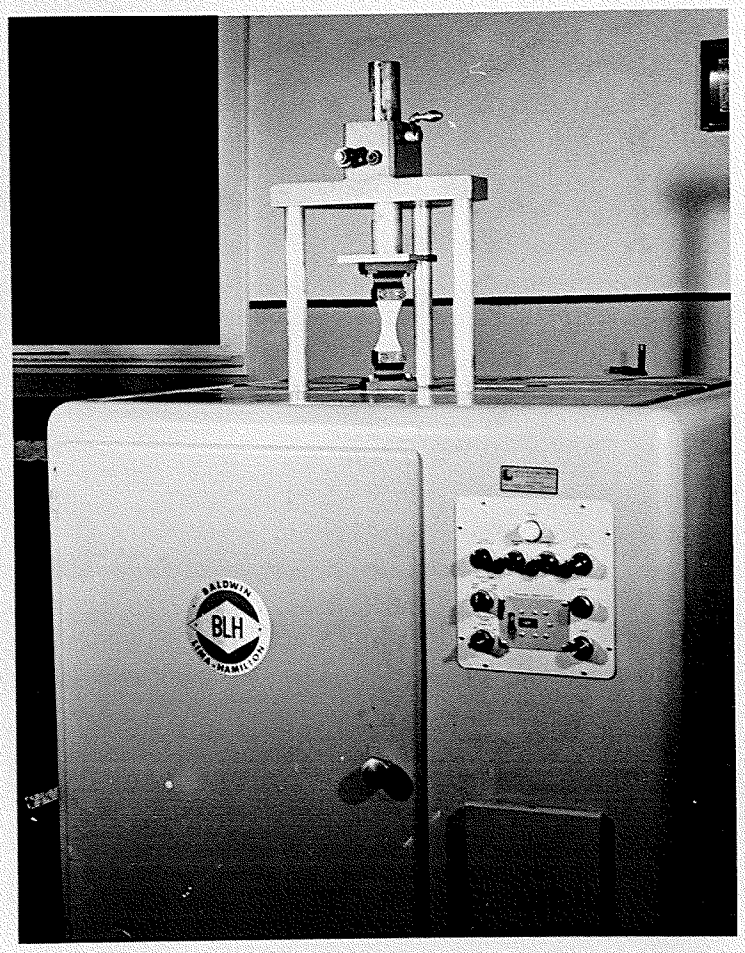

Figure 6.2 Sonntag Baldwin fatigue testing machine (Model SF-1-U)

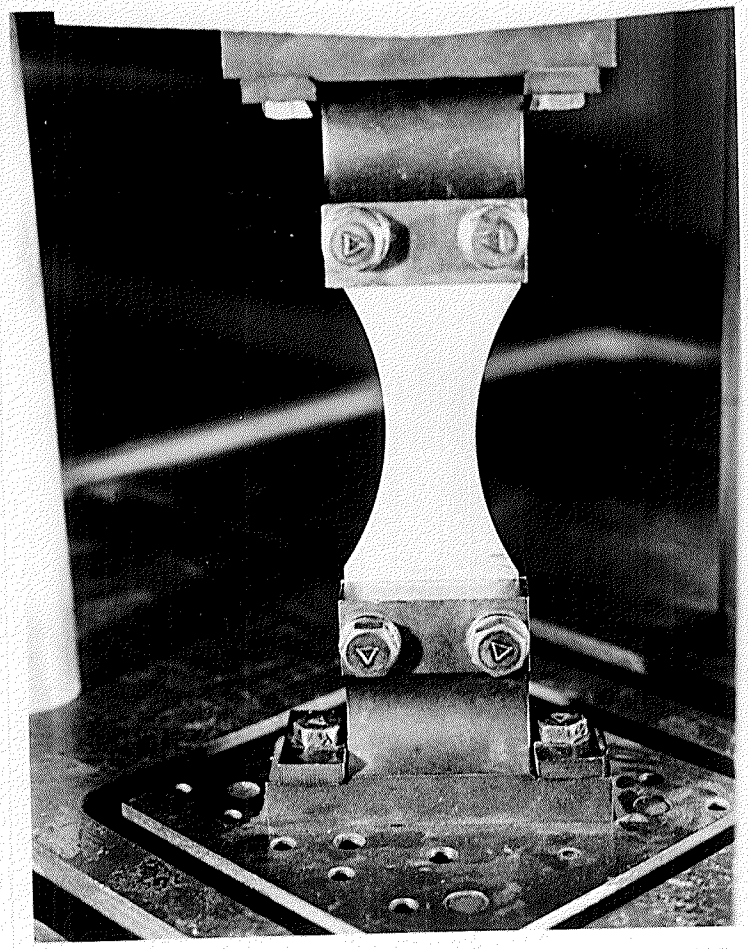

(a) Front View

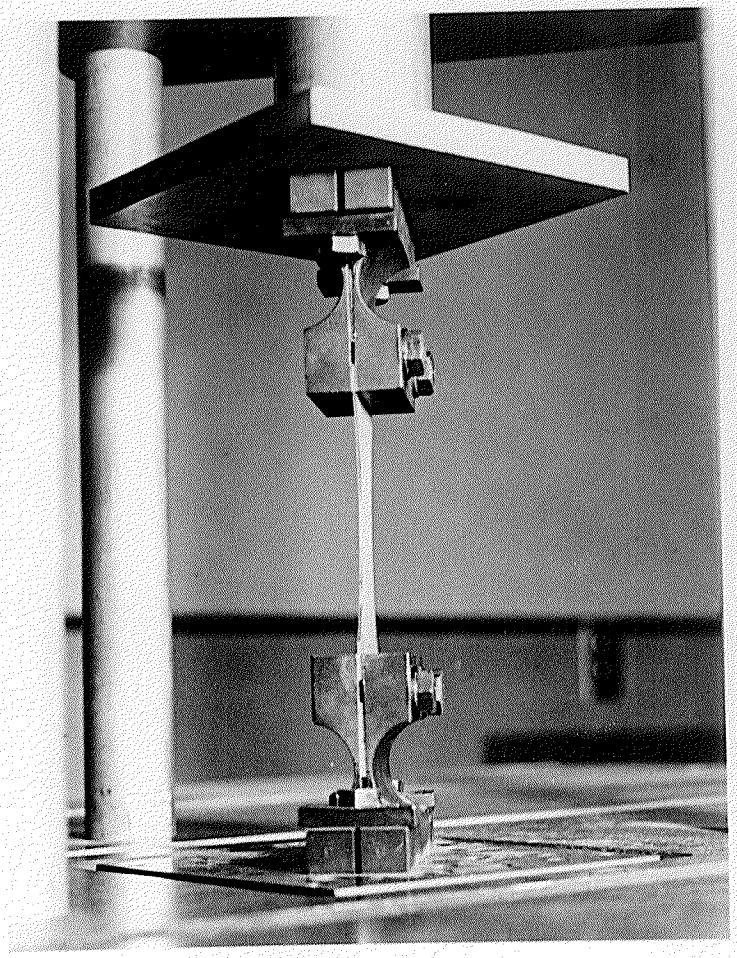

(b) Side View

Figure 6.3 Specimen type-B as clamped.

6.2.3 TEST PROCEDURE

Groups of specimens each containing at least five units were tested at several stress levels. Zero-to-tension load was applied with a nominal fatigue stress ratio of zero. The fatigue stress ratio is the algebraic ratio of the minimum stress to the maximum stress in one load cycle.

All specimens were cycled until complete rupture at the test section. In the long life range the test was terminated at ten million cycles even if complete fracture had not occurred. Specimens which run out at this arbitrary limit of cycling are indicated as runouts. However, specimens may fracture outside the test section and thus create a discrepancy. The specimen life, in this case, does not represent the life of the specimen but rather it indicates an early termination of testing with respect to the test section. Sufficient data may be collected by testing extra specimens but such data points are distinguished in the results.

Eight different fatigue test series were planned to fulfill the objectives of the experimental fatigue testing program.

Series 1 tests were carried out for preliminary optimization purposes. Thirty type-A specimens were dimpled to different levels. The control parameter which was the average edge strain was selected in the range from 0 to 2.25 percent. The lowest value was for undimpled specimens while the highest value was determined by the practical limit for maintaining the specimens flat after dimpling. This limit was determined by visual inspection of specimens. All specimens were notched

and tested to failure at the same stress level of 23 ksi (162 MPa). An optimum dimpling was determined from this test series.

Series 2, 3, and 4 were carried out to measure the improvement in the fatigue strength reduction factor, FSRF, which could be obtained in an edge notched specimen by edge dimpling. The FSRF is the ratio of the fatigue strength of a specimen with no stress concentration to the same with stress concentration. Three S-N curves were obtained for notched, dimpled-notched and plain specimens, respectively. Each series contained a minimum of five different stress levels.

Series 5 to 8 were conducted to investigate the effect of preloading on edge dimpling. In Series 5, specimens type-A were dimpled to the optimum dimpling strain and then preloaded to prestress ratios of 0, 0.4, 0.6, 0.8, 1.0, 1.2 and 1.6. The preloaded samples were cycled to failure at the same stress level. From the results of Series 5 three different prestress levels were selected below, equal to and above the yield strength of the material. Preloaded specimens were used to obtain a full range S-N curve for each prestress value. Test series 6, 7 and 8 were carried out to obtain the three S-N curves.

6.3 RESULTS AND ANALYSIS

The results of the fatigue testing program are pesented and statistically analyzed in Appendix A in five sections.

The results of preliminary optimization are given in Appendix A.2. The analysis indicates a continuous fatigue life improvement as the average

edge strain increases. Although the results do not indicate a peak improvement the optimum average edge strain, as determined from practical considerations, may be taken as 2 percent. This optimum value was used in all dimpling.

The results of fatigue test series 2, 3 and 4 are reported in Appendix A.4. The results are fitted to three S-N curves as shown in Figure 6.4. Each S-N curve represents the best fitting expression of the form

$$S = S_e + A\,(N + B)^{-m} \qquad 6.1$$

to the experimental data, where S is the maximum fatigue strength for a given number of cycles N and S_e, A, B and m are parameters.

The results of fatigue test series 5, 6, 7 and 8 are reported in Appendix A.5. The resulting S-N curves for the selected values of pre-load are plotted in Figure 6.5.

6.4 DISCUSSION

6.4.1 THE FATIGUE STRENGTH IMPROVEMENT

The results of fatigue testing shown in Figure 6.4 indicate a considerable improvement in fatigue strength. The improvement in fatigue strength is plotted against the fatigue life in Figure 6.6. The improvement in fatigue strength is simply determined by the ratio of the change in fatigue strength to the strength of undimpled specimens. It increases with the increase of fatigue life and it appears to reach a peak value at a life longer than ten million cycles. The fatigue strength is almost

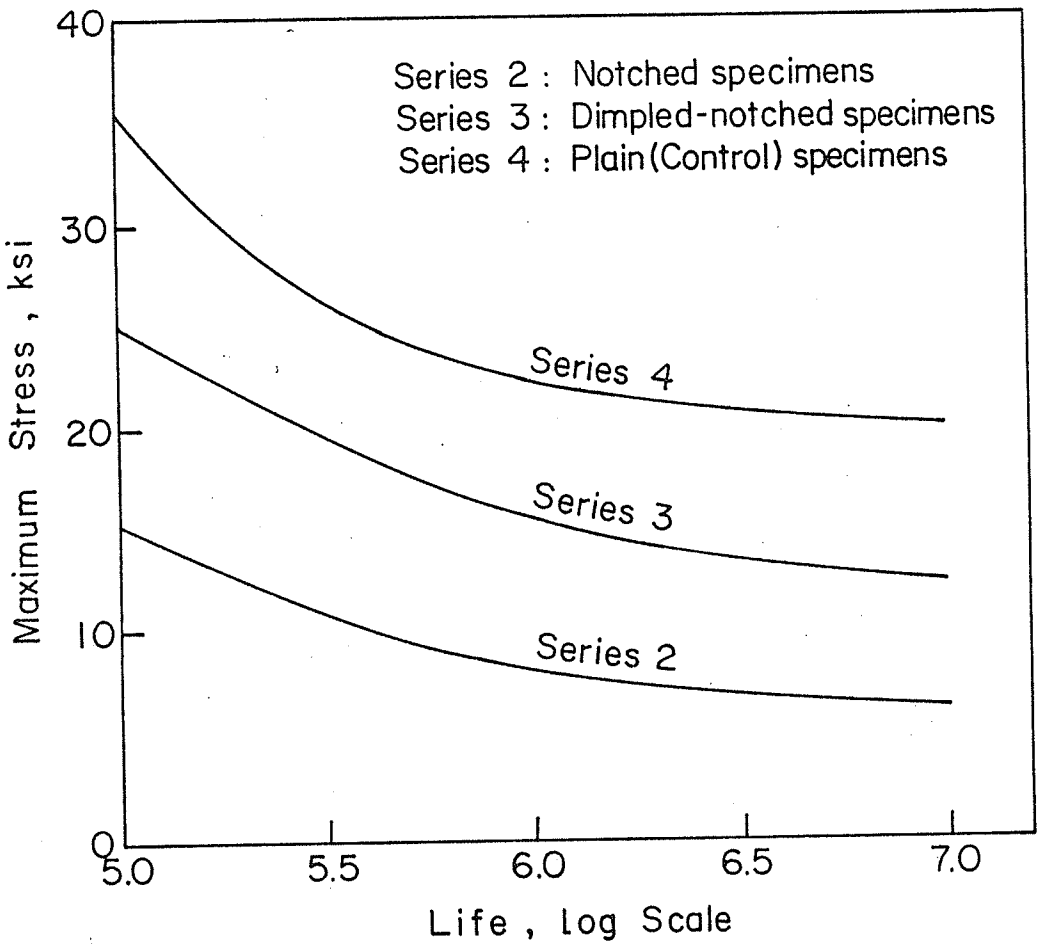

Figure 6.4 Best fitting S-N curves for fatigue testing - strength improvement results.

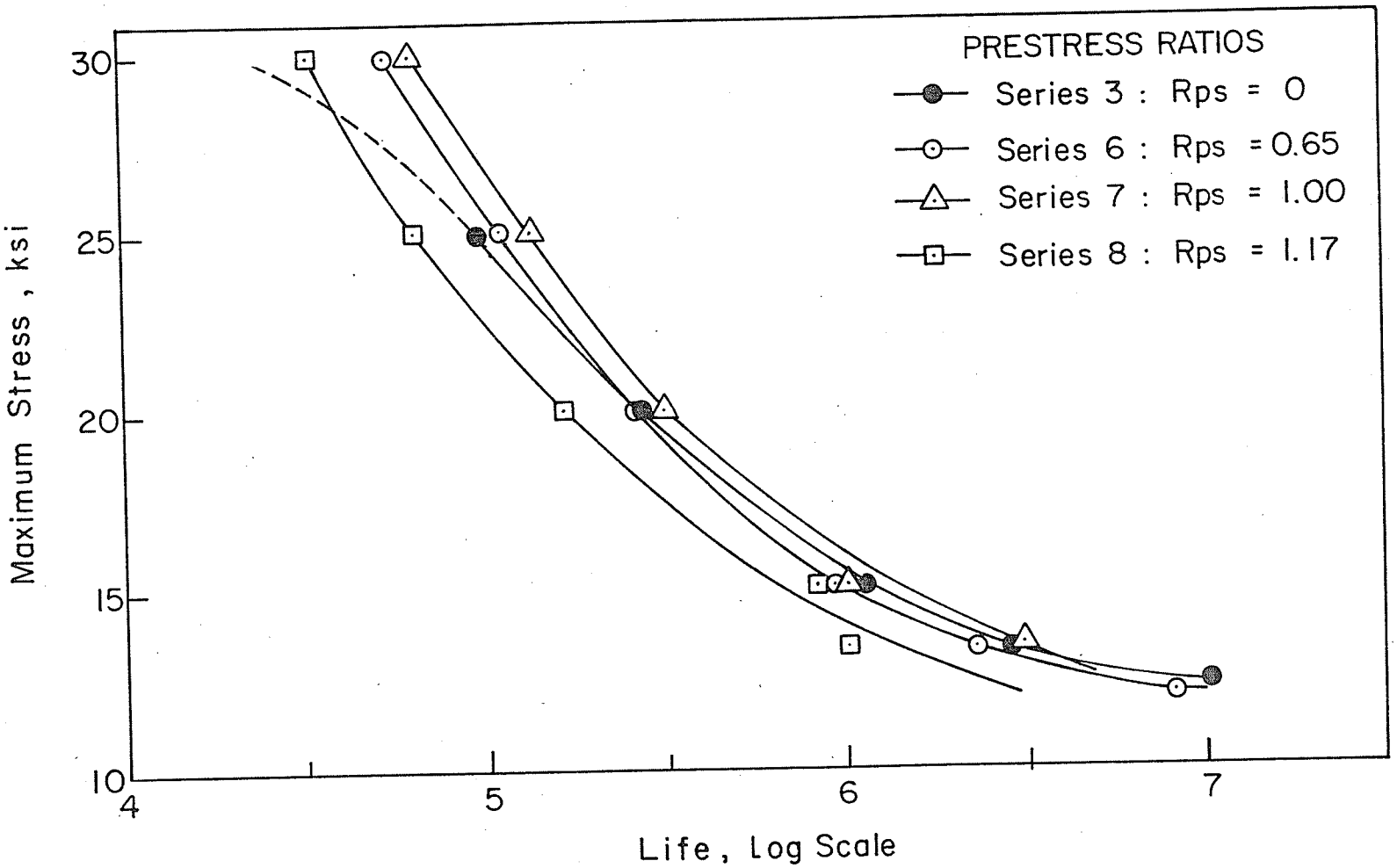

Figure 6.5 Best fitting S-N curves for fatigue testing results - preloading effect.

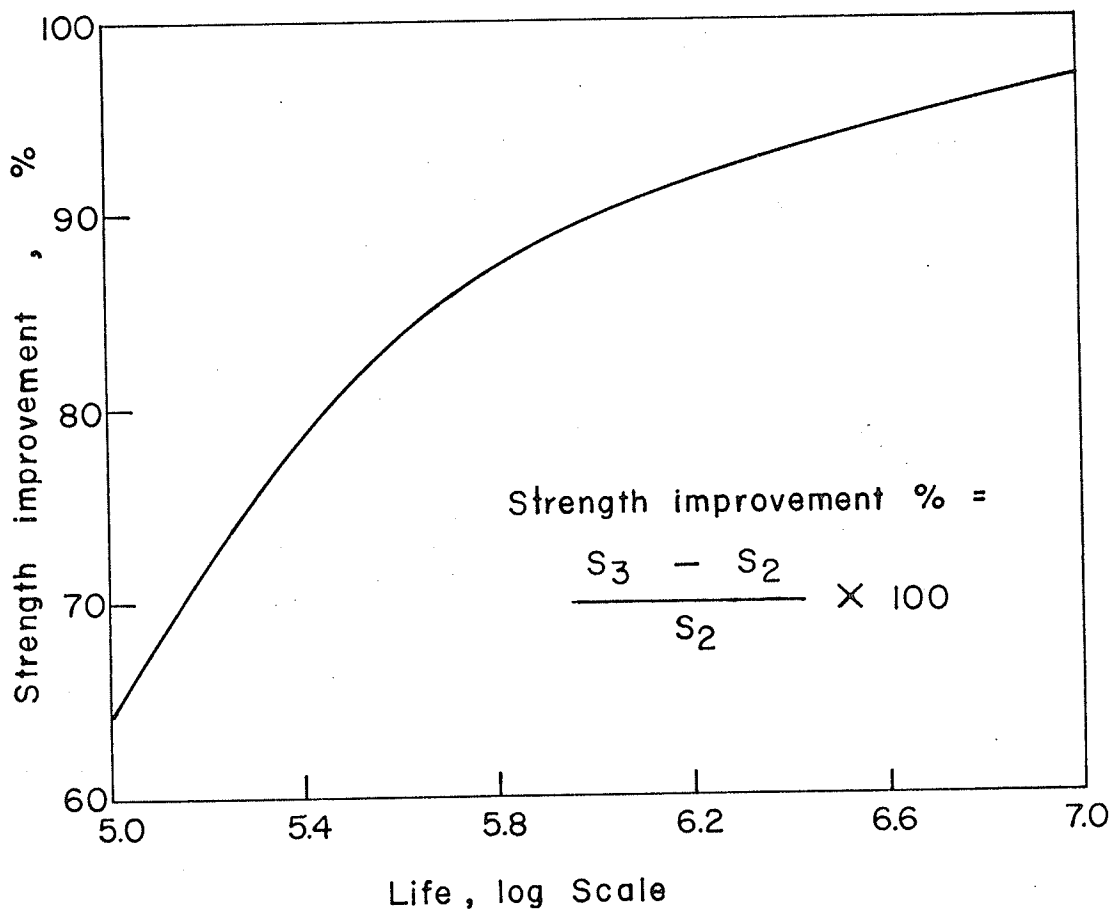

Figure 6.6 Fatigue strength improvement vs. life (log scale).

doubled at this life. As the life decreases the strengthening effect of dimpling is reduced to approximately 63 percent at 100 kilocycles. Lesser strengthening is expected in the low cycle fatigue range. The advantage of dimpling is lost by the redistribution of residual stresses due to plastic flow at high loads. However, rough extrapolation of the curve of Figure 6.6 indicates that some 15 percent improvement in strength would still be feasible at 10 kilocycles. The nature of residual stresses created by edge dimpling in the intermediate cycle range, however, requires further investigation in order to come to a solid conclusion of whether or not dimpling has a favourable effect in that range.

The improvement may be expressed in terms of the decrease in the FSRF as shown in Figure 6.7. This decrease approaches the 50 percent figure at 10 million cycles to failure. This parameter indicates the same trend of variation of the strength improvement parameter but it exhibits a narrow range of variation. Further examination of the variation of the FSRF with life as shown in Figure 6.8 indicates that the FSRF of dimpled specimens is practically independent of the fatigue life. This implies that a single value of FSRF of dimpled specimens determined at an arbitrary life may be sufficient to obtain the full range S-N curve from available data for plain material. This tendency of having a constant FSRF is observed in the cycle range from 100 kilocycles to 10 million cycles.

It should be remarked that a higher percentage of improvement may be obtained in practical applications of edge treatment. If edge dimpling

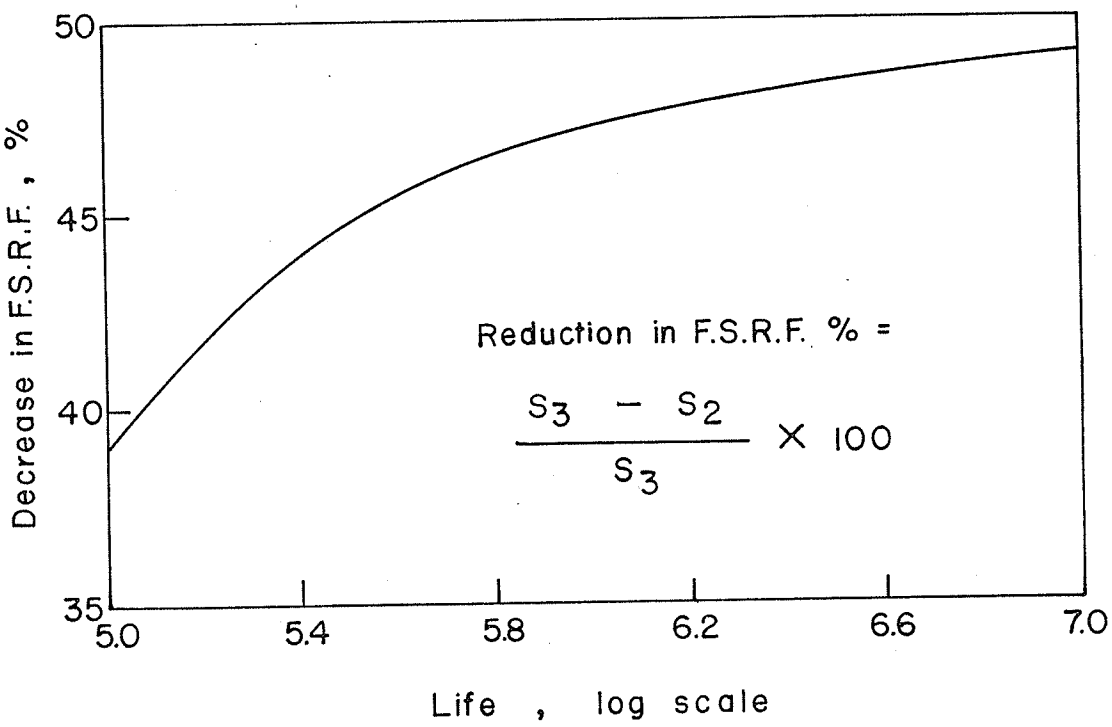

Figure 6.7 The decrease in F.S.R.F. vs. life.

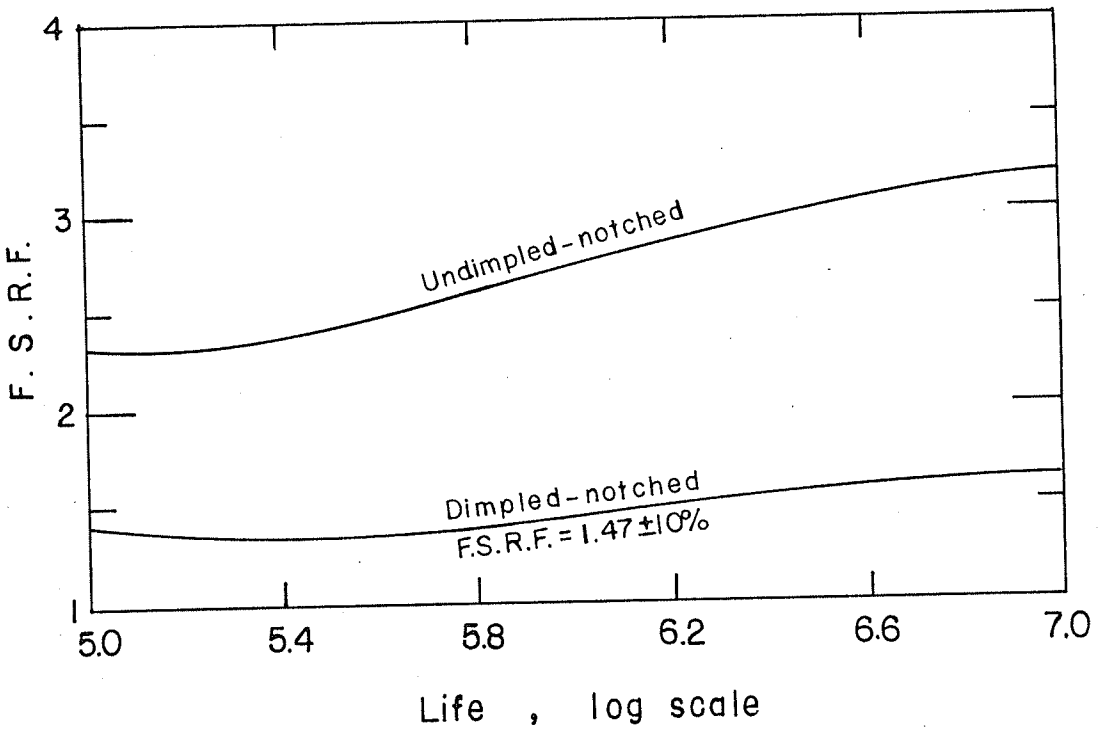

Figure 6.8 The variation in F.S.R.F. due to dimpling

is performed on the edge of a wide plate rather than a narrow specimen the rigidity of the undimpled region will be greater and will constrain the relaxation. This will result in residual stresses closer to the MPRS and, hence, in a higher fatigue strength improvement.

6.4.2 THE EFFECT OF PRELOADING ON FATIGUE STRENGTH

Preloading of specimens does not appear to have drastic influence on the fatigue strength improvement achieved by dimpling. From a statistical viewpoint, as detailed in Appendix A.5, the observed differences due to preloading are insignificant. Although the changes are minor, the analysis of Figure 6.5 clarifies certain effects associated with preloading. The ratio of the logarithms of fatigue life with and without preloading is plotted vs. the prestress ratio as shown in Figure 6.9. For prestress ratios less than approximately 0.5 there is no significant change in fatigue life. This confirms the results obtained in Appendix A.5 at a single stress level. A comparison with the limit of 0.65 based on the analytic solution of residual stress, indicates a slight difference. However, the limit is in agreement with the value obtained from experimental measurement of residual stresses. The actual residual tension appears to be in the vicinity of 0.5 the yield strength.

It is observed that at any stress level and for a prestress ratio $R_{ps} = 0.92$, the fatigue life is affected favourably by preloading. Meanwhile, for higher or lower ratios a decrease in fatigue life results at lower stress levels. To maintain the improvement gained by edge dimpling,

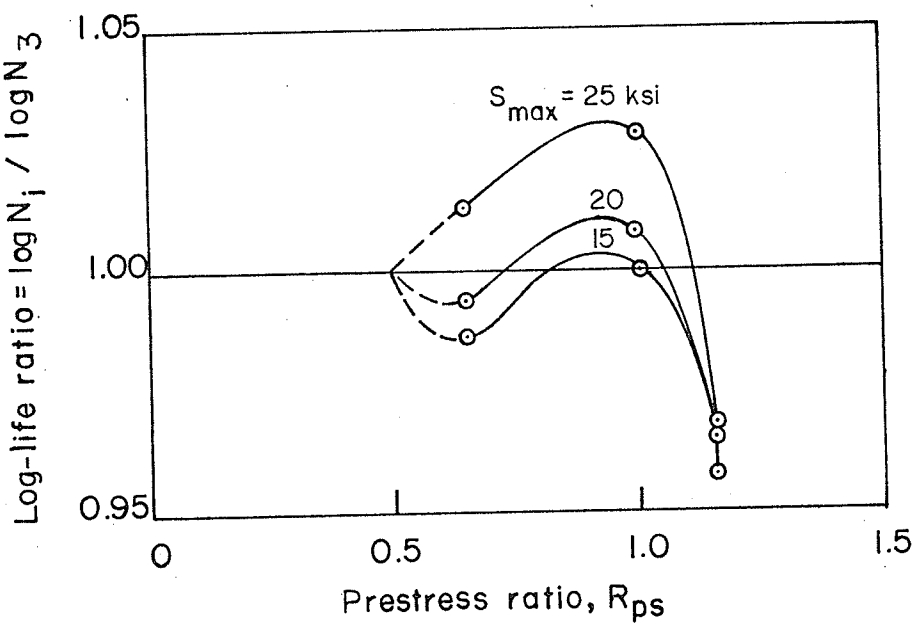

Figure 6.9 Log-life ratio vs. prestress ratio at various preload levels. N_i, i=6,7,8; is the life of respective series. N_3, is the life of specimens without preload.

prestress should not exceed the yield strength of the material, otherwise the improvement will be lowered.

Figure 6.10 illustrates the effect of preloading in terms of fatigue strength improvement. Prestress within the yield point of the material results in a slight variation in strength improvement. At 100 kilocycles fatigue strength increases from 64 percent to up to 78 percent for $R_{ps} = 1.0$. Meanwhile, a reduction of the strength improvement of approximately 8 percent at 10 million cycles is found for low prestress values. However, at this life the remaining strength improvement amounts to 90 percent. The high prestresss ratio reduces the improvement to about 48 percent at 100 kilocycles. For undimpled specimens such a high prestress would slightly improve the fatigue strength by strain hardening. The FSRF also changes with prestress as shown in Figure 6.11. The FSRF slightly increases or decreases for $R_{ps} \leq 1.0$ but it remains constant within ± 5 percent.

6.4.3 THE CORRELATION OF FATIGUE STRENGTH IMPROVEMENT AND RESIDUAL STRESS

The fatigue strength improvement has been studied in the foregoing sections. A relation between the strength improvement and the residual stress is desirable to expedite the prediction of such improvements from knowledge of residual stress. Such a relation is most valuable to the designer.

Residual stresses due to edge dimpling were determined analytically in Chapter 4 and experimentally in Chapter 5. Evidently, these

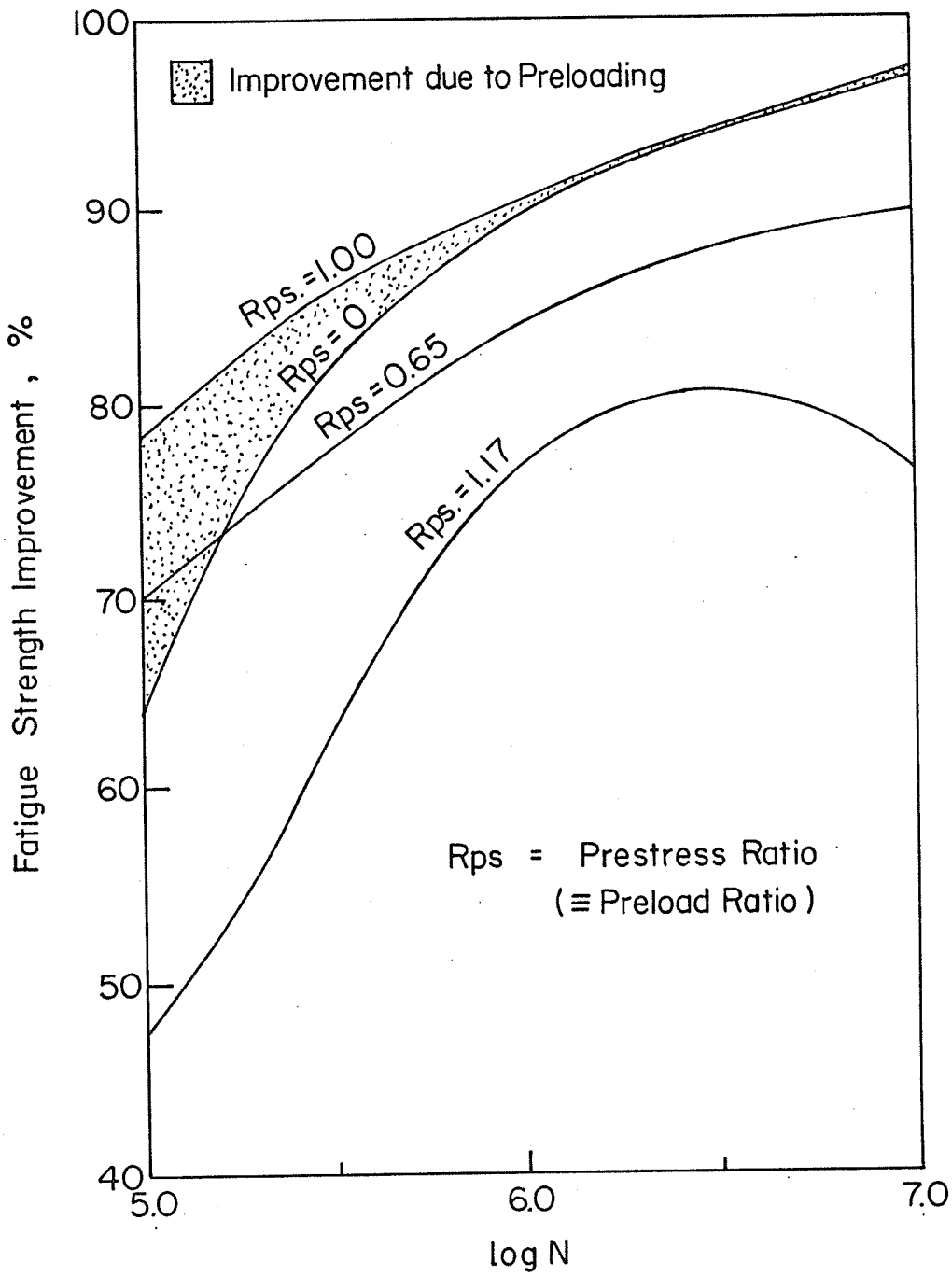

Figure 6.10 Change of fatigue strength improvement by preloading

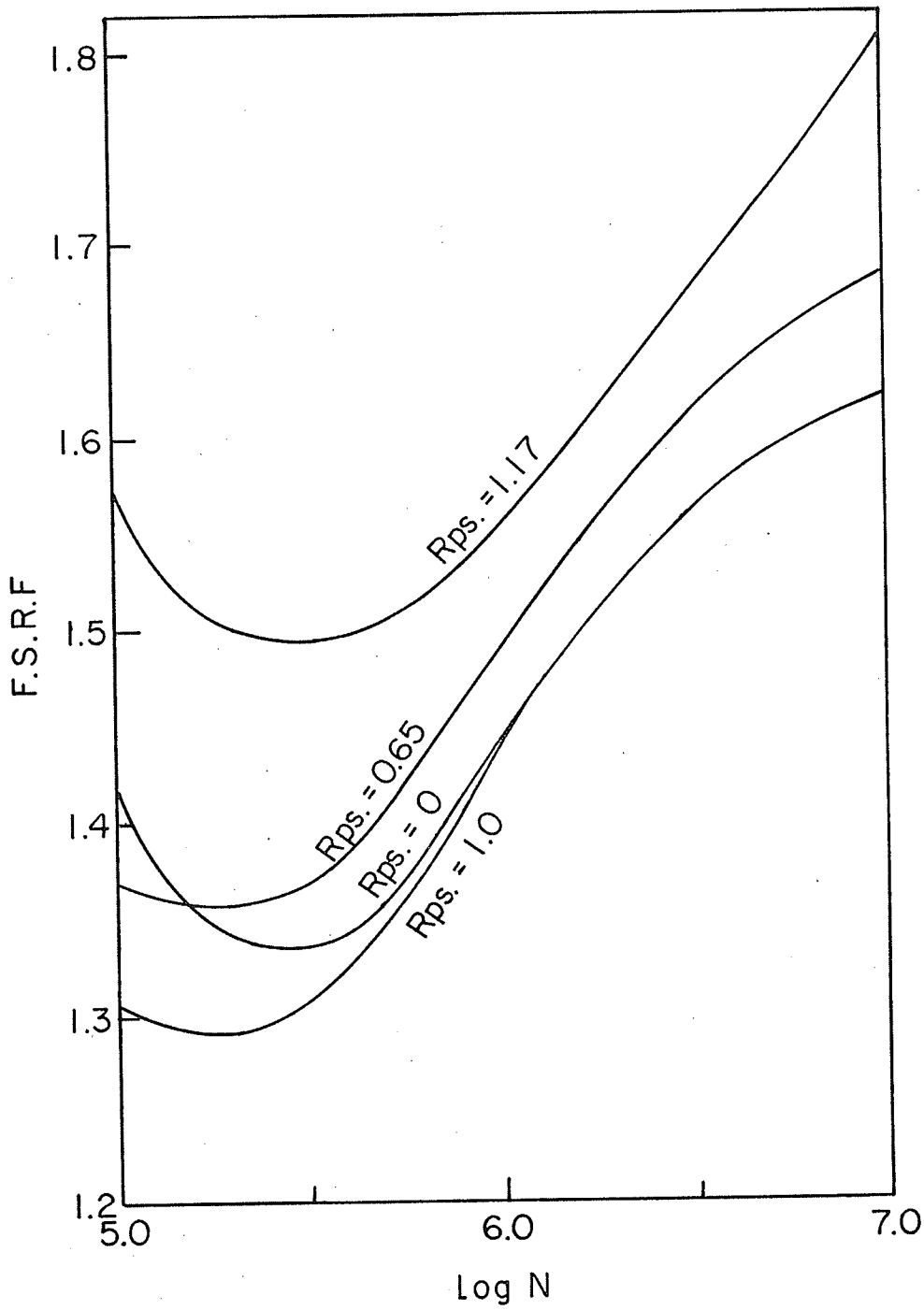

Figure 6.11 Change of F.S.R.F. of dimpled specimens by preloading

stresses will be modified in fatigue test specimens due to notching. The resulting stress distribution is determined by the notch depth and geometry. When the specimen is notched, a part of the material causing the misfit will be removed. Accordingly, a deep notch through the dimpled area may cause the complete loss of residual stress in the remaining cross section. Conversely, a small notch will remove only a small volume of the misfit region leaving an essentially unchanged residual stress at the notch root. However, changes in the interior regions are expected. The presence of the notch as a discontinuity in the stress field causes the residual compression at the notch root to approach the yield strength of the material in compression. This high residual stress will be local to the notch root and will be associated with a very steep positive stress gradient.

As noted previously, the presence of high residual compression at the notch root lowers the actual stress concentration effects, thus delaying both crack initiation and propagation. The reduction of stress concentration may be employed to estimate the improvement in fatigue strength of dimpled-notched specimens. The procedure is presented in the following.

For a small notch of root radius, r, Heywood [19] suggested the following relationship between the FSRF at 10^7 cycles, K_f , and the theoretical stress concentration factor, K_t :

$$K_f = K_t/[1 + 2\sqrt{a/r}] \qquad 6.2$$

where a is the material notch alleviation factor, which depends on the

tensile strength of the material. Equation 6.2 may be written:

$$K_f = q \cdot K_t \qquad 6.3$$

where q is the notch sensitivity factor given by

$$q = 1/[1 + 2\sqrt{a/r}] \qquad 6.4$$

For aluminum alloys the notch alleviation factor is [19]

$$\sqrt{a} = (24/\sigma_{ut})^3 \qquad 6.5$$

where σ_{ut} is the ultimate tensile strength of the material.

For dimpled notched specimens subjected to a nominal stress σ and having a notch root residual stress of σ^{RS}, the effective stress concentration factor, K_t', will be:

$$K_t' = [K_t \cdot \sigma - \sigma^{RS}]/\sigma$$

$$= K_t - \sigma^{RS}/\sigma \qquad 6.6$$

Due to the reduction of stress concentration effect the FSRF for dimpled-notched specimens, K_f', will be:

$$K_f' = q \cdot K_t' \qquad 6.7$$

Substituting Equation 6.6 into Equation 6.7 obtain

$$K_f' = q \cdot [K_t - \sigma^{RS}/\sigma] \qquad 6.8$$

Using Equation 6.3,

$$K_f' = K_f - q \cdot \sigma^{RS}/\sigma \qquad 6.9$$

By definition, the FSRFs for both notched and dimpled-notched

specimens are given by:

$$K_f' = S_p/S' \quad , \quad K_f = S_p/S \qquad 6.10$$

where S_p , S' , and S are the fatigue strengths at 10^7 cycles of plain, dimpled-notched, and notched specimens, respectively.

Substituting Equations 6.10 into Equation 6.9 and noting that $\sigma = S'$, obtain:

$$S' = S \cdot [1 + q \cdot \sigma^{RS}/S_p] \qquad 6.11$$

This relation permits the prediction of fatigue strength S' from information of the fatigue strength of plain material at 10^7 cycles, S , the notch sensitivity factor, q , and the fatigue strength of notched specimens at 10^7 cycles or alternatively the FSRF of notched specimens, K_f . The upper limit for S' is S_p for which $K_f' \to 1$. This signifies that the notch weakening effect is entirely eliminated by the introduction of residual stress. In this case, as the material as a whole should have unit value for the FSRF, failure should occur at other weak points that may exist in the material.

For the present case, a notch having 0.005-in. root radius in 2024-T3 alclad aluminum alloy should have a notch alleviation factor $\sqrt{a} = 0.05$. Therefore, from Equation 6.4,

$$q = 0.414$$

From the mathematical models of the S-N curves determined in Appendix A.4 calculated at 10^7 are:

$$S_p = 19.92 \text{ ksi}$$

$$S = 6.25 \text{ ksi}$$

The residual stress σ^{RS} = 45 ksi. Substituting these values into Equation 6.11 obtain the estimate of S' = 12.10 ksi. This is in excellent agreement with the experimental value of 12.31 ksi.

At this point it is of interest to note that the notch root residual stress is not the only significant parameter. The stress gradient created by edge dimpling and altered by preloading seems to have an influence on the rate of crack propagation. Preloading produces changes in the stress gradient and subsequent notching raises the stress at the notch root to the yield stress. Therefore, in both preloaded and non-loaded specimens the notch root stress will be the same. But experiments indicate a certain trend of change in fatigue resistance which can only be attributed to the effect of the change in stress gradient. However, the slight changes which were observed in fatigue behaviour are shown to be statistically insignificant (Appendix A.5). A more fundamental study of the effect of stress gradients on the various aspects of fatigue crack initiation and propagation is required.

From knowledge of the FSRF or the fatigue strength of dimpled-notched specimens at 10^7 cycles it is possible to construct the predicted S-N curve for dimpled-notched specimens. The S-N curve for plain specimens is essential and one of two general assumptions has to be made:

i. The predicted FSRF for dimpled-notched specimens remains constant at the entire life spectrum. That is a value of 1.65.

ii. The predicted FSRF decreases in some continuous manner as fatigue life decreases. Heywood [19] suggests an empirical relation between

the FSRF at 1000 cycles, $K_f'(1)$, and K_f' :

$$[K_f'(1) - 1]/[K_f' - 1] = f \qquad 6.12$$

where f is an empirical material constant. It is suggested that K_f' be applied at 10^7 cycles and then progressively reduced until 10^3 cycles. Therefore, at any life N, in kilocycles

$$K_f'(N) = K_f'(1) + [K_f' - K_f'(1)]\cdot[(\log N - 3)/4] \qquad 6.13$$

For the present case, f = 0.55 [5] and hence at N, kc:

$$K_f(N) = 1.36 + 0.0725 \log N$$

A prediction of the S-N curve of dimpled-notched specimens based on the S-N curve for plain material and both assumptions regarding the change of FSRF is made. A comparison of the predicted and experimental values if presented in Table 6.2. The results indicate good agreement between predictions based on the second assumption and results from experiments. The first assumption seems to yield more conservative predictions. In general, it may be observed that the predicted values tend to be in the lower side from experiment which provide a safe application to design purposes.

6.5 SUMMARY

An experimental fatigue testing program was carried out in order to assess the fatigue strength improvement by edge dimpling. The study, backed by extensive statistical analysis of data, indicates considerable fatigue strength improvement which is not significantly affected by

TABLE 6.2

COMPARISON OF PREDICTED AND EXPERIMENTAL
FATIGUE STRENGTHS FOR ROTCHED DIMPLED SPECIMENS

N, Kc	Sp, Ksi	Predictions			Experimental S', Ksi
		Assumption (ii)		(i)	
		$K_f'(N)$	$S'=Sp/K_f'$	$S'=S_p/1.65$	
100	35.32	1.51	23.39	21.41	24.88
300	26.27	1.54	17.06	15.92	19.67
1,000	22.13	1.58	14.01	13.41	15.34
3,000	20.60	1.61	12.80	12.48	13.29
10,000	19.92	1.65	12.07	12.07	12.31

preloading. An attempt was made to correlate the strength improvement and residual stress which resulted in a procedure for predicting the S-N curve for dimpled notched specimens. The prediction was based on the S-N curve for plain material and the notch geometry. The predicted curve was found to be in good agreement with experiment.

CHAPTER 7

SUMMARY AND CONCLUSIONS

7.1 SUMMARY

A new technique for improving the fatigue strength of sheet and thin plate material by edge treatement has been described. The technique induces residual stresses highly compressive at the free edge where stress concentration caused by geometric discontinuity exists.

The edge treatment was induced by edge dimpling which is a mechanical method of producing a controllable gradient of plastic strain in a finite length of the free edge of sheet metallic materials. An apparatus was designed and constructed to perform the process in order to experimentally optimize the technique and investigate its influence on fatigue behaviour of specimens.

The determination of the influence of edge dimpling required the determination of residual stresses in the critical region. Therefore, residual stresses due to edge dimpling were determined by means of an approximate analytical procedure. The finite element method was used to determine parts of the solution. Residual stresses were verified by measurement. A modified hole-drilling technique was developed for the measurement of residual stresses in thin material. The modified technique was employed to measure the residual stress distribution due to edge dimpling. The analytical and experimental results were found to be in good agreement.

The experimental fatigue testing program was carried out to evaluate the edge dimpling technique. An optimum edge dimpling procedure was found to give the largest fatigue life improvement. This optimal edge dimpling was then utilized in all subsequent fatigue testing. Full-scale high-cycle fatigue testing with and without preloading was conducted. The analysis of data and correlation with residual stresses was made. The results indicate a high and stable level of fatigue strength improvement. Furthermore, the fatigue strength of dimpled-notched specimens may be predicted with high accuracy if the residual stresses and notch configuration are given.

7.2 CONCLUSIONS

Supported by data obtained from the experiments described in this thesis, the following conclusions are made:

1. The edge dimpling technique is capable of inducing high levels of residual compression at the free edge of sheet or thin plate material. The high compression is balanced by tensile stresses of much lower magnitude in the "interior" regions.
2. The modified hole-drilling technique may be used to measure residual stress gradients with a satisfactory degree of accuracy.
3. Residual stresses due to edge dimpling may be determined analytically if the various parameters are given and the material is of known behaviour.
4. Optimum edge dimpling significantly improves the edge notch fatigue

strength of 2024-T3 alclad aluminum alloy specimens under zero-to-tension fatigue cycling.

5. The fatigue strength reduction factor of the edge dimpled specimens tends to be constant regardless of fatigue life.
6. Preloading does not appear to induce significant statistical differences in the fatigue strength improvement obtained by edge dimpling. However, prestress higher than the yield strength may prove to be detrimental.
7. A nominal prestress in the vicinity of the yield strength of the material is generally favourable.
8. The S-N curve for dimpled-notched specimens may accurately be predicted from knowledge of the S-N curve for plain material and the notch geometry.

7.3 SUGGESTIONS FOR FURTHER STUDY

1. A fundamental study of the influence of stress gradient on fatigue crack propagation is in order. Since the crack propagation rate is a function of the effective stress, further study to incorporate the stress gradient in evaluating the effective stress is desirable.
2. The modified hole-drilling technique requies data on the machining effects induced in various materials by various drilling tools and at different conditions. Since this type of data is scarce, experiments are required to generate them and determine the optimum drilling combinations for different materials.

3. A better evaluation of residual stresses induced by edge dimpling may be obtained numerically. This may be achieved by a three dimensional finite element computerized solution. Such a solution will provide the best means of optimizing the technique and adapting it to various practical applications.
4. The edge dimpling apparatus was designed to adapt to a wide range of specimen configurations. Therefore, this advantage may be used to edge dimple structural parts or plates with large scale stress concentrations. Component fatigue testing should emphasize the practical value of the technique.
5. Since large structural openings in aircraft structures, for instance, are usually surrounded by a row of small holes for fastening purposes, it is interesting to study the influence of edge dimpling in such cases. This may require the re-optimization of the depth of dimpling to place the holes into the region of high residual compression.
6. Experimental study of the effect of preloading on residual stress distribution. This study may be extended to include the effect of gusts in a load spectrum by applying high overloads at different intervals during the fatigue testing.

BIBLIOGRAPHY

1. Sines, G. and Waisman, J.L., eds., Metal Fatigue, McGraw-Hill, 1959.

2. Forrest, P.G., Fatigue of Metals, Pergamon Press, 1962.

3. Speakman, E.R., "Stress Coining Procedures for Fatigue Improvement", Report No. MDC-J5588, Douglas Aircraft Co., June 1972.

4. Norton, J.T., Rosenthal, D., and Maloof, S.D., "X-ray Diffraction Study of the Effect of Residual Compression on Fatigue of Notched Specimens", The Welding J., v. 25, n. 11, Res. Suppl., pp. 729S-736S, 1946.

5. Juvinall, R.C., Engineering Considerations of Stress, Strain and Strength, McGraw-Hill, 1967.

6. Smith, C.R., "Design Applications for Improving Fatigue Resistance of Airplane Structures", Proc. ASTM, v. 60, pp. 589-601, 1960.

7. Smith, C.R., "Interference Fasteners for Fatigue-Life Improvement", Experimental Mechanics, v. 5, n. 8, pp. 19A-23A, Aug. 1965.

8. Mittenberg, A.A. and Beall, L.G., Jr., "Effects of Pin-Interference and Bolt Torque on Fatigue Strength of Lug Joints", Proc. ASTM, v. 63, pp. 671-683, 1963.

9. Ligenza, S.L., "Cyclic-Stress Reduction Within Pin-loaded Lugs Resulting from Optimum Interference Fits", Experimental Mechanics, v. 3, n. 1, pp. 21-28, 1963.

10. Koplik, B. and Klassen, D.D., "Reduction of Alternating Stress Range Around Holes in Flat Plates by Use of Inserts", Trans. ASME, J. of Engrg. for Ind., v. 93, n. 2, pp. 683-687, May 1971.

11. Lee, E.H. and Rogers, T.G., "On the Generation of Residual Stresses in Thermoviscoelastic Bodies", Trans. ASME, v. 87, J. Appl. Mech., Series E, v. 32, pp. 874-880, 1965.

12. Rathbun, F.O., Jr. and Coffin, L.F., Jr., "An Experimental Investigation of Residual Stress in Quenched Flat Plates", Experimental Mechanics, v. 6, n. 10, pp. 519-527, Oct. 1966.

13. Hsu, T.R., "Application of the Laser Beam Technique to the Improvement of Metal Strength", unpublished.

14. Hsu, T.R. and Trasi, S.R., "On the Analysis of Residual Stresses Introduced in Sheet Metals by Thermal Shock Treatment", Trans. ASME, J. Appl. Mech., Paper No. 76-APM-13, 1976.

15. Horger, O.J., ed., ASME HBK, Metals Engineering - Design, McGraw-Hill, pp. 42-62, 1953 (168 References).

16. Weiner, J.H. and Huddleston, J.V., "Transient and Residual Stresses in Heat Treated Cylinders", Trans. ASME, v. 81, J. Appl. Mech., Series E, v. 26, pp. 31-39, 1959.

17. Bühler, H. and Scheil, E., "Zusammenwirken von Wärme - und Umwandlungspannungen in abgeschreckten Stählen", (The Combined Effect of Heat and Transformation Stresses in Quenched Steels) Archiv für das Eisenhüttenwesen, v. 6, pp. 283-288, 1933.

18. Landau, H.G. and Zwicky, E.E., Jr., "Transient and Residual Thermal Stresses in an Elastic-Plastic Cylinder", Trans. ASME, v. 82, J. Appl. Mech., Series E, v. 25, pp. 481-488, 1960.

19. Heywood, R.B., Designing Against Fatigue, Chapman and Hall, London, 1962.

20. Dugdale, D.S., "Effect of Residual Stresses on Fatigue Strength", Welding J., v. 38, Res. Suppl., pp. 45S-48S, 1959.

21. Rosenthal, D., Sines, G., and Zizicas, G., "Effect of Residual Compression on Fatigue", Welding J., v. 28, n. 3, Res. Suppl., pp. 98S-103S, 1949.

22. Heller, R.A., Seki, M., and Freudenthal, A.M., "The Effect of Residual Stress on Random Fatigue Life", Proc. ASTM, v. 64, pp. 516-535, 1964.

23. Taira, S. and Murakomi, Y., "Effect of Residual Stresses on Fatigue Strength", Proc. 5th Jap. Con. Test. Mat., pp. 27-31, 1962.

24. Heywood, R.B., "The Effect of High Loads on Fatigue", Proc. of IUTAM, Colloquium on Fatigue, ed. by W. Weibull and F.K.G. Odqvist, pp. 92-102, Stockholm, 1955.

25. Vitovec, F.H., "Effect of Static Prestrain on the Fatigue Properties Under Uniformly Increasing Stress Amplitude", Proc. ASTM, v. 58, pp. 552-569, 1958.

26. Esquivel, A.L. and Evans, K.R., "X-ray Diffraction Study of Residual Macrostresses in Shot-peened and Fatigued 4130 Steel", Experimental Mechanics, v. 8, n. 11, pp. 496-503, Nov. 1968.

27. Boggs, B.D. and Byrne, J.G., "Fatigue Stability of Residual Stress in Shot-Peened Alloys", Metallurgical Trans., v. 4, n. 9, pp. 2153-2157, Sept. 1973.

28. Straub, J.C. and May, D., "Stress Peening", Iron Age, 21/4/49.

29. Fuchs, H.O., "Techniques of Surface Stressing to Avoid Fatigue", Metal Fatigue, ed. by G. Sines and J.L. Waisman, McGraw-Hill, ch. 9, pp. 197-231, 1959.

30. Mattson, R.L. and Roberts, J.G., "The Effect of Residual Stresses Induced by Strain Peening upon Fatigue Strength", Internal Stresses and Fatigue in Metals, ed. by G.M. Rassweiler and W.L. Grube, Elsevier, pp. 337-357, 1959.

31. Phillips, A., "Improvement of Fatigue Life of Aircraft Components by Coining", ASME Paper No. 61-AV-35, March 1961.

32. Whaley, R.E., "Improvement in 7075-T651 Aluminum Alloy Fatigue Life by Coining", Proc. ASTM, v. 63, pp. 692-705, 1963.

33. Kasgard, P.V., Day, E.E., and Kobayashi, A.S., "Exploratory Study on Optimum Coining for Improvement of Fatigue Life", Experimental Mechanics, v. 4, n. 10, pp. 297-305, 1964.

34. Speakman, E.R., "Fatigue Life Improvement Through Stress Coining Methods", Achievement of High Fatigue Resistance in Metals and Alloys, ASTM STP-467, pp. 209-227, 1970.

35. Smith, C.R., "Preventing Fatigue Failures", Assembly Engg., in 3 parts, from March - May, 1968.

36. Speakman, E.R., Private Communication, Sept. 12, 1973.

37. Shewchuk, J. and Roberts, F.A., "Increasing the Fatigue Strength of Loaded Holes by Dimpling", Trans. ASME, J. Engg., Materials and Technology, v. 96, n. 3, pp. 222-226, July 1974.

38. Shewchuk, J., "Decreasing the Fatigue Strength Reduction Factor by Dimpling", ASTM, JTEVA (J. of Testing and Evaluation), v. 2, n. 5, pp. 425-428, Sept. 1974.

39. Kuc, A.P. and Shewchuk, J., "The Effect of Interference Fit on the Dimpled Loaded-hole Fatigue Strength of 2024-T_3 Aluminum Alloy", SESA Paper No. WR-42-1975, Meeting Silver Spring, MD, May 9-14, 1976.

40. Timoshenko, S.P. and Goodier, J.N., Theory of Elasticity, 3rd ed., McGraw-Hill, 1970.

41. Wang, N.M., "Large Plastic Deformation of a Circular Sheet Caused by Punch Stretching", General Motors Research Publications, GMR.862, March 1969.

42. Metha, H.S. and Kobayashi , S., "Finite Element Analysis and Experimental Investigation of Sheet Metal Stretching", Trans. ASME, v. 95, J. of Engg. for Ind., pp. 874-880, 1973.

43. Osadchuk, V.A., "Determination of Residual Stresses in a Spherical Shell", Soviet Materials Science, v. 7, n. 4, pp. 476-478, Dec. 1973 (Translation from Russian).

44. D'lsa, F.A., Mechanics of Metals, Addison-Wesley, Don Mills, Ontario, 1968.

45. Gupta, S.P. and Kodali, S.P., "The Effect of Pre-Strain on the Bauschinger Effect", Scripta Metallurgica, v. 10, n. 2, pp. 111-114, February 1976.

46. Desai, C.S. and Abel, J.F., Introduction to the Finite Element Method, Van Nostrand Reinhold, 1972.

47. McGonagle, W.J. and Yun, S.S., "Measurement of Surface-Residual Stress by Nondestructive Methods", Proc. 5th Int. Conf. on Nondestruct. Test., Montreal, Canada, pp. 159-164, May 21-26, 1967.

48. Martin, D.L., ed., "Evaluation of Methods for the Measurement of Residual Stresses", SAE TR-147, 1960.

49. Donachie, M.J., Jr. and Norton, J.T., "Residual Stresses in Shot-Peened Aluminum Bars", Experimental Mechanics, v. 2, n. 7, pp. 222-224, July 1962.

50. Koistinen, D.P. and Marburger, R.E., "Internal Stresses Induced by Phase Transformation", Internal Stresses and Fatigue in Metals, ed. by G.M. Rassweiler and W.L. Grube, Elsevier, pp. 110-119, 1959.

51. Marburger, R.E. and Koistinen, D.P., "X-ray Measurement of Residual Stresses in Hardened Steel", Ibid, pp. 98-109.

52. Roberts, F.A., "Improving the Fatigue Strength of Loaded Holes by the Dimpling Process", M.Sc. Thesis, The Univ. of Manitoba, Canada, 1973.

53. Benson, R.W. and Raelson, V.J., "Acoustoelasticity - A New Technique", Product Engineering, v. 30, n. 29, pp. 56-59, July 20, 1959.

54. Noronha, P.J., Chapman, J.R., and Wert, J.J., "Residual Stress Measurement and Analysis Using Ultrasonic Techniques", ASTM JTEVA (J. of Testing and Eval.), v. 1, n. 3, pp. 209-214, May 1973.

55. Abuku, S. and Cullity, B.D., "A Magnetic Method for the Determination of Residual Stress", Experimental Mechanics, v. 11, n. 5, pp. 217-223, May 1971.

56. Oppel, G.U., "Biaxial Elasto-Plastic Analysis of Load and Residual Stresses", Experimental Mechanics, v. 4, n. 5, pp. 135-140, May 1964.

57. Underwood, J.H., "Residual-Stress Measurement Using Surface Displacement Around an Indentation", Experimental Mechanics, v. 13, n. 9, pp. 373-380, Sept. 1973.

58. Sachs, G., "Residual Stresses; Their Measurement and Their Effects on Structural Parts", The Failure of Metals by Fatigue, Proc. of a Symp. held in the Univ. of Melbourne, Melbourne Univ. Press, Australia, ch. 15, pp. 237-247, 1947.

59. Bühler, H., "Complete Determination of the State of Residual Stress in Solid and Hollow Metal Cylinders", Residual Stresses in Metals and Metal Constructions, ed. by W.R. Osgood, Reinhold, New York, pp. 305-329, 1954.

60. Lambert, J.W., "A Method of Deriving Residual Stress Equations", Proc. SESA, v. 12, n. 1, pp. 91-96, 1954.

61. Weiss, V., "Residual Stresses in Cylinders", Proc. SESA, v. 15, n. 2, pp. 53-56, 1958.

62. Horger, O.J., Neifert, H.R., and Regen, R.R., "Residual Stresses and Fatigue Studies", Proc. SESA, v. 1, n. 1, pp. 10-18, 1943.

63. Mack, D.R., "Measurement of Residual Stress in Discs from Turbine-rotor Forgings", Experimental Mechanics, v. 2, n. 5, pp. 155-158, May 1962.

64. Weiss, S., Baker, G.S., and DasGupta, R.D., "Vibrational Residual Stress Relief in Plain Carbon Steel Weldments", Welding J., v. 55, n. 2, Res. Suppl., pp. 47S-51S, Feb. 1976.

65. Golsby, R.J., "Measurement of Residual Stresses in a Noryl Tele-communications Co-ordinate Selector Switch", Strain (J. of the Brit. Soc. for Strain Measurement), v. 11, n. 4, pp. 148-153, Oct. 1975.

66. Letner, H.R., "Application of Optical Interference to the Study of Residual Surface Stresses", Proc. SESA, v. 10, pp. 23-36, 1953.

67. Zapel, E.J., "Method of Determining Residual Stresses in a Biaxial Stress Field", Experimental Mechanics, v. 2, n. 8, pp. 245-248, 1962.

68. Waisman, J.L. and Phillips, A., "Simplified Measurement of Residual Stresses", Proc. SESA, v. 11, n. 2, pp. 29-44, 1954.

69. Hospers, F. and Vogelesang, L.B., "Determination of Residual Stresses in Aluminum-Alloy Sheet Material", Experimental Mechanics, v. 15, n. 3, pp. 107-110, March 1975.

70. Kalakoutsky, N., "The Study of Internal Stresses in Cast Iron and Steel", London, 1888.

71. Tebedge, N., Alpsten, G., and Tall, L., "Residual Stress Measurement by the Sectioning Method", Experimental Mechanics, v. 13, n. 2, pp. 88-96, Feb. 1973.

72. Alpsten, G.A. and Tall, L., "Residual Stresses in Heavy Welded Shapes", Fritz Laboratory Reprint No. 70-6 from Welding J., v. 49, March 1970.

73. Tebedge, N., Alpsten, G., and Tall, L., "Measurement of Residual Stresses - A Study of Methods", Fritz Engg. Lab., Report No. 337.8, Lehigh University, USA, Feb. 1970.

74. Mather, J., "Determination of Initial Stresses by Measuring the Deformations Around Drilled Holes", Trans. ASME, v. 56, pp. 249-254, 1934.

75. Soete, W. and Vancrombrugge, R., "An Industrial Method for the Determination of Residual Stresses", Proc. SESA, v. 8, n. 1, pp. 17-28, 1950.

76. Riparbelli, C., "A Method For the Determination of Initial Stresses", Proc. SESA, v. 8, n. 1, pp. 173-196, 1950.

77. Kelsey, R.A., "Measuring Non-Uniform Residual Stresses by Hole-Drilling Method", Proc. SESA, v. 14, n. 1, pp. 181-194, 1956.

78. Bathgate, R.G., "Measurement of Non-Uniform Biaxial Residual Stresses by the Hole-Drilling Method", Strain, v. 4, n. 2, pp. 20-29, April 1968.

79. Rendler, N.J. and Vigness, I., "Hole-Drilling Strain-Gage Method of Measuring Residual Stresses", Experimental Mechanics, v. 6, n. 12, pp. 577-586, Dec. 1966.

80. Lake, B.R., Appl, F.J., and Bert, C.W., "An Investigation of the Hole-Drilling Technique for Measuring Planar Residual Stress in Rectangularly Orthotropic Materials", Experimental Mechanics, v. 10, n. 6, pp. 233-239, June 1970.

81. Cordiano, H.V. and Salerno, V.L., "Study of Residual Stresses in Linearly Varying Bi-axial-Stress Fields", Experimental Mechanics, v. 9, n. 1, pp. 17-24, Jan. 1969.

82. Gupta, B.P., "Hole-Drilling Technique: Modifications in the Analysis of Residual Stresses", Experimental Mechanics, v. 13, n. 1, pp. 45-48, Jan. 1973.

83. Dini, J.W., Benedetti, G.A., and Johnson, H.R., "Residual Stresses in Thick Electrodeposits of Nickel-Cobalt Alloy", Experimental Mechanics, v. 16, n. 2, pp. 56-60, Feb. 1976.

84. Beaney, E.M. and Procter, E., "A Critical Evaluation of the Centre Hole Technique for the Measurement of Residual Stresses", Strain, v. 10, n. 1, pp. 7-14, Jan. 1974.

85. Schwaighofer, J., "Determination of Residual Stresses on the Surface of Structural Parts", Experimental Mechanics, v. 4, n. 2, pp. 54-56, Feb. 1964.

86. Vaidyanathan, S. and Finni, I., "Determination of Residual Stresses from Stress Intensity Factor Measurements", Trans. ASME, v. 93, J. Basic Engrg., pp. 242-246, June 1971.

87. Nawwar, A.M., McLachlan, K., and Shewchuk, J., "A Modified Hole-Drilling Technique for Determining Residual Stresses in Thin Plates", SESA Paper No. 2388, May 1975.

88. Wu, C.T., "Transverse Sensitivity of Bonded Strain Gages", Experimental Mechanics, v. 2, n. 11, pp. 338-344, Nov. 1962.

89. Meyer, M.L., "A Simple Estimate for the Effect of Cross Sensitivity on Evaluated Strain-gage Measurements", Experimental Mechanics, v. 7, n. 11, pp. 476-480, Nov. 1967.

90. Beaney, E.M., "The Effect of Cross-Sensitivity on the Determination of Stress by Strain Gauges", Strain, v. 6, n. 2, pp. 71-73, April 1970.

91. Machin, K.E. and Hassan, Y.E., "Transverse-Sensitivity Error in Strain-gage Measurement", Experimental Mechanics, v. 16, n. 1, pp. 38, 40 Jan. 1976.

92. Savin, G.N., Stress Concentration Around Holes, Pergamon Press, 1961 (Translated from Russian).

93. Peterson, R.E., Stress Concentration Factors, John Wiley, 1974.

94. Machinary's Handbook, 14th ed., p. 1116, 1949.

95. Manson, S.S., "Avoidance, Control and Repair of Fatigue Damage", Metal Fatigue Damage, ASTM STP 495, pp. 254-346, 1971.

96. ASTM Committee E9 on Fatigue, "A Guide for Fatigue Testing and the Statistical Analysis of Fatigue Data", ASTM STP-91-A, 2nd ed., 1963.

97. Weibull, W., Fatigue Testing and Analysis of Results, Pergamon Press, 1961 (1266 references).

98. Sinclair, G.M. and Dolan, T.J., "Effect of Stress Amplitude on Statistical Variability in Fatigue Life of 75 S - T6 Aluminum Alloy", Trans. ASME, v. 75, pp. 867-872, 1953.

99. Anonymous, "Subroutine NLMAX", 360/75 FORTRAN IV Subroutine Library, "Least Squares Fitting and Optimization", Package B - Computing Centre, Univ. of Waterloo, Ont., Dec. 1970.

100. Weibull, W., "Statistical Handling of Fatigue Data and Planning of Small Test Series", FFA (The Aeronautical Research Institute of Sweden), Report No. 69, 1957.

101. Wilson,E.L., "Structural Analysis of Axisymmetric Solids", AIAA Journal, v. 3, n. 12, December 1965.

APPENDIX A

PRESENTATION AND STATISTICAL ANALYSIS OF FATIGUE DATA

A.1 COMPARISON OF NOTCHED SPECIMENS TYPES-A AND -B

The purpose of this test was to find out whether specimens having the same test section and the same notch but different in shape would survive the same number of load cycles until failure. Two samples of specimens type-A and type-B were notched and fatigue cycled to failure at the same stress level. The results of fatigue testing are given in Table A.1.

To answer the question whether the observed differences in the values are due to chance or due to some differences in the results of both types of specimens, two methods may be employed. The first is the rank test which does not require knowledge of the shape of the fatigue life distribution. It assumes that the two groups are drawn from populations that have the same shape but may differ in their medians. The second method assumes the normality of the fatigue life distribution and applies tests of significance to both the means and standard deviations of the samples. The hypothesis that the two samples are drawn from the same population will now be tested using both methods.

i. THE RANK TEST

In this test the rank of each observation in the two samples combined is determined and the ranks for the two samples are totalled

TABLE A.1

RESULTS OF COMPARATIVE TESTS

Maximum stress level 12 644 psi

Nominal stress ratio 0.0

Sample No.	Specimen type	Sample size	Lives to failure, Kilocycles	(Rank total)
23	A	5	114, 163, 174, 213, 300 (3), (4), (6), (9), (10)	(32)
23B	B	6	60, 61, 165, 188, 205, 328 (1),(2),(5), (7), (8),(11)	(34)

separately and then the smaller total is compared to the critical range at the desired level of significance. In Table A.1 the ranks are indicated in parentheses and the totals are shown in the last column. The rank total for type-A specimens, which has the smaller number of measurements, is 32. From Table II [96] the critical lower and upper rank totals for 5% level of significance are 19 and 41, respectively, and for 1% level of significance they become 16 and 44. Since the observed value falls within the critical range, the conclusion may be confidently drawn that the difference in sample means is insignificant and it may be attributed to chance.

ii. TESTS OF SIGNIFICANCE

The assumed normality of fatigue life distribution requires transformation of N to logN . Let the sample mean and standard deviation of logN be: $\bar{x}_1$, s_1 and $\bar{x}_2$, s_2 for samples type-A of size n_1 and type-B of size n_2. Two tests must be conducted. The first is to check the difference in sample standard deviations and the second is to test the difference between the means. Table A.2 gives a summary of the results.

1. Testing the difference between s_1 and s_2:

$$\text{The ratio} \quad \nu = s_1^2 / s_2^2 = 0.256$$

For a chosen level of significance $\alpha = 0.05$; compute $\beta = 1 - \alpha = 0.95$ and by using the F-distribution tables [96] the value F_β corresponding to degrees of freedom $(n_1 - 1)$ and $(n_2 - 1)$ are found to be $F_\beta = 5.19$. Therefore, $1/F < \nu < F$ and the sample variances, and thus standard deviations are considered to be not significantly different.

TABLE A.2

TESTS OF SIGNIFICANCE - SUMMARY OF RESULTS

Specimen type	A	B
Sample size	$n_1 = 5$	$n_2 = 6$
Mean logN	$\bar{x}_1 = 2.2630$	$\bar{x}_2 = 2.1465$
Sample standard deviation	$s_1 = 0.1383$	$s_2 = 0.2733$

2. Testing the difference between $\overline{x}_1$ and $\overline{x}_2$:

Firstly, an estimate of the common variance is computed by

$$s^2 = \frac{(n_1 - 1)\, s_1{}^2 + (n_2 - 1)\, s_2{}^2}{(n_1 + n_2 - 2)} = 0.05$$

Then, the test statistic t' is computed from

$$t' = \frac{\overline{x}_1 - \overline{x}_2}{s \cdot \sqrt{(1/n_1) + (1/n_2)}} = 0.85$$

This test statistic t' is compared with the value t obtained from the t-distribution tables [96]. For a 0.05 significance level, $\beta = 0.95$ and corresponding to $(n_1 + n_2 - 2)$ degrees of freedom, $t_\beta = 1.83$. Since $t_\beta > t'$, therefore, the sample means are not significantly different at the 0.05 level of significance.

The final conclusion based on the foregoing analysis is that there is no significant difference between notched specimens type-A and type-B.

A.2 OPTIMIZATION TESTING: SERIES 1

A total of thirty type-A specimens with an average edge strain ranging from 0 to 2.25 percent were tested at the same stress level. The results are given in Table A.3. For each sample, the median is taken as the best estimate of population mean, and the confidence limits of the mean are calculated for a confidence level $\gamma = 0.95$. If $\overline{x}$ and s are the median and standard deviation of logN for each sample, therefore, the confidence limits of the population mean are calculated from:

$$\mu = \overline{x} \pm (t_\beta / \sqrt{n}) \cdot s$$

where $(t_\beta / \sqrt{n}) = 1.24$ for $\gamma = 0.95$ and a sample size $n = 5$.

The experimental results, as plotted, are shown in Figure A.1. It is evident that there is a continuous improvement in fatigue life as the average edge strain increases. The trend of improvement is expected to be similar in shape to the characteristic edge dimpling curve discussed in Section 3.2.4. This expectation is based on the fact that fatigue improvement is directly related to the magnitude of residual compression induced in the critical region. Therefore, in the characteristic elastic region no life improvement is expected. In the developing region, a rapid increase in residual stress prompts a similar trend in the life improvement. While in the stability region, slight fatigue life change is expected. This behaviour is represented by the dotted curve in Figure A.1.

It is evident that the experimental data is in partial disagreement with the expected behaviour, in the lower range of up to approximately 1.2 percent average edge strain. This deviation of the life

TABLE A.3

TEST SERIES NO. 1:

RESULTS OF PRELIMINARY OPTIMIZATION TESTING

Maximum Stress Level = 23,158 psi
Nominal Stress Ratio = 0.0
Notch Depth = 1.6 mm (0.063 in)

Sample		Dimpling	$\bar{\varepsilon}_e$ %	Lives to Failure, Kc.					$\bar{x}$	$\bar{\bar{x}}$	S	$\frac{t_\beta}{\sqrt{n}}$ S
No.	Size	Ratio R_t							Median	Mean		
11	5	0.00	0.00	19	21	22	22	24	4.342	4.333	0.033	0.041
12	5	1.00	0.52	27	37	42	53	59	4.623	4.624	0.120	0.149
13	5	1.25	0.82	36	54	73	89	109	4.863	4.828	0.169	0.210
14	5	1.50	1.25	45	51	54	72	77	4.732	4.767	0.090	0.111
15	5	1.75	1.73	75	109	128	130	184→	5.107	5.080	0.126	0.157
16	5	2.00	2.25	93	123	143	149	215→	5.155	5.144	0.119	0.147

→Fracture occurred outside the test section but visual crack was observed at the test section.

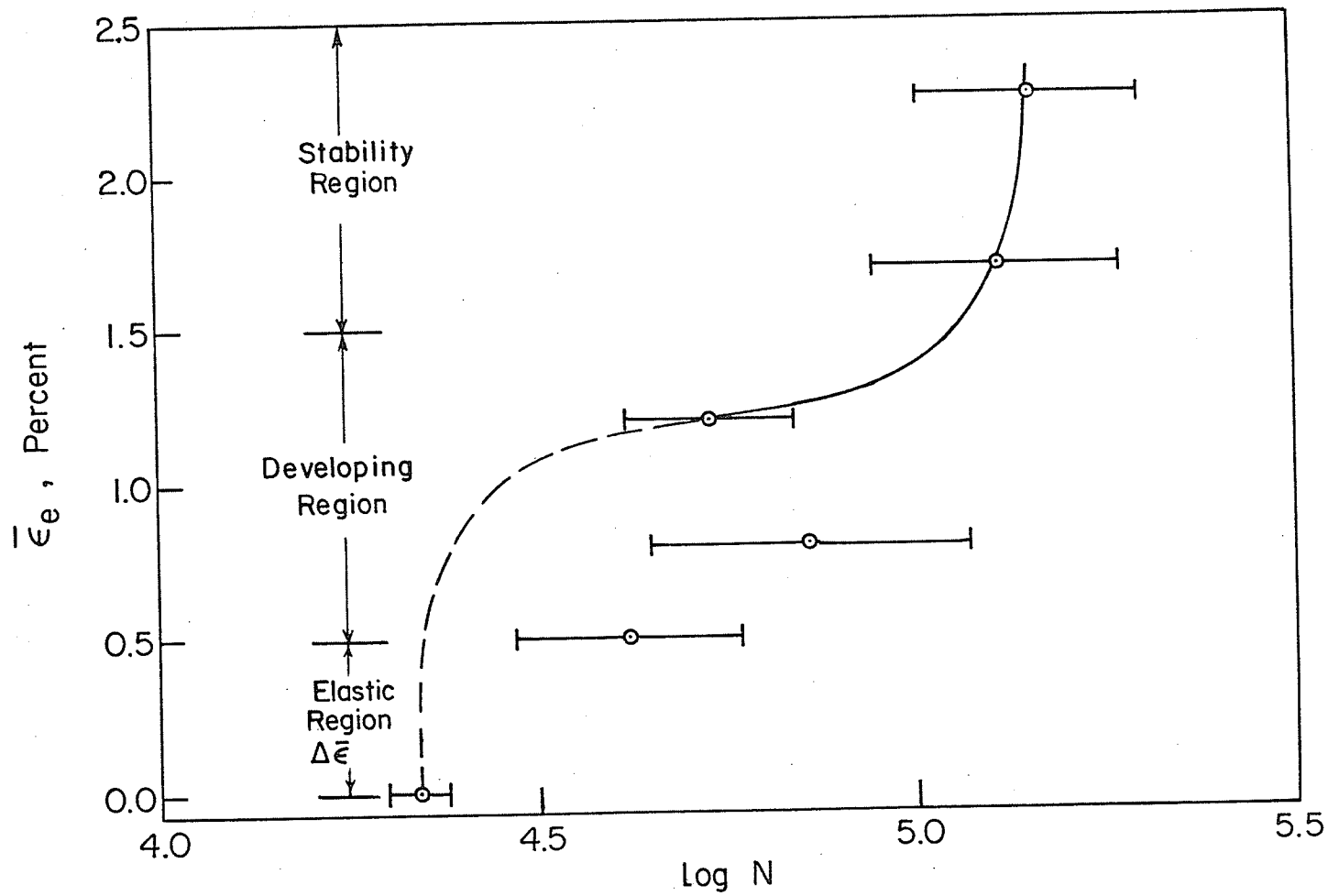

Figure A.1 Average edge strain , $\bar{\epsilon}_e$, vs. log N plot

improvement, although favourable, may be explained in view of the undesirable bending discussed in Section 3.2.1. In the elastic region, although the average edge strain at the neutral axis does not exceed the elastic limit, both surfaces of the dimpled region experience stresses in excess of the elastic limit. Therefore, the resulting residual stress distribution will be of the quality shown in Figure A.2 and the effective value of residual stress will be the least of the stresses at the corners. This effect of bending appears gradually and disappears more rapidly as the whole plate thickness experiences plastic stretching.

It may also be observed that the favourable improvement due to bending effects in the elastic and developing regions is accompanied by considerable scatter. This scatter which was predicted in Section 3.2.4 is due to the high sensitivity of residual stress to the dimpling ratio. As the average edge strain increases, the surface strains increase, and the residual stresses in the corners will be in the stability region. Hence, the scatter may decrease again for values of average edge strain in the upper range of the developing region. The results, however, confirm that the stability region is the most desirable range of edge dimpling.

To permit easy comparison of the results with the characteristic curve, the data are represented in terms of a median life improvement factor. It is defined as the ratio of the number of cycles to failure (median life) of an edge-dimpled specimen to those of a non-edge-dimpled specimen. The results are shown in Figure A.3. A thorough examination of the curve would lead to the recommendation of values of average edge

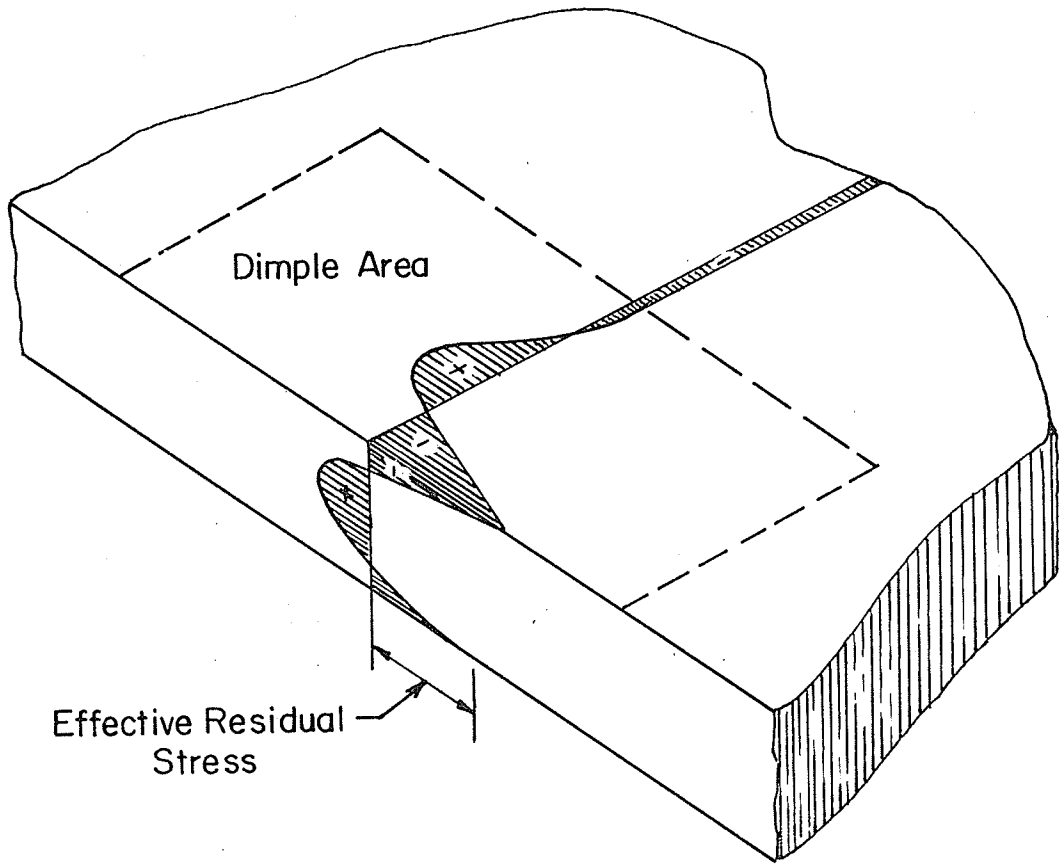

Figure A.2 Residul stress distribution for $\bar{\epsilon}_e$ in the elastic stage.

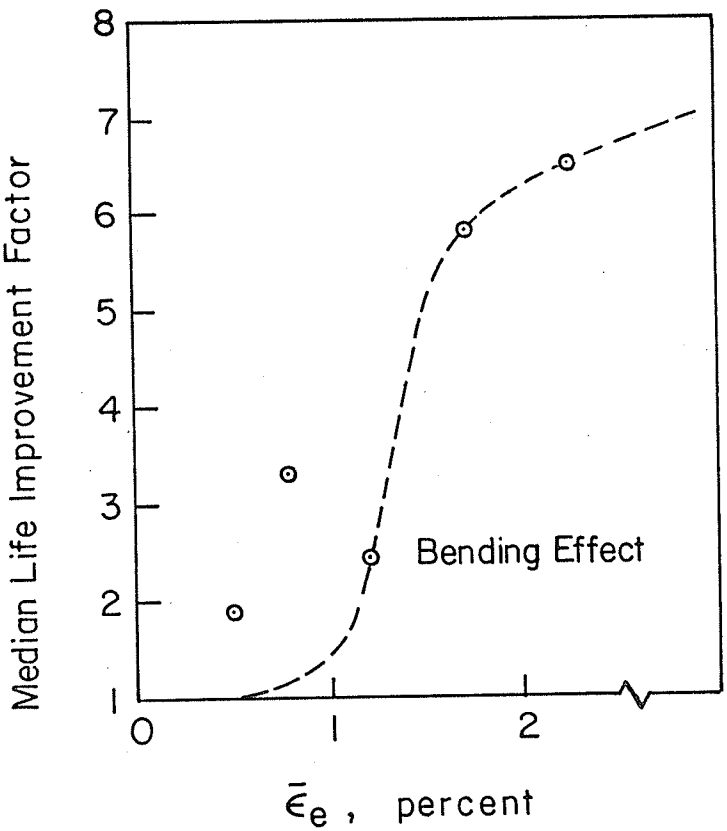

Figure A.3 Median life improvement factor vs. $\bar{\epsilon}_e$.

strain, $\bar{\varepsilon}_e$, greater than 1.5 percent. As $\bar{\varepsilon}_e$ increases, the improvement will continue to increase up to a limit determined by the maximum dimpling strain that can be reached. When the strain at the outer surfaces approaches the ultimate strain, sub-micro cracks will form and cause the deterioration of fatigue strength. However it is not likely that this limit will be reached. The limit is practically determined by the value of average edge strain at which the dimpled region could be flattened without local buckling. This limit was found to be 2 percent and was used in all subsequent fatigue testing.

A.3 FATIGUE LIFE DISTRIBUTION OF DIMPLED SPECIMENS

The following test is aimed at finding the form of distribution of fatigue lives of dimpled specimens. To be useful, the distribution shape should satisfy the following conditions:

1. The results predicted by the distribution should be in good agreement with the experimental data.
2. The distribution form should be mathematically tractable.

Therefore, the experimental data should be plotted on different probability scales for different distribution shapes and the best fitting form could be determined. However, the normal distribution mathematical form provides unmatchable ease in data manipulation, and hence, an approximately normal fit may be preferred over other forms that result in better fitting.

A total of 34 specimens type-A with optimal edge treatment (2% average edge strain) were cycled to failure at a maximum stress level of 17 ksi (113 MPa). The results were ordered from least to greatest as shown in Table A.4. The probability of failure, P, was computed from:

$$P_W = k/(n + 1)$$

where k is the cumulative number of specimens failed, and

n is the total number of specimens tested.

This is the most frequently used form for P employed by Weibull (1939) and Gumbel (1954) [97]. Blom (1956) suggested that

$$P_B = (k - a) / (n - a - b + 1)$$

in which a and b are fractional constants to be chosen with regard to the distribution of fatigue life. For the normal distribution Blom's

TABLE A.4

TEST SERIES NO. 9:

RESULTS OF FATIGUE LIFE DISTRIBUTION

Maximum stress level = 16 858 psi

Nominal stress ratio = 0.0

All specimens type-A.

Order (k)	N, kc.	logN	P_W,%	P_B,%
1	153	5.185	2.86	1.82
2	325	5.512	5.71	4.74
3	355	5.550	8.57	7.66
4	356	5.551	11.43	10.56
5	374	5.573	14.29	13.50
6	432	5.635	17.14	16.42
7	450	5.653	20.00	19.34
8	473	5.675	22.86	22.26
9	475	5.677	25.71	25.18
10	488	5.688	28.57	28.10
11	489	5.689	31.43	31.02
12	527	5.722	34.29	33.94
13	533	5.727	37.14	36.86
14	548	5.739	40.00	39.78
15	577	5.761	42.86	42.70
16	598⊕	5.777	45.71	45.62
17	599	5.777	48.57	48.54
18	622	5.794	51.43	51.46
19	632	5.801	54.29	54.38
20	633	5.801	57.14	57.30
21	634	5.802	60.00	60.22
22	647	5.811	62.86	63.14
23	682⊕	5.834	65.71	66.06
24	689	5.838	68.57	68.98
25	724	5.860	71.43	71.90
26	750⊕	5.875	74.29	74.82
27	770	5.886	77.14	77.74
28	813	5.910	80.00	80.66
29	831	5.920	82.86	83.58
30	853→	5.931	85.71	86.50
31	909	5.959	88.57	89.42
32	996→	5.998	91.43	92.34
33	1394→	6.144	94.29	95.26
34	2377	6.376	97.14	98.18

→ Fracture occured outside the test section.

⊕ Same as above but visual cracks were observed at the test section.

equation becomes

$$P_B = (k - 3/8) / (n + 1/4)$$

and the results will fit in a straight line. Both Weibull's and Blom's estimates are given in Table A.4.

When the results are plotted on log-linear scale, as shown in Figure A.4, it appears that the best fitting line is a curve which represents the desired mathematical form. It is evident that it is not an easy task to fit the data to a curve. It is rather convenient to transform the data and fit it to a straight line. This can be done by using probability paper. Figure A.5 shows the log-normal probability plot of the present data. A comparison of Figures A.4 and A.5 indicates that the tails of the distribution are slightly recitifed by plotting on log-normal probability paper and the results reasonably fit a linear relation. However, it should be pointed out that the presence of extreme points in the log-normal plot is not unexpected. In general, fatigue as a physical phenomenon is always associated with variable amounts of scatter, which is dependent on a number of factors. In edge dimpling a further source of scatter is that arising from minor variations in the residual compressive stress distribution from one specimen to the other. In addition to that is the possibility of scatter due to the accuracy of notching of specimens. Such factors could possibly account for the extreme data points.

In conclusion, the life distribution of dimpled-notched specimens type-A could be assumed normal.

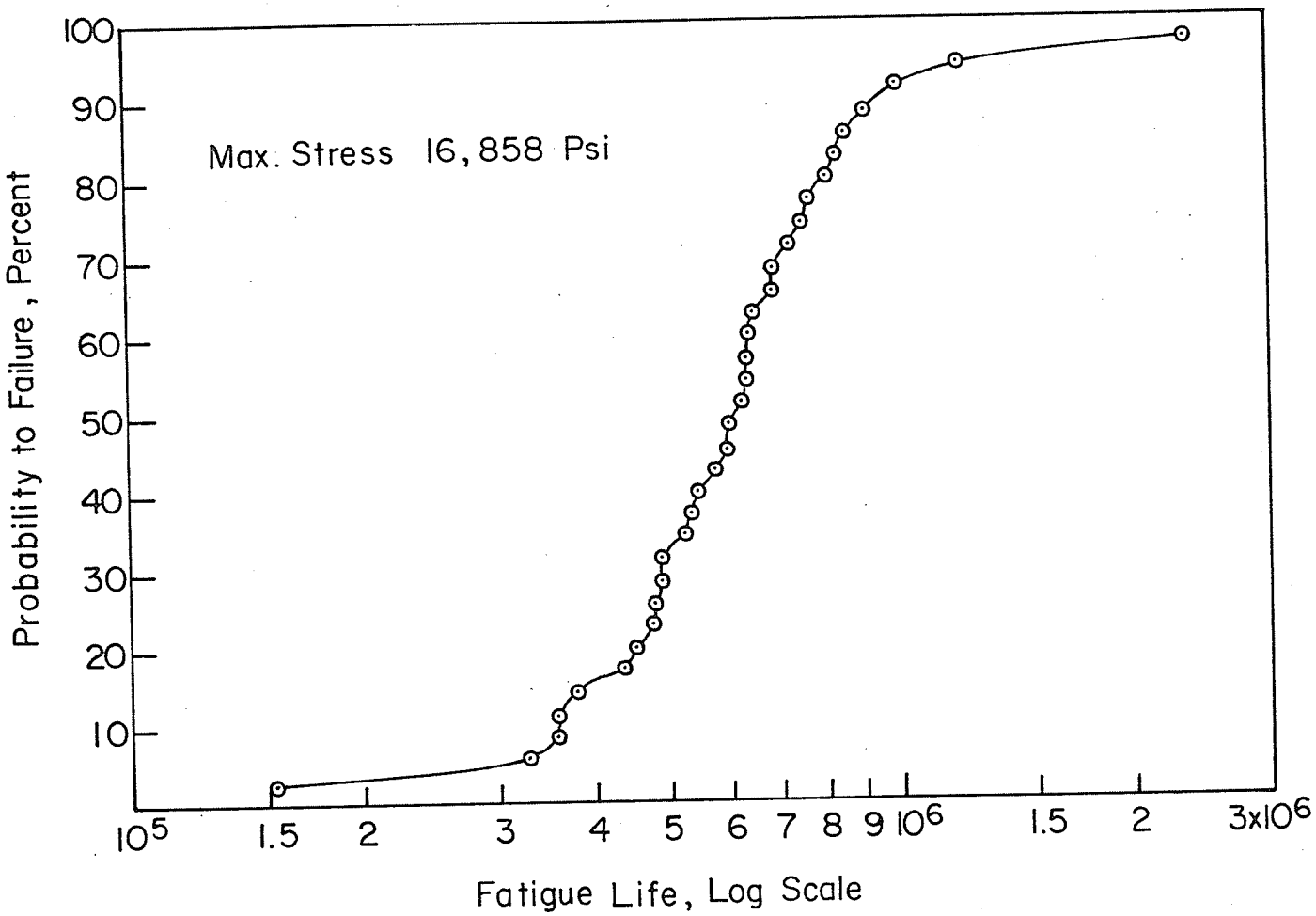

Figure A.4 Comulative Probability plot for data Series 9.

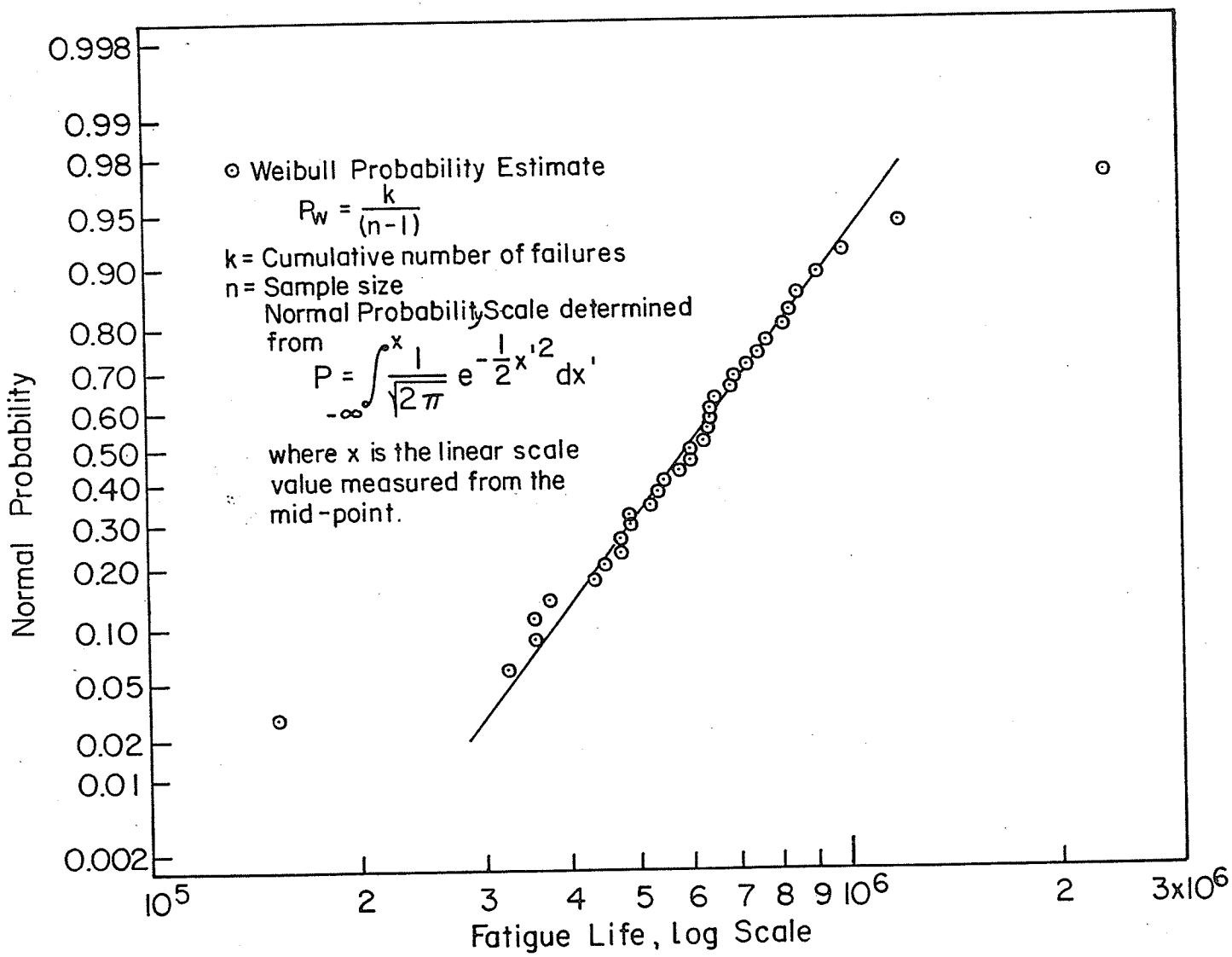

Figure A.5 Log - Normal probability plot for data of Series 9.

A.4 PRIMARY FATIGUE TESTING: SERIES 2, 3 AND 4

The results of fatigue test series 2, 3 and 4 are given in Tables A.5, A.6 and A.7, respectively. The results are fitted to three S-N curves according to the general mathematical expression of the power function; which has been used extensively by several investigators such as Weibull [97] and Sinclair and Dolan [98]. It is in the form:

$$S = S_e + A\,(N + B)^{-m}$$

where S is the maximum fatigue strength,

N is the fatigue life,

S_e is the fatigue strength corresponding to an infinite number of cycles,

A is the general parameter which has the units of stress,

B is the time scale parameter, and

m is the shape parameter of the curve.

The parameters B and m determine the inflection point, N_i, of the semi-log plot, where $N_i = B/m$.

Such a model is desirable to permit accurate and reliable comparison of different test series and to enable extrapolation to higher number of cycles which is not covered by experiments. The best fitting curve to the data is determined by means of a computerized version of the least squares method (first proposed by Legendre in 1805) and using the Gauss-Newton iteration technique [99]. The models should be fitted to the median lives for the following statistical reasons [96, 100]:

TABLE A.5

TEST SERIES NO. 2:

RESULTS OF FATIGUE TESTING FOR NOTCHED SPECIMENS

Sample No.	Sample Size	Stress Level, S_{max}, psi	Lives to Failure, Kilocycles
21	6	21,073	18, 19, 25, 26, 33, 39
22	7	16,858	50, 58, 70, 71, 73, 74, 83
23	5	12,644	114, 163, 174, 213, 300
24	6	8,429	752, 837, 944, 963, 1014, 1027
25	3	7,158	942, 1741, 10055*
26	1	6,322	10088*
27	1	5,053	10008*

*Runouts: Test terminated at indicated life.

TABLE A.6

TEST SERIES NO. 3:

RESULTS OF FATIGUE TESTING FOR DIMPLED-NOTCHED SPECIMENS

Sample No.	Sample Size	Stress Level, σ_{max}, psi	Lives to Failure, Kilocycles
31	5	25,304	44, 81, 91, 94, 105
32	10	21,073	95, 159, 160, 185, 211, 227, 252, 278⁺, 308⁺, 365
33	34	16,858	See results of Test Series No. 9
34	6	14,751	919, 1156, 1164, 1270, 2127, 3300*
35	5	12,644	2531, 2794, 6256, 13650*, 14609*

*Runouts: Test terminated at this life.

⁺Fracture occurred outside the test section, but visual cracks were observed at the test section.

TABLE A.7

TEST SERIES NO. 4:

RESULTS OF FATIGUE TESTING FOR PLAIN SPECIMENS

Sample No.	Sample Size	Stress Level, σ_{max}, psi	Lives to Failure, Kilocycles
41	5	36,018	94, 97, 116, 120, 126
42	6	32,031	62, 94, 129, 146, 170, 220
43	6	28,027	142, 189, 203, 241, 242, 261
44	6	24,023	214, 472, 547, 589, 617, 828
45	6	22,029	475, 622, 679, 1273, 1493, 2162
46	2	20,019	10000*, 10000*

*Runouts: Test terminated at this life.

i. The distribution of individual fatigue life values is usually skewed. In cases where the distribution shape is unknown, the analysis of data may be done with no specific assumptions of the shape. In this case the median is chosen to express the central tendency of data points at each stress level. The median, being the middle point value of observations, determines the 50 percent probability S-N curve which is sufficient for purposes of comparison.

ii. The median holds the same relative position with respect to the other observations after transformation in which the order of observations is preserved, whereas other estimates do not.

iii. In small samples, the median value is not greatly influenced by outlying and abnormal data points. Therefore, the central tendency of the population of specimens is estimated more accurately by the median and not the mean of small sample data.

It is readily seen that the median analysis provides an average S-N curve without knowledge of the shape of the fatigue life distribution. However, in small sample data, serious inaccuracies may result in estimating the confidence intervals for the median life. In order to sharpen the inferences which may be made from the data, particular functional forms can be assumed for the fatigue life distribution. It has been found that semi-log presentation of data results in approximately normal distribution. Having assumed the normality of the distribution it is then possible to use the data to obtain more

precise estimates of the confidence interval of the median (which is equal to the mean in case of normal distributions). Therefore to gain the advantages of using the median together with the accuracy acquired by assuming normality, the mean of the population will be estimated by the sample median. The assumption of normality could safely be made for data of plain or notched specimens. Meanwhile, it is shown in Section A.3 that the fatigue life distribution of edge dimpled specimens is essentially normal. Therefore, the assumption of normality is valid for the present study.

For each S-N curve the following steps of solution were taken:

1. For each sample find the median $\bar{x} = \log\bar{N}$; where $\bar{N}$ is the median life, and the standard deviation of the sample $s = \sqrt{\Sigma(x - \bar{x})^2/n}$; where $x = \log N$. From which the best estimate of the population mean, μ, and the population standard deviation, σ, are:

$$\mu = \bar{x}$$

$$\sigma = s \cdot \sqrt{n/(n - 1)} = \sqrt{\Sigma(x - \bar{x})^2/(n - 1)}$$

2. For a confidence level γ, usually 0.95 [1], calculate the confidence limits of the standard deviation; the lower limit, σ_ℓ, and the upper limit, σ_u, as follows:

$$\sigma_\ell = s/\sqrt{P_{\beta_2}}, \quad \sigma_u = s/\sqrt{P_{\beta_1}}$$

where the P-values are taken from Chi-square distribution tables, which may be found in any statistical tables handbook or in Reference 96. If γ is an arbitrary confidence level the percentiles $\beta_1 = (1 - \gamma)/2$ and $\beta_2 = (1 + \gamma)/2$ may be calculated.

3. Plot the standard deviation versus the stress level on log-log paper and determine the best fitting straight line which represents the expression

$$\sigma = \sigma_0 \cdot s^{-q}$$

where σ_0 is the intercept and q is the slope of the transformed straight line relation. This formula was proposed by Sinclair and Dolan [98]. The linear relation is thus used to calculate the corrected best estimate of the standard deviation of the population, $\hat{\sigma}$, at each stress level.

4. Determine the confidence interval of the population mean for a confidence level $\gamma = 0.95$:

$$\text{the lower limit} \quad \mu_\ell = \mu - (t_{\beta_1}/\sqrt{n}) \cdot \hat{\sigma}$$

$$\text{the upper limit} \quad \mu_u = \mu + (t_{\beta_2}/\sqrt{n}) \cdot \hat{\sigma}$$

where the t-values are determined from the t-distribution tables [96] for (n - 1) degrees of freedom.

For convenience the parameters $1/\sqrt{P_{\beta_2}}$, $1/\sqrt{P_{\beta_1}}$ and $t_\beta/\sqrt{n}$ are are calculated for a confidence level of 0.95 and for a sample size ranging from $n = 2$ to 40 (linear interpolation may be used). The resulting values appear in Table A.8 and may be used directly to determine the confidence limits of both the standard deviation and mean of the population.

5. Use the μ-values at each stress level to find the 50 percent probability S-N curve with the constraints $\mu_\ell \leq \mu \leq \mu_u$.

TABLE A.8

STATISTICAL PARAMETERS FOR DETERMINING

CONFIDENCE LIMITS OF THE MEAN AND STANDARD DEVIATION

Confidence level $\gamma = 0.95$

Confidence limits for $\mu = \bar{x} \pm (t_\beta/\sqrt{n}).\hat{\sigma}$

Confidence limits for $\sigma = s.(1/\sqrt{P_{\beta 2}})$, $s.(1/\sqrt{P_{\beta 1}})$

Sample size $= n$

n	$(t_\beta/\sqrt{n})^*$	$(1/\sqrt{P_{\beta_2}})$	$(1/\sqrt{P_{\beta_1}})$
2	8.98	0.45	31.94
3	2.48	0.52	6.29
4	1.59	0.57	3.73
5	1.24	0.60	2.87
6	1.05	0.62	2.45
7	0.93	0.64	2.20
8	0.83	0.66	2.04
9	0.77	0.68	1.92
10	0.71	0.69	1.83
20	0.47	0.76	1.46
30	0.37	0.80	1.34
40	0.32	0.82	1.29
∞	0.00	1.00	1.00

* Note that $t_\beta = t_{\beta_1} = t_{\beta_2}$

The foregoing procedure was applied to results of test Series 2, 3 and 4. Numerical results are presented in Table A.9 and values of $\hat{\sigma}$ are determined from figure A.6. The median lives and their confidence intervals are plotted in Figure A.7 as well as the best fitting S-N curves determined by the least squares technique.

TABLE A.9

STATISTICAL ANALYSIS OF SERIES 2, 3 & 4

Sample No.	n	$\bar{x}$ (mean)	$\bar{\bar{x}}$ (median)	σ	σ_ℓ	σ_u	$\hat{\sigma}$	μ	$t_\beta \frac{\hat{\sigma}}{\sqrt{n}}$	μ_ℓ	μ_u	S_{max}, ksi
21	6	4.409	4.406	0.131	0.081	0.321	0.047	4.406	0.049	4.357	4.455	21.073
22	7	4.830	4.851	0.074	0.047	0.163	0.077	4.851	0.072	4.779	4.923	16 858
23	5	5.263	5.241	0.155	0.093	0.444	0.147	5.241	0.182	5.059	5.423	12.644
24	6	5.963	5.979	0.053	0.033	0.129	0.390	5.979	0.410	5.569	6.389	8.429
25	3	6.406	6.241	0.534	0.277	3.357	0.565	6.241	1.401	4.840	7.642	7.158
31	5	4.901	4.959	0.150	0.090	0.431	0.147	4.959	0.182	4.777	5.141	25.304
32	10	5.323	5.340	0.169	0.117	0.310	0.170	5.340	0.121	5.219	5.461	21.073
33	34	5.777	5.786	0.200	0.162	0.264	0.200	5.786	0.070	5.716	5.856	16.858
34	6	6.174	6.085	0.208	0.129	0.509	0.220	6.085	0.231	5.854	6.316	14.751
35	5	6.789	6.796	0.363	0.218	1.042	0.250	6.796	0.310	6.486	7.106	12.644
41	5	5.041	5.064	0.057	0.034	0.164	0.057	5.064	0.071	4.993	5.135	36.018
42	6	5.102	5.137	0.195	0.121	0.479	0.082	5.137	0.086	5.051	5.223	32.031
43	6	5.320	5.345	0.097	0.058	0.239	0.122	5.345	0.128	5.217	5.473	28.027
44	6	5.703	5.754	0.200	0.124	0.490	0.200	5.754	0.210	5.544	5.964	27.023
45	6	5.986	5.968	0.256	0.159	0.627	0.256	5.968	0.269	5.699	6.237	22.029

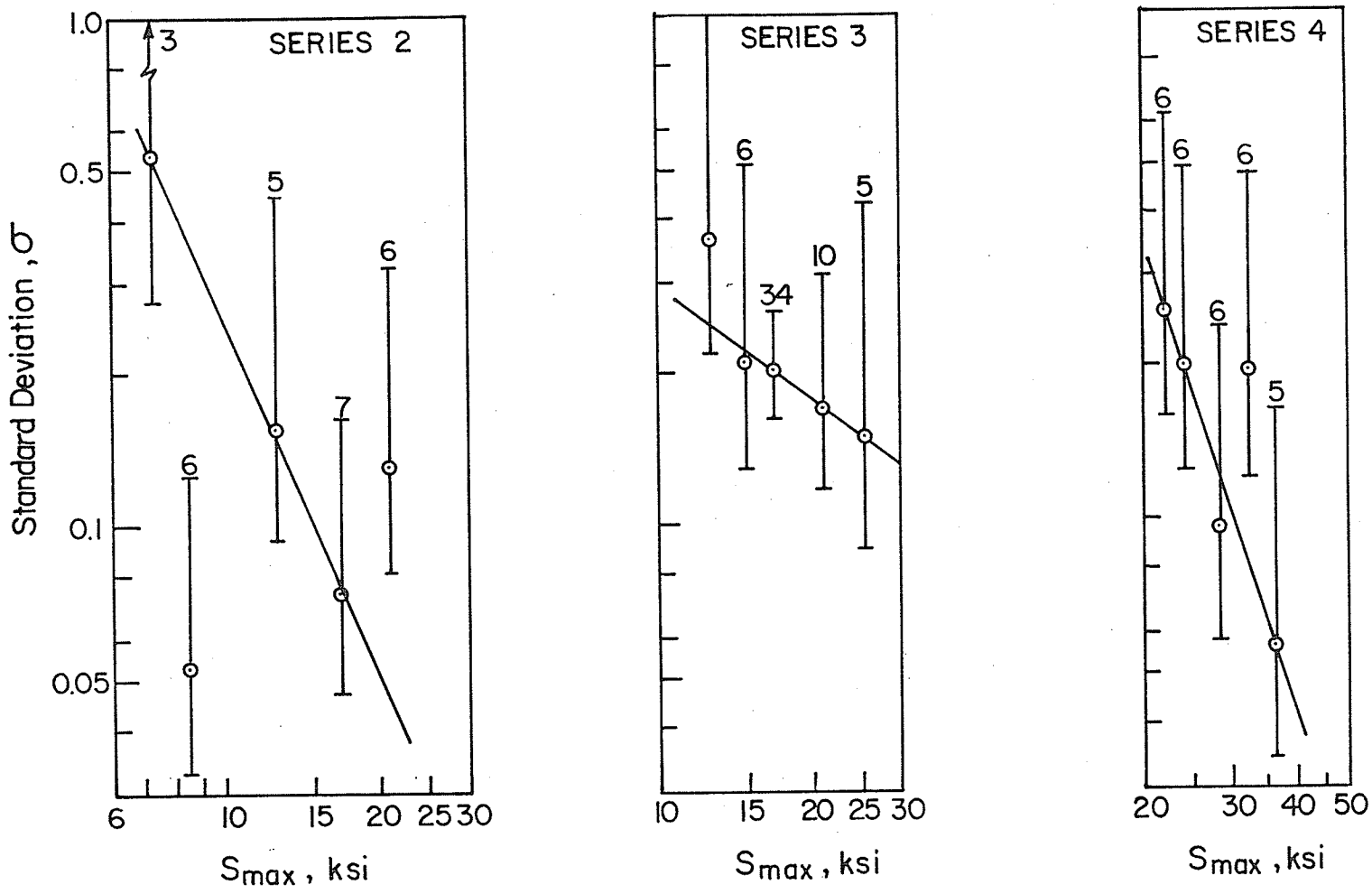

Figure A.6 Log - Log plots of the best estimate of standard deviation of the population, σ, vs. the maximum fatigue stress, S_{max}.

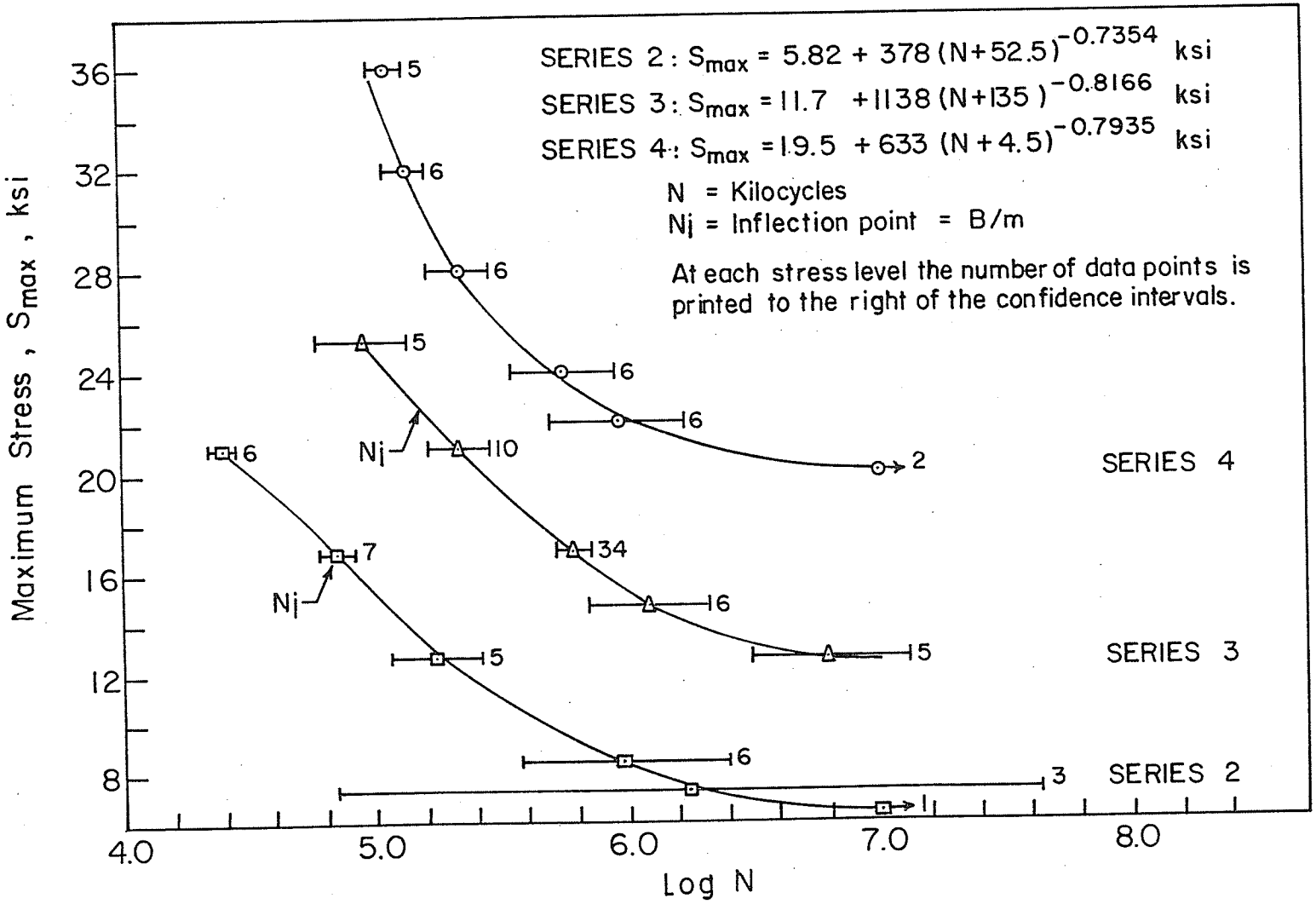

Figure A.7 S-N Curves for fatigue strength test series.

A.5 PRELOADING FATIGUE TESTING: SERIES 5, 6, 7 AND 8

Test series 5, 6, 7 and 8 were carried out to investigate the influence of prior overloading or "preloading" on the fatigue improvements achieved by edge dimpling. In series 5, preliminary testing was carried out to roughly determine the trend of change of fatigue life with different values of preload. The test results are given in Table A.10. The results are represented in Figure A.8 in which logN is plotted versus the prestress ratio. The prestress ratio, R_{ps}, is the ratio of prestress to the yield strength of the material (this is the ratio of preload to the yield load). The following observations may be made:

a. The indicated trend of behaviour was determined at a high stress level and will probably be different at lower levels.

b. The effect of preloading seems to be insignfiicant for prestress ratio less than 0.5.

c. A gradual improvement follows and continues until a peak is reached in the vicinity of $R_{ps} = 1.0$.

d. This is followed by rapid deterioration of fatigue life and the improvement gained by edge dimpling entirely disappears at a prestress ratio of approximately 1.2. Thereafter, the steep decrease of fatigue life continues.

As a result of the preliminary speed test, Series 5, three values of prestress were selected for further testing:

$R_{ps} = 0.65$ where the improvement due to preloading starts,

$R_{ps} = 1.0$ in the vicinity of the peak improvement, and $R_{ps} = 1.17$

TABLE A.10

TEST SERIES NO. 5:

RESULTS OF PRELIMINARY PRELOADING TESTING

Maximum stress level = 23 158 psi

Nominal stress ratio = 0.0

Yield strength of material= 45 000 psi

Sample		Prestress ksi	Prestress R-tio, R_{ps}	Lives to Faiure, kc.
No.	Size			
51	3	0	0.00	113, 113, 135
52	3	20	0.44	90, 101, 105
53	3	30	0.67	109, 132, 143
54	3	40	0.89	163, 184, 223
55	3	50	1.11	119, 184, 196
56	2	60	1.33	23, 31

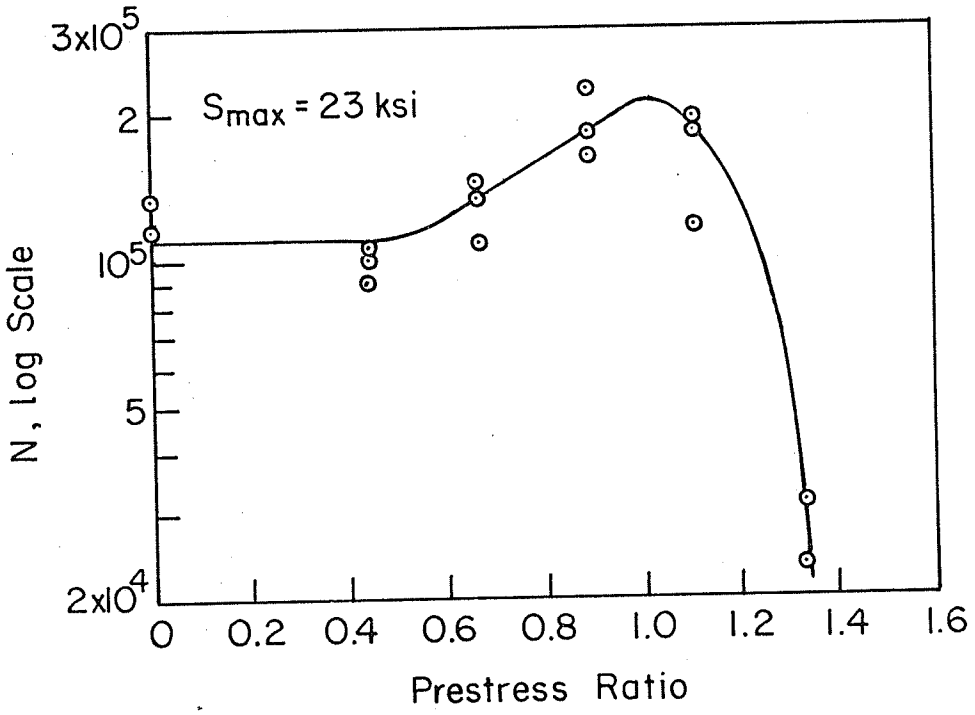

Figure A.8 The effect of prestress ratio on fatigue life, at the same stress level.

slightly before the sharp deterioration occurs to avoid wide scatter in the results.

Test series 6, 7 and 8 were conducted for the three selected values of preload ratio. The results are given in Tables A.11, A.12 and A.13, respectively. Three S-N curves were fitted to the results using the method described in Section A.4. The details of the various statistics are given in Table A.14. Figure A.9 was used to determine the best estimate of standard deviation for each test series. The results of least squares curve fitting are shown in Figure A.10 along with the corresponding models.

From a statistical point of view the means of the three samples were examined to determine whether they were significantly differnt or not. Consider the most divergent results at the highest stress level, namely, samples numbers 71 and 81. Assume that the samples are drawn from normally distributed populations. The sample sizes, means and standard deviations are:

$$n_1 = 5 \quad , \quad \bar{x}_1 = 4.675 \quad , \quad s_1 = 0.201$$

$$n_2 = 6 \quad , \quad \bar{x}_2 = 4.543 \quad , \quad s_2 = 0.194$$

Calculate the variance ratio

$$\nu = s_1^2 / s_2^2 = 1.081$$

At a significance level of $\gamma = 0.95$, and using the F-distribution tables [96] determine

$$F_{0.95} = 5.19 \quad , \quad 1/F_{0.95} = 0.193$$

TABLE A.11

TEST SERIES NO. 6:

RESULTS OF FATIGUE TESTING WITH PRIOR OVERLOADING

PRESTRESS RATIO, R_s = 0.65

Sample No.	Sample Size	Stress Level, S_{max}, psi	Lives to Failure, Kilocycles
61	6	30,000	40, 54, 54, 55, 56, 109→
62	6	25,000	81, 104, 112, 125, 170, 249→
63	6	20,000	189, 257, 261, 293, 368, 614→
64	6	15,000	273→, 757, 807, 928, 1095, 2545*
65	5	13,250	1916, 2006, 2295, 2352, 4412
66	1	12,000	10288

*Runouts: Test terminated at indicated life.

→Fracture occurred outside the test section.

TABLE A.12

TEST SERIES NO. 7:

RESULTS OF FATIGUE TESTING WITH PRIOR OVERLOADING

PRESTRESS RATIO, R_s = 1.00

Sample No.	Sample Size	Stress Level, S_{max}, psi	Lives to Failure, Kilocycles
71	6	30,000	26, 28, 64, 67, 76, 105→
72	6	25,000	47, 90, 135, 140, 148, 256→
73	6	20,000	241, 263, 298, 320, 388, 529
74	5	15,000	834, 920, 944, 1001, 2168
75	7	13,250	1881, 2128, 2660, 3630, 5928, 7394→, 10219*

*Runouts: Test terminated at indicated life.

→Fracture occurred outside the test section.

TABLE A.13

TEST SERIES NO. 8:

RESULTS OF FATIGUE TESTING WITH PRIOR OVERLOADING

PRESTRESS RATIO, R_s = 1.17

Sample No.	Sample Size	Stress Level, S_{max}, psi	Lives to Failure, Kilocycles
81	6	30,000	18, 26, 28, 38, 55, 66
82	6	25,000	52, 54, 64, 103, 105, 146$^{\rightarrow}$
83	6	20,000	74, 121, 128, 221, 320, 525
84	5	15,000	591, 693$^{\rightarrow}$, 1192, 1812$^{\rightarrow}$, 2072*
85	5	13,250	448, 969, 1006, 1761, 10542*

*Runouts: Test terminated at indicated life.

$^{\rightarrow}$Fracture occurred outside the test section.

TABLE A.14

STATISTICAL ANALYSIS)F SERIES 6, 7 & 8

Sample No.	n	$\bar{x}$ (mean)	$\bar{\bar{x}}$ (median)	σ	σ_ℓ	σ_u	$\hat{\sigma}$	μ	$\frac{t_\beta \hat{\sigma}}{\sqrt{n}}$	μ_ℓ	μ_u	S_{max}, ksi
61	5	4.711	4.732	0.061	0.037	0.175	0.074	4.732	0.092	4.640	4.824	30.000
62	5	5.060	5.049	0.118	0.071	0.339	0.090	5.049	0.112	4.937	5.161	25.000
63	5	5.427	5.417	0.105	0.063	0.301	0.116	5.417	0.144	5.273	5.561	20.000
64	5	6.040	5.968	0.214	0.128	0.614	0.160	5.968	0.198	5.770	6.166	15.000
65	5	6.392	6.361	0.146	0.088	0.419	0.185	6.361	0.229	6.132	6.590	13.250
66	1	7.012	7.012	(POINT ESTIMATE)				7.012	(NOT APPLICABLE)			12.000
71	5	4.675	4.806	0.225	0.135	0.646	0.188	4.806	0.233	4.573	5.039	30.000
72	5	5.015	5.130	0.210	0.126	0.603	0.190	5.130	0.236	4.894	5.366	25.000
73	6	5.516	5.490	0.124	0.077	0.304	0.195	5.490	0.205	5.285	5.695	20.000
74	5	6.040	5.975	0.168	0.101	0.482	0.200	5.975	0.248	5.727	6.223	15.000
75	6	6.562	6.492	0.283	0.175	0.693	0.202	6.492	0.212	6.280	6.704	13.250
81	6	4.543	4.513	0.212	0.131	0.519	0.171	4.513	0.180	4.333	4.693	30.000
82	5	4.858	4.806	0.149	0.089	0.428	0.202	4.806	0.250	4.556	5.056	25.000
83	6	5.271	5.226	0.312	0.193	0.764	0.250	5.226	0.263	4.964	5.489	20.000
84	3	5.924	5.924	0.215	0.112	1.352	0.330	5.924	0.818	5.106	6.742	15.000
85	5	6.182	5.994	0.516	0.310	1.481	0.372	5.994	0.461	5.533	6.455	13.250

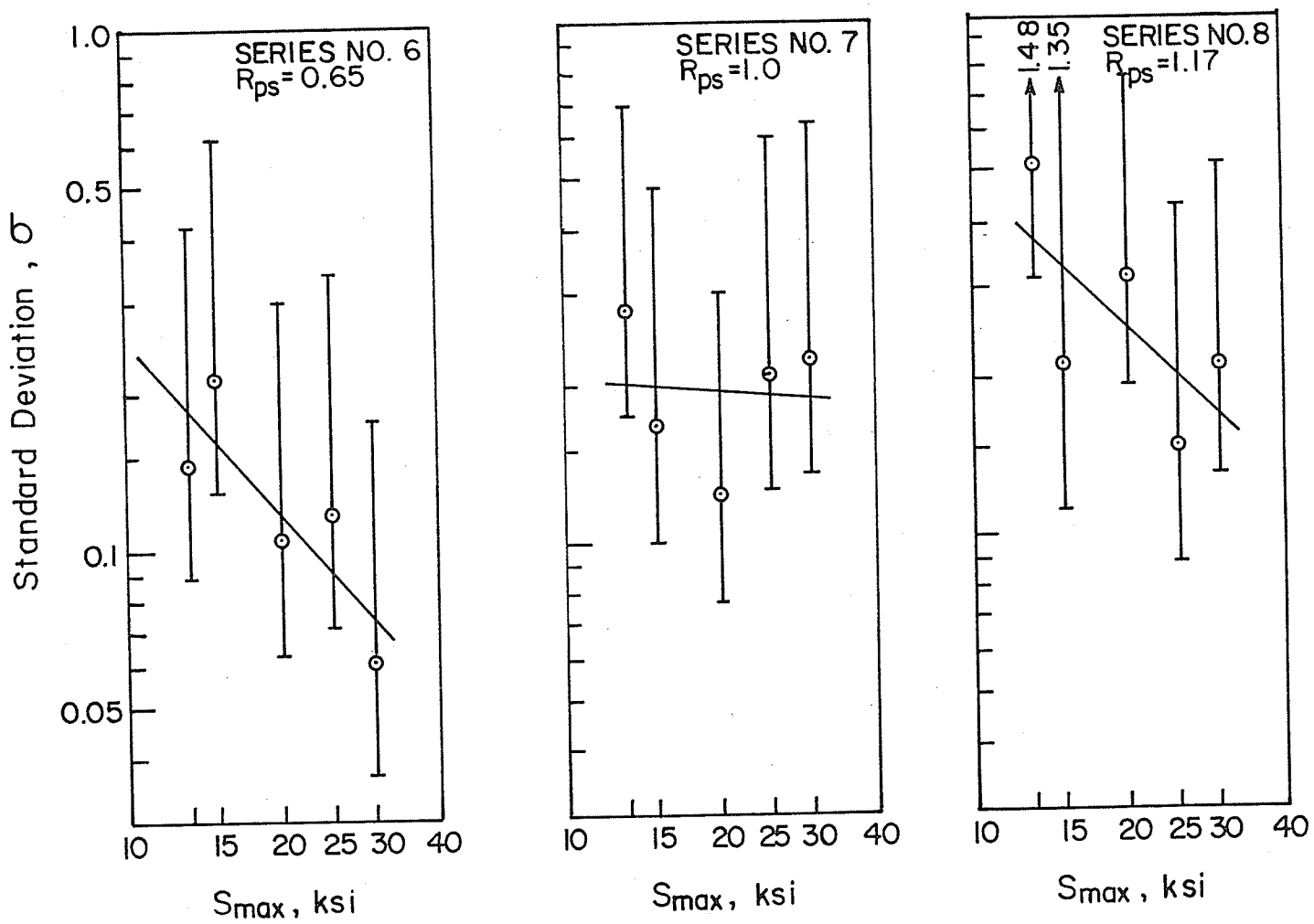

Figure A.9 Log-log plots of the best estimate of standard deviation of the population, σ, vs. the maximum fatigue stress, S_{max}.

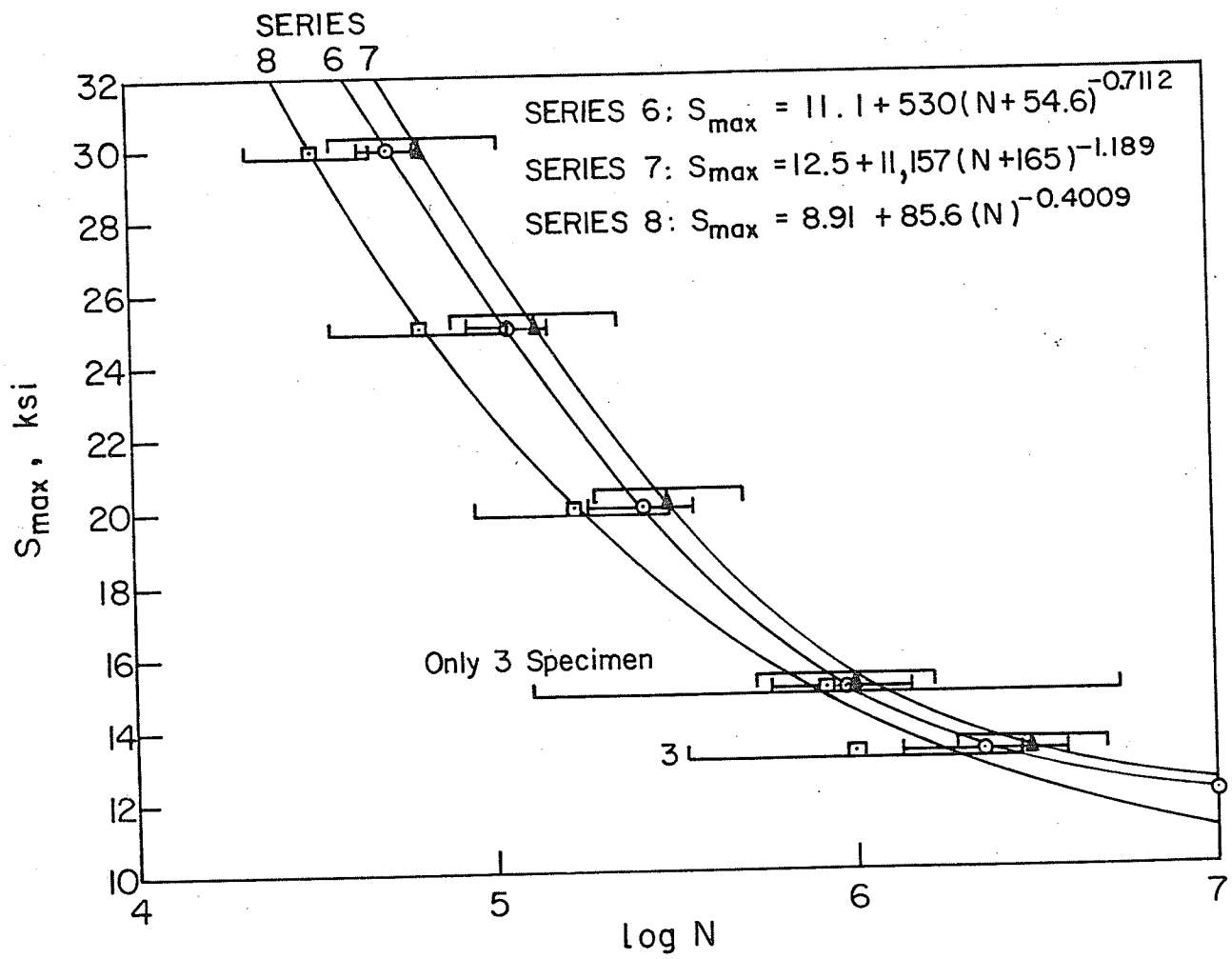

Figure A.10 Effect of preloading

and by comparison it is found that ν is within the critical limits. In this case, the sample standard deviations are said to be not significantly different. To test the difference between the means of the two samples first compute an estimate of the common variance $s^2 = 0.039$ and, therefore, the common standard deviation is $s = 0.197$. Then calculate the statistic $t' = 1.107$. For a risk $\alpha = 0.05$ and degrees of freedom d.f. = 9, use the t-distribution tables to determine

$$t_{0.95} = 1.83 > t'.$$

Therefore, the means and standard deviations of the two samples are not significantly different. Since the two samples were the most divergent it may be concluded that from a statistical viewpoint, preloading ratios of up to 1.17 do not produce improvements in the fatigue life that are statistically significant. This conclusion is valid in the cycle range of testing as shown in Figure A.10.